# THE ROLE OF WNT SIGNALING IN BONE MECHANOTRANSDUCTION

Whitney Ann Bullock

Submitted to the faculty of the University Graduate School
in partial fulfillment of the requirements
for the degree
Doctor of Philosophy
in the Department of Anatomy and Cell Biology,
Indiana University

November 2019

Accepted by the Graduate Faculty of Indiana University, in partial fulfillment of the requirements for the degree of Doctor of Philosophy.

Doctoral Committee

_____
Alexander Robling, PhD, Chair

_____
Joseph Bidwell, PhD

September 13, 2019

_____
Lilian Plotkin, PhD

_____
Uma Sankar, PhD

_____
Kenneth White, PhD

# DEDICATION

This work is dedicated to my parents, Fred and Eliza, for instilling a passion for science and learning at a young age. To my family- Gil, Claire and Emma – for endless support and encouragement.

ACKNOWLEDGEMENT

I would like to thank the National Institutes for Health for funding support, which allowed me to conduct these experiments and present my work at numerous conferences.

To the many members of the Robling lab, for assistance with these studies and moral and emotional support. A special thank you to April Hoggatt- without her countless hours of help and patience, this work would not have been possible.

Thank you to Amgen, for use of the Scl-Ab used in these studies. Thank you to Gabriela Loots for assistance with RNAseq, and Matthew Warman for assistance with digital droplet PCR.

Lastly, thank you to Dr. Robling, for encouragement and guidance, both when experiments went well and when they spectacularly failed. To my committee, for their expertise, guidance and input. And to the Deparment of Anatomy and Cell Biology, IBMG, ICMH and the IU School of medicine for the opportunity to complete this work.

Whitney Ann Bullock

THE ROLE OF WNT SIGNALING IN BONE MECHANOTRANSDUCTION

The aging US population is experiencing a growing incidence of osteoporosis, characterized by increased fracture risk and low bone mass. In skeletal tissue, canonical Wnt signaling is a critical regulator of bone mass, and dysregulation of the Wnt pathway has been implicated in numerous skeletal displasias. Some components of the Wnt signaling pathway have a clear role in bone homeostasis, particularly in the response of bone to altered mechanical environment. Other pathway components are more poorly defined. One important intracellular signal transduction node in the Wnt cascade is β-catenin, which modulates gene expression and cell-cell junctions, among other functions. During periods of disuse, β-catenin is degraded, leading to inhibition of Wnt targets. Here, I characterize the role of β-catenin in bone during a disuse challenge, using a genetic mouse model expressing an inducible constitively-active mutant form of β-catenin in the osteocyte population. I hypothesize that prevention of β-catenin degradation during disuse will prevent the bone wasting effects of mechanodeprivation. As a second goal, I focus on upstream (membrane-bound) modulation of Wnt. Here, I investigate the low-density lipoprotein receptor-related receptor 4 (Lrp4), in the regulation of bone mass and mechanotransduction. I generated an Lrp4 knockin mouse model harboring a missense mutation found among human patients with abnormally high bone mass. I hypothesize that the mutation compromises sclerostin action on bone cells. Understanding how each of these components of the Wnt signaling pathway interact, may lead to novel therapeutic targets for treatment of bone diseases.

Alexander Robling, PhD, Chair

TABLE OF CONTENTS

List of Tables ..... ix
List of Figures ..... x
List of Abbreviations ..... xi
Chapter 1: The Role of Wnt Signaling in Bone Mechanotransduction ..... 1
Mechanotransduction in bone: concepts and mechanisms ..... 2
Fluid flow and tissue strain in bone ..... 5
Molecular basis for mechanotransduction in bone ..... 7
Integrins/Focal Adhesions ..... 8
G-protein and receptor tyrosine kinase signaling in mechanotransduction ..... 10
Gap Junctions/Ion Channels in mechanotransduction ..... 12
Biochemical responses to mechanical stimuli ..... 14
Prostaglandin and NO signaling ..... 14
Wnt signaling impacts bone mass and strength ..... 16
Wnt signaling participates in mechanotransduction ..... 17
Osteocytes are the cell type of action for Wnt-mediated modulation of bone mass ..... 19
Osteocytes are the cell type of action for Wnt-mediated mechanotransduction ..... 20
Wnt-mediated mechanotransduction during mechanodeprivation ..... 22
Chapter 2: Materials and Methods ..... 27
Generation of mouse models ..... 27
β-catenin Constitutively Active mouse models ..... 27
Cre induction ..... 28
Lrp4 R1170W knock-in mice ..... 28
Dmp1-hSost mice ..... 29
Dual-energy x-ray absorptiometry (DEXA) ..... 29
Micro-computed tomography (μCT) ..... 30
Hindlimb suspension ..... 30
Botulinum toxin (Botox)-induced muscular paralysis ..... 30
Protein extraction and Western Blotting ..... 31
Protein extraction from mouse bones ..... 31
Gel electrophoresis and transfer to nitrocellulose ..... 32
Antibodies ..... 32
Quantitative cortical bone histomorphometry ..... 32
dd-PCR assay for genomic recombination of the conditional β-catenin alleles ..... 33
RNA sequencing of osteocyte-enriched cortical bone lysates in tail suspended mice ..... 34
Sclerostin inhibition *in vivo* ..... 35
Biomechanical measurements of whole-bone strength ..... 36
Muscle function testing ..... 36
Statistical analysis ..... 37
Chapter 3: Constitutive activation of β-catenin in osteocytes protects bones from disuse-associated bone wasting ..... 38
Recombination of β-catenin in bone following tamoxifen injection ..... 38
Tail Suspension Induced Bone Wasting ..... 39
Botulinum Toxin (Botox)-Induced Bone Wasting ..... 43

Gene Expression in Osteocyte-Enriched Lysates .....49
Chapter 4: The R1170W mutation in Lrp4 increases bone mass via loss of facilitator function with sclerostin.....50
Mice with the Lrp4 R1170W mutation exhibit increased bone mass .....50
$Lrp4^{KI}$ mice have increased bone formation, sclerostin expression and mildly impaired muscle function .....52
Overexpression of Sost in bone tissue causes osteopenia in WT but not $Lrp4^{KI}$ mice .....56
Inactivation of sclerostin elicits a blunted osteogenic effect in $Lrp4^{KI}$ mice.....59
$Lrp4^{KI}$ mice are partially protected from disuse-induced bone wasting .....59
Chapter 5: Discussion .....66
Regulation of β-catenin in osteocytes is necessary for mechanotransduction in disuse .....66
Lrp4 mediates bone homeostasis and mechanotransduction through Sost.....73
Future directions .....76
Appendix 1: Permissions .....80
References.....85
Curriculum Vitae

LIST OF TABLES

Table 1: Radiographic and biomechanical analysis of female Lrp4 WT, HET and KI mice....57
Table 2: Radiographic and biomechanical analysis of male Lrp4 WT, HET and KI mice....58
Table 3: Radiographic analysis and serum measurements in WT and Lrp4-KI female mice with and without a Dmp1-hSost transgene....64
Table 4: Radiographic analysis and serum measurements in WT and Lrp4-KI male mice with and without a Dmp1-hSost transgene....65

LIST OF FIGURES

Figure 1: The bone microenvironment .....3
Figure 2: Osteocytes are the mechanosensor of bone.....6
Figure 3: Mechanotransduction signaling in osteocytes.....10
Figure 4: Gap junctions and hemichannels in osteocytes .....13
Figure 5: Wnt signaling pathways in bone.....17
Figure 6: Lrp5 is critical for the response to mechanical load in bone.....18
Figure 7: Lrp5 mutations in bone alter bone mass.....19
Figure 8: Sost prevents loading response in bone.....22
Figure 9: Mutations in the 3rd beta-propeller central domain increase bone mass in patients with sclerosteosis.....24
Figure 10: Constitutive activation of β-catenin in bone.....38
Figure 11: Mice with constitutive activation of β-catenin are protected from mechanodeprivation-induced bone loss during 4 weeks of tail suspension .....42
Figure 12: μCT measurements of cancellous bone properties in the tibiae of ground control and tail suspended Cre-positive and Cre-negative βcat CA mice .....44
Figure 13: Dynamic histomorphometry of Cre-positive and Cre-negative βcat CA mice following tail suspension.....45
Figure 14: Mice with constitutive activation of β-catenin are not protected from mechanodeprivation-induced bone loss during 4 weeks of muscle paralysis disuse.....47
Figure 15: μCT measurements of cancellous bone properties in the tibiae of saline-injected control and Botox in βcat CA Cre-positive and Cre-negative mice .....48
Figure 16: RNAseq of bones from βcatCA mice.....49
Figure 17: Generation of Lrp4 R1170W knockin mouse model .....50
Figure 18: $Lrp4^{KI}$ mice have a high bone mass phenotype.....53
Figure 19: $Lrp4^{KI}$ mice display supernumerary teeth and altered molar cusp patterns .....54
Figure 20: $Lrp4^{KI}$ mice have increased bone formation, increased circulating and Local sclerostin, and reduced skeletal muscle function.....55
Figure 21: $Lrp4^{KI}$ mice are protected from the osteopenic effects of Sost overexpression .....60
Figure 22: Response to pharmalogic inhibition of Sost is blunted in $Lrp4^{KI}$ mice.....62
Figure 23: $Lrp4^{KI}$ mice are partially protected from disuse-induced bone loss.....63

LIST OF ABBREVIATIONS

| | |
|---|---|
| FAK: | Focal Adhesion Kinase |
| Pyk2: | Proline-rich kinase2 |
| GPCR: | G-protein coupled receptor |
| FRET: | Fluorescence resonance energy transfer |
| PTH1R: | Parathyroid hormone 1 receptor |
| RTK: | Receptor Tyrosine kinase |
| IGF1R: | Insulin-like growth factor 1 receptor |
| PKG: | Protein Kinase G |
| Cx43: | Connexin 43 |
| PGE2: | Prostaglandin E2 |
| VGCC: | Voltage-gated calcium channels |
| COX2: | Cyclooygenase 2 |
| NO: | Nitric oxide |
| Lrp5: | Low density lipoprotein receptor-related protein 5 |
| OPPG: | Osteoporosis pseudoglioma |
| BMD: | Bone mineral density |
| HBM: | High bone mass |
| WT: | Wild-type |
| LDL: | Low density lipoprotein |
| Lrp4: | Low-density lipoprotein receptor-related protein 4 |
| Dmp1: | Dentin matrix protein |
| DMF: | Dimethyl formamide |
| DEXA: | Dual-energy x-ray absorptiometry |
| BMC: | Bone mineral content |
| HRP: | Horseradish peroxidase |
| uCT: | Micro-computed tomography |
| ddPCR: | Digital droplet PCR |
| CA: | Constitutively active |
| LOF: | Loss-of-function |
| GOF: | Gain-of-function |
| TG: | Transgene/transgenic |
| NTG: | Non-transgenic |
| BV/TV: | Bone volume/total volume |
| Tb.N.: | Trabecular number |
| Tb.Th.: | Trabecular thickness |
| pQCT: | Peripheral quantitative computed tomography |
| SEM: | Standard error of mean |
| SOST2: | Sclerosteosis2 |
| NMJ: | Neuromuscular junction |
| L5: | Lumbar vertebra 5 |
| LiCl: | Lithium chloride |
| CMS: | Congenital myasthenic syndrome |

## ***Chapter 1: The Role of Wnt Signaling in Bone Mechanotransduction***

Osteoporosis—a disease characterized by low bone mass and increased fracture risk—is a growing problem among the aging US population [6, 7]. The prevalence of low bone mass, especially among post-menopausal women, highlights the need for therapies to increase bone mass. Each of the FDA-approved therapies for treating osteoporosis is associated with unwanted side effects (blood clots associated with SERM use, bisphosphonate storage in bone tissue associated with atypical fractures, cancer concerns with teriparatide, cardiovascular risk with sclerostin antibody), so understanding additional pathways that regulate bone mass could provide new potential drug targets that might have fewer side effects.

The mechanical environment of bone tissue represents a key regulator in the maintenance of bone mass, and absence of mechanical stimulation (disuse) has profound bone wasting effects. Paralysis, long-term bed rest, and space flight all result in reduced mechanical stimulation and a reduction in bone mass, leading to increased risk of fracture. In the absence of a steady-state mechanical environment, osteoblast activity decreases, while bone resorption by osteoclasts increases. Osteocytes are the mechanosensors in the skeletal system, and they regulate osteoblast and osteoclast differentiation and activity through multiple mechanisms (Figure 1). The altered mechanical environment experienced by the osteocyte induces biochemical changes in the local cell populations that ultimately facilitate bone adaptation. These changes–collectively known as mechanotransduction—involve activation and inhibition of numerous pathways that coordinate to achieve an adapted structure.

**Mechanotransduction in bone: concepts and mechanisms**

Detection of mechanical stimuli, and transformation of mechanical signals into biochemical responses, is facilitated by the vast network of cytoplasmic processes that extend from the osteocyte cell body throughout the lacuna-canalicular network in mineralized bone. Cell surface molecules and structures (integrins/cadherins, ion channels, G-protein coupled receptors, primary cilia) and intracellular signaling pathways (Wnt/β-catenin, mitogen-activated protein kinases, tyrosine kinases, cGMP/cAMP pathways) detect and transduce mechanical signals from osteocyte "sensor cells" into altered bone remodeling by "effector cells" (osteoblasts, osteoclasts, bone lining, Figure 1). Several fundamental processes that control skeletal adaptation to mechanical loading have been identified and integrated with signaling pathways, leading to a better understanding of bone tissue engineering and physiology [8], creating new opportunities for clinical/pharmaceutical and exercise strategies to promote skeletal health.

Cells within bone detect, coordinate and mediate mechanical loading on the skeleton. Key questions include 1) how the cells embedded within and on the surfaces of bone sense and respond to externally applied mechanical loads, 2) whether the mechanical stimulus is direct tissue strain from loading/bending of bone, or an indirect consequence of the load (i.e., load-induced fluid flow over the surfaces of bone cells), and 3) how cells translate a mechanical signal detected at the cell surface into an appropriate sequence of biochemical changes inside the cell that results in a coordinated anabolic or catabolic response.

The cells most likely to function as the "mechanosensors" in bone are the osteocytes. Intuitive considerations and abundant experimental evidence supports the assignment of osteocytes as the bone cells most directly responsible for detecting mechanical signals and orchestrating the skeletal response to those signals. Osteocytes within individual lacunae are perfectly positioned as mechanosensors since they are distributed uniformly throughout cortical and trabecular bone and are connected by system of canals. This allows osteocytes to function in a network capable of sensing load-induced signals virtually anywhere in the skeleton. Long cytoplasmic processes (~50/cell) interconnect the cells comprising this vast network to each other via gap junctions, which facilitate cell-cell communication. However, these same properties make osteocytes unlikely candidates for effector cells that directly add or remove bone from bone surfaces. Although osteocytes can mediate localized removal of mineralized matrix and calcium release from their own lacuna, this localized activity has little effect on the size, shape, and structural properties of the skeleton. Osteoblasts, bone lining cells and

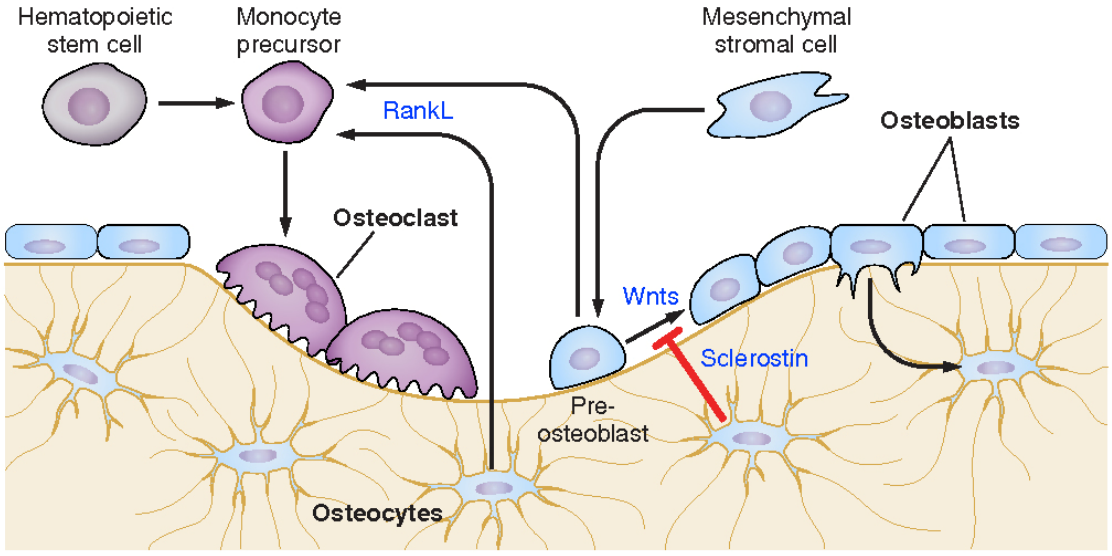


Figure 1. The bone microenvironment. The bone microenvironment is a complex system consisting of bone-forming osteoblasts, bone-resorbing osteoclasts and mechanosensitive osteocytes. These cells coordinate bone homeostasis through complex signaling mechanisms. Figure from [4].

osteoclasts function as the “effector” cells that add or remove bone under the direction of signals from the osteocyte network.

To understand how physical stimuli affect bone cells, I must consider the vastly different microenvironments that different bone cells inhabit. Stromal (MSC) cells for instance reside in the bone marrow space of long bones and vertebrae, have minimal extracellular space surrounding them, and no rigid substrate to contact. In contrast, osteoblasts, osteocytes and bone lining cells attached to the hard surfaces of bone, experience higher surface strains as well as movement of fluid over their surfaces. The physical environment of the osteocyte is truly unique. Osteocytes encase themselves in mineralized matrix. Importantly, they create a small fluid filled form-fitting cavity within their lacuna and extend cell processes that course through the matrix in narrow canaliculi. The canaliculi average about 260 nm in diameter and the space between the projection membrane and the canalicular wall is very narrow (~80 nm), creating the potential for high velocity fluid movement driven by load-induced pressures or matrix strains. Finite element modeling indicates that typical macroscopic level strains on bone can result in greatly amplified strains at the microscopic level of the perilacunar space [9]. For years the strongest argument favoring the osteocyte network as the primary mechanosensory system in bone was based on these characteristics. Fortunately, experimental support for this hypothesis now exists. Osteocytes are more sensitive and respond differently to fluid flow-induced shear stress compared to osteoblasts *in vitro* [10, 11], and experiments in mice demonstrated a key functional role for osteocytes in detecting disruptions to normal mechanical loading. A transgenic mouse was created that enabled efficient ablation of the majority of osteocytes without affecting osteoblasts and osteoclasts [12]. These mice

were protected from disuse-induced bone loss, demonstrating a key role for the osteocyte network in sensing the loss of normal skeletal loading. Although inflammatory effects, including enhance osteoclast formation, following induction of such massive osteocyte death, complicate this analysis [13], there is an overwhelming consensus that osteocytes are the primary mechanosensory cells in bone.

**Fluid flow and tissue strain in bone**

There is a strong argument in favor of mechanically generated oscillatory fluid movement within the lacunocanalicular network being the most physiologically relevant cell level mechanical stimulus. Although tissue strains produced by bending the bone matrix can induce mechanical signals detected by osteocytes, the vast array of cytoplasmic processes of the osteocyte positions these cells to sense fluid flow. Indeed, the ability of the extracellular domains of integrins expressed on the long cytoplasmic osteocyte processes appear to be capable of "amplifying" relatively small fluid forces into disproportionally large biochemical responses inside osteocytes [14]. Osteocytes are physically connected to the extracellular glycocalyx within the canalicular walls *via* integrin heterodimers. Subtle changes in the conformation of integrin extracellular domains are transduced to the cell interior via short cytoplasmic tails. Growing evidence suggests that integrin-associated signaling and cytoskeletal proteins transmit mechanical signals directly to the nucleus to alter gene expression.

Experimental limitations must be considered when evaluating mechanical sensory mechanisms and the relative contributions of fluid flow and substrate strain in osteocytes. First, most published studies are based on *in vitro* cell culture experiments using osteoblasts or osteocyte-like cell lines; since primary osteocytes are difficult to isolate in

sufficient numbers for experimental study. Determining the contribution of tissue level strains in bone as biologically relevant osteocyte stimuli is also challenging [15]. Measurements of tissue strain collected on the periosteal surface of long bones indicate that the peak strain generated during strenuous activity is approximately 3,000 με. When bone cells grown on 2-dimensional culture substrates are exposed to 3,000 με no detectable response can be measured. In fact, greater than 10,000 με must be applied before most *in vitro* models will yield a measurable response. Application of 10,000 με is beyond the yield point of bone *in vivo* and fracture occurs before sufficient tissue strain stimulates bone cells. However, application of loads generating ~2000 με on a bone's surface may generate local strains up to 30,000 με on the osteocyte lacunar wall. This

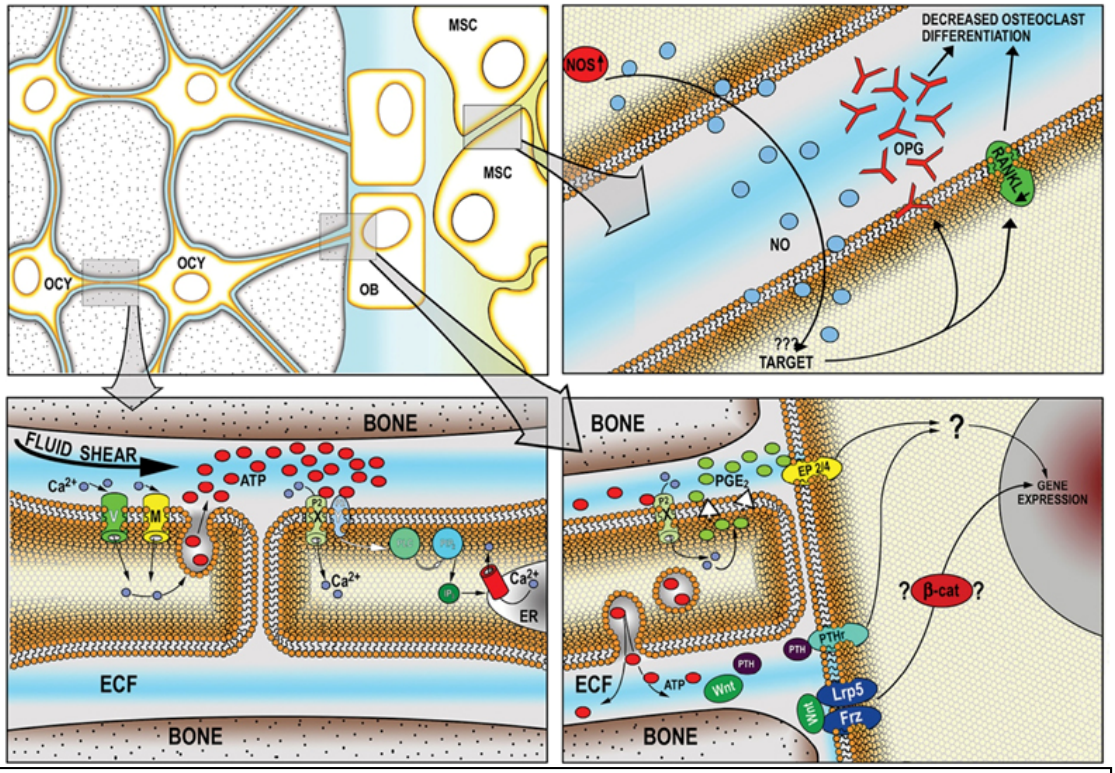


Figure 2. Osteocytes are the mechanosensor of bone. Mechanotransduction in osteocytes is dependant on fluid flow in the osteocyte canalucilar network. Fluid flow during mechanical loading in bone results in osteocyte-osteocyte, osteocyte-osteoblast and MSC paracrine signaling. Figure from [2].

difference in macro vs micro level strain is possibly a consequence of stress-concentrating effects of the voids produced by osteocyte lacunae [14].

Much less controversial is the impact of shear stress generated as extracellular fluid moves across osteocyte surfaces from areas of higher to lower pressure when a long bone is bent during loading (Figure 2). Fluid shear stress potently stimulates osteocytes and other bone cells *in vitro*. Enhanced transport of growth factors and nutrients, removal of waste products of metabolism (chemotransport), and generation of electrical streaming potentials may also affect osteocyte responses to fluid flow. Chemotransport also affects the response of bone cells to fluid flow independent of mechanical signal transduction [16].

An intriguing model for osteocyte mechanotransduction has been developed by the Schaffler and Weinbaum laboratories [14] based upon microscopic level studies of osteocytes in bone piece. Their model considers the observation that the cytoplasmic processes appear to be suspended from the canalicular wall via integrin adhesion complexes attached to tethering structures made from the glycocalyx . They suggest that fluid flow through the space between the membrane and the glycocalyx wall "deflects" these tethering structures, resulting in deformation referred to as "hoop strain" Deformation of these tethering structure results in a strain amplification that is radial, like a hoop. As a result of this amplification, estimates suggest that local cell membrane strains may be 10-100-fold higher than grossly measured tissue strains.

**Molecular basis for mechanotransduction in bone**

Having considered both the physical environment and the mechanical forces to which osteocytes are exposed, how do osteocytes respond appropriately to relevant mechanical

stimuli? This complex question must consider the contributions of membrane proteins, lipids, intracellular signals, and the cytoskeleton, all of which convert mechanical forces into biochemical signals that ultimately alter gene expression. No aspect of mechanotransduction in bone may be more fundamental than, yet as controversial as, identification of the predominant cell surface mechanoreceptor. It is probable that no single mechanoreceptor protein or structure is singularly responsible for sensing and transducing mechanical stimuli into altered bone formation. Fortunately excellent progress is being made and great potential exists to therapeutically manipulate mechanotransduction pathways to treat human bone mass diseases.

Bone cell mechanoreceptors can be classified into broad categories; i) integrins, ii) G-protein coupled receptors/receptor tyrosine kinases, and iii) ion channels/connexin hemichannels). A role for the primary cilium is also gaining acceptance. Inhibition of a specific protein's ability to blunt normal mechanotransduction is the standard of proof that a protein is involved *in vitro.* However, most *in vitro* studies fail to recapitulate the complex 3-dimensional environment of osteoblasts and osteocytes *in vivo*, and it is more challenging to determine which proteins are essential *in vivo*. While it is likely that any predominant mechanoreceptor would be activated within milliseconds of stimulation, temporal and quantitative assessment of mechanical signaling activity in real time in living cells within bone is extremely difficult.

*Integrins/Focal Adhesions*

Integrins as mechanosensors at specialized sites of cell-matrix adhesion, known as "focal adhesions", have been intensively studied [17]. Integrin-containing focal adhesions mediate both cell-matrix adhesion and transmembrane signaling. Responses to strain and

fluid flow mediated by integrins in bone cells, initially studied in osteoblast-like cells, and more recently in osteocytes, include changes intracellular tension via reorganization of the actin cytoskeleton, increased MAP kinase and tyrosine kinase activity, release of paracrine signaling molecules (prostaglandins and nitric oxide), and altered gene expression. These findings led to the "mechanosome hypothesis" (Figure 3) which postulated that protein complexes (mechanosomes) capable of associating with cell adhesion molecules (integrins and cadherins) are "launched" from the membrane to the nucleus in response to mechanical stimuli, leading to alteration of gene expression [18]. DNA-binding proteins localized in adhesion molecule-associated complexes are translocated to the nucleus in response to mechanical loading, thereby transferring mechanical information from adhesion complexes at the cell surface to target genes [19]. Experimental support is based largely on the effects of deleting/inhibiting specific mechanosome proteins on signaling and load-induced bone formation.

Evidence that integrins are activated by fluid flow is compelling and comes both from direct demonstration of changes in integrin conformation and from studies using integrin-specific inhibitory antibodies and function inhibiting Arg-Gly-Asp (RGD) peptides. Thus, focal adhesions exhibit many properties implicating them as primary mechanosensory structures [20]. Importantly, integrins have two interrelated roles: a structural (load-bearing) function in which they link (indirectly) to the actin cytoskeleton, and a signal transduction/scaffolding function in which they bind and organize proteins that have significant downstream effects on the cell. Although cytoskeletal reorganization received considerable initial attention as a mechanism for transducing mechanical signals, many biochemical responses to mechanical stimulation in bone cells do not

require an intact cytoskeleton [21]. Conformational changes induced by mechanical stimuli expose binding sites in the cytoplasmic tails of integrin subunits. These are binding sites for kinases (focal adhesion kinase [FAK], proline rich kinase-2 [Pyk2], Src kinase) and adaptor proteins (e.g., paxillin, β-actinin, Nmp4, zyxin, p130$^{cas}$, among many others) that can stimulate signaling cascades and translocate mechanosome complexes from the cell membrane into the nucleus in a multi-stop process involving detection of a mechanical signal, activation of membrane-associated proteins, formation of mechanosome complexes at the membrane, and then their translocation to the nucleus where they alter transcription of genes that regulate bone remodeling.

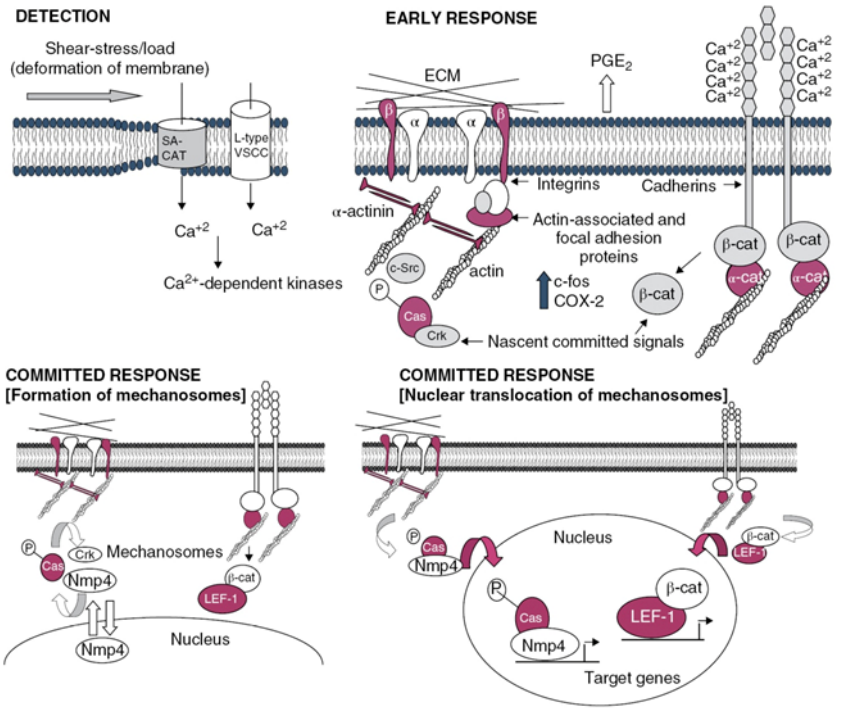


Figure 3. Mechanotransduction signaling in osteocytes. In response to mechanical stimulation (fluid flow or ECM deformation), numerous signaling pathways are activated. Figure from [2].

*G-protein and receptor tyrosine kinase signaling in mechanotransduction*

Osteocyte responses to mechanical load include activation of G-protein coupled receptors (GPCRs). GPCRs are a large class of surface receptors stimulated by a wide range of ligands. The most common method of monitoring GPCR activity is though measuring

hydrolysis of the G-proteins that they activate. The Frangos lab showed that fluid shear stimulates G-protein signaling and that pharmacologic inhibition of G-proteins inhibits activation of downstream signals [22]. The temporal and spatial advantages of fluorescence resonance energy transfer (FRET) microscopy allowed them to demonstrate that a conformational change occurs in the parathyroid hormone 1 receptor (PTH1R) and $B_2$ bradykinin receptor within milliseconds of applying fluid shear stress [23]. This response did not require the presence of either receptor's ligand and could be modulated by changing membrane fluidity, showing that these receptors exhibit the characteristics required of direct cell surface sensors of mechanical stimuli.

Molecular interplay between receptor tyrosine kinase (RTK) signaling and integrins was shown by the Bikle laboratory who reported that signaling through the insulin-like growth factor 1 receptor (IGF1R) is required for optimal transduction of fluid shear induced signaling and is also regulated by direct interaction with integrins [24]. This led to their proposing a model in which the bone forming effects of IGF1 are not only mediated by interactions with IGF1R but can simultaneously be modulated by mechanical stimulation of integrins and pathways downstream of integrins. The Pilz lab showed that fluid shear mediated activation of nitric oxide, cyclic GMP and protein kinase G signaling in osteoblasts was dependent on Src activation downstream of integrins [25]. This process involved PKG II dependent Src dephosphorylation via a fluid shear induced PKG II/Src/Shp mechanosome. Whether GPCRs and RTKs are able to sense mechanical stimuli directly, or do so primarily via cross-communication with integrin mechanosensor remains to be determined.

*Gap Junctions/Ion Channels in mechanotransduction*

Gap junction channels formed by connexins (Cx) mediate communication among osteocytes and between osteocytes and cells on the bone surface [26]. All bone cells express connexins, Cx43 being the most abundant. *In vitro* and *in vivo* studies showed that Cx43 protein levels and function are increased by mechanical stimulation and conversely, lack of mechanical signals decreases Cx43 expression.

Cx43 also forms hemichannels that enable communication between cells and the extracellular environment [27] and are opened by mechanical stimulation [26], although their function is still under debate. It has been proposed that hemichannels are required for ATP and prostaglandin release induced by mechanical stimulation. However, another study showed that activation of purinergic receptors increases prostaglandin E2 (PGE2) release independent of hemichannels, and that blockade of P2X7 receptors, which are activated by ATP, prevents PGE2 release from osteoblastic and osteocytic cell lines. Further, it was recently shown that that osteoblastic cells derived from Cx43-/- mice still respond to mechanical stimulation by releasing PGE2 [26]. This later study proposes that hemichannels formed by Pannexin1, a transmembrane protein with topology similar to connexins [28], rather than Cx43 are responsible for channel activity induced by ATP in osteoblastic cells.

*In vitro* studies, together with early evidence showing the existence of gap junctions between osteocytes and osteoblasts on the bone surface [29], led to the hypothesis that Cx43 is required for the response to mechanical stimulation *in vivo*. This was proven in mice lacking Cx43 in pre-osteoblasts, osteoblasts and osteocytes, which exhibit an attenuated anabolic response to mechanical stimulation on the tibial

endocortical surface [26]. However, all studies in which periosteal bone formation was investigated showed, surprisingly, an enhanced response to mechanical loading in the absence of Cx43 in osteochondroprogenitors, osteoblasts, and osteocytes. The molecular bases for this effect remains unknown.

Mechanotransduction can be modulated by extracellular nucleotides [30]. ATP and UTP are released by osteoblasts and osteocytes subjected to mechanical stimulation *in vitro*, and can activate P2X ligand-gated ion channels and metabotropic P2Y GPCRs [31]. Receptor activation leads to various responses depending on the nucleotide and type of receptor, including Ca2+ wave propagation, intracellular kinase activation, modulation of osteoblast function and survival. In particular, P2X7-deficient mice exhibit a deficient anabolic response to mechanical stimulation in vivo, suggesting an important role for these channels in mechanotransduction [32]. Further, a complex formed by P2X7

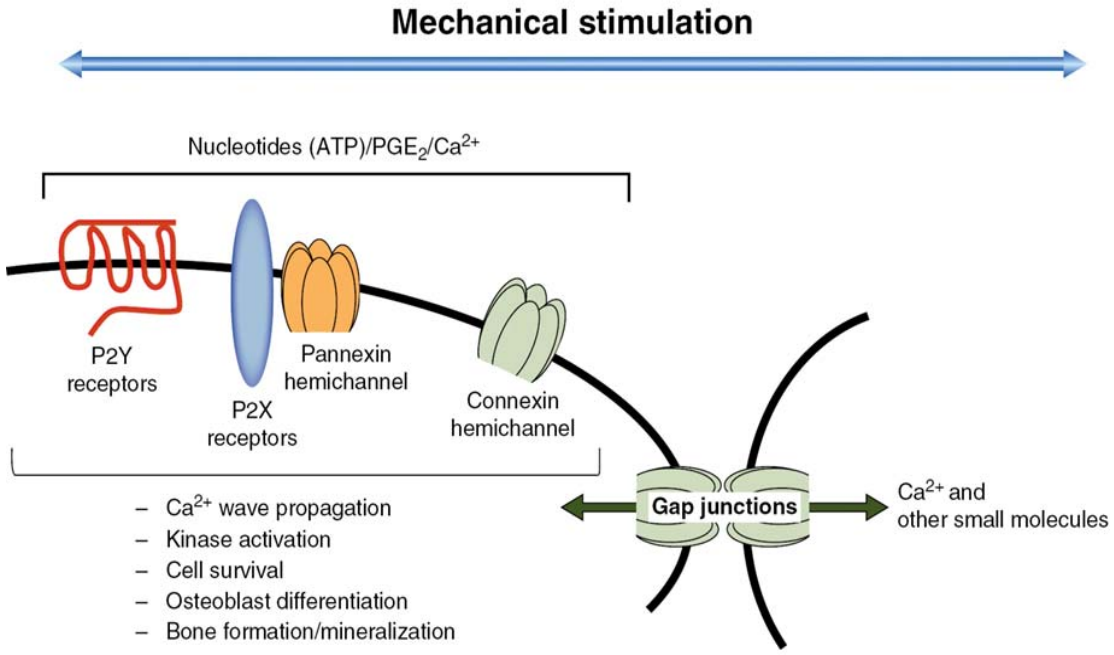


Figure 4. Gap junctions and hemichannels in osteocytes. Gap junctions are necessary of mechanotransduction in osteocytes. Cx43 in osteocytes is involved in the response to mechanical stimulation in bone. Figure from [2].

receptors and pannexin1 channels mediates ATP release induced by mechanical stimulation in vitro [33]. The relevance for this complex in transmission of mechanical signals in vivo remains to be determined (Figure 4).

Ion channels sensitive to mechanical stimulation are also found in osteoblastic cells [34, 35]. Among them, gadolinium-sensitive stretch-activated cation channels are involved in the response to stretching in vitro. In addition, transient receptor potential channels and voltage gated calcium channels (VGCC) mediate the propagation of calcium waves following mechanical stimulation in osteoblastic cells. Interestingly, osteoblast to osteocyte differentiation is accompanied by changes in the type of VGCC from L-type in osteoblasts to T-type in osteocytes, a change associated with the different sensitivity of the two cell types to mechanical stimulation [36]. The role of VGCC channels in mechanotransduction has been demonstrated *in vivo*, as inhibition of L-type channels in rats blocks the anabolic response to loading [34].

**Biochemical responses to mechanical stimuli**

Detection of a molecular response to mechanical stimulation does not prove that it is important for mechanotransduction in bone. Determining which are important to regulating bone responses to mechanical stimulation and which are merely tangential is a critical question if we are to effectively target mechanotransduction pathways for therapeutic benefit. The following signaling pathways have been verified *in vivo* to affect the skeleton.

*Prostaglandin and NO signaling*

Osteoblasts and osteocytes secrete prostaglandin E2 (PGE2) and upregulate expression of cyclooxygenase 2 (COX2) in response to substrate strain and fluid flow [37]. COX2 is

necessary for PGE2 production, and inhibition of COX2 using inhibitors such as NS398 blocked PGE2 release *in vitro*. PGE2, a lipid generated from arachidonic acid via COX enzymes that functions like a hormone, is secreted in response to a number of stimuli including PTH, estrogen and mechanical loading. Vigorous exercise in humans results in rapid release of PGE2 from loaded lower limb bones [38]. In mice, mechanical loading upregulated COX2 mRNA and protein within minutes [39]. A functional role for PGE2 signaling on the skeleton in response to mechanical loading was shown *in vivo* by pharmacologic inhibition of both COX1 and COX2 using indomethacin, or via selective inhibition of COX2 alone using NS398 [40]. In both cases, inhibition of PGE2 production prior to loading reduced the osteogenic response. PGE2 secretion studies from bone cells in vitro suggest PGE2 is released through connexin-43 hemichannels or from purinergic P2X7 protein complexes [41]. Downstream of PGE2 release, autocrine and/or paracrine effects may be mediated via Ep receptors.

Nitric oxide (NO), a free radical that diffuses like a gas very rapidly through the plasma membrane, is released from osteoblasts and osteocytes in response to fluid shear and strain. Depletion of NO *in vivo* prior to loading in rats using NOS inhibitors attenuates the osteogenic response to loading. Unlike WT animals, mice null for inducible NOS ($iNOS^{-/-}$), failed to reform bone that is lost during hindlimb unloading upon returning to normal ambulation, suggesting that the cellular response to mechanical stimulation in bone requires NO signaling [42].

One of the key pathways that osteocytes use to facilitate mechanotransduction is the Wnt signaling pathway, which is gaining recognition as a key player in adaptive bone modeling and remodeling.

**Wnt signaling impacts bone mass and strength**

The role of Wnt signaling in bone mechanotransduction is of critical importance, and it serves as the basis for most of the work associated with this dissertation. Our understanding of osteocyte mechanotransduction took a significant leap forward when the importance of Wnt signaling in bone was identified (Figure 5). Prior to the turn of this century, research on the Wnt signaling cascade was confined largely to the cancer (e.g., tumor biology and proliferation) and developmental biology (e.g., axis patterning) fields. However, two key clinical discoveries changed our view on where and how Wnt signaling is important in the body, bringing the skeleton into direct focus as a major Wnt-dependent system. The first of these discoveries was the finding that loss-of-function mutations in the Wnt co-receptor *Low density lipoprotein receptor-related protein 5* (LRP5) are a genetic cause of the rare, debilitating disease Osteoporosis Pseudoglioma (OPPG) [43]. Patients with OPPG can present clinically with bone mineral density (BMD) values that are approximately 5 standard deviations below age-matched normal values, resulting in frequent fractures and impaired mobility. At around the same time, other groups reported that gain-of-function mutations in LRP5 are a genetic cause for endosteal hyperosteosis, a high bone mass (HBM) condition [44, 45]. These patients have BMDs that are approximately 5 standard deviations above normal, but their skeletons are relatively normal in shape, and they present with none of the clinical manifestations associated with other, osteoclast-mediated sclerosing bone disorders (e.g., osteopetrosis). Thus, within a few short years, a single Wnt co-receptor was identified as causative for two very different rare skeletal diseases, one associated with very high bone mass and the other associated with very low bone mass. As LRP5 has no other well-

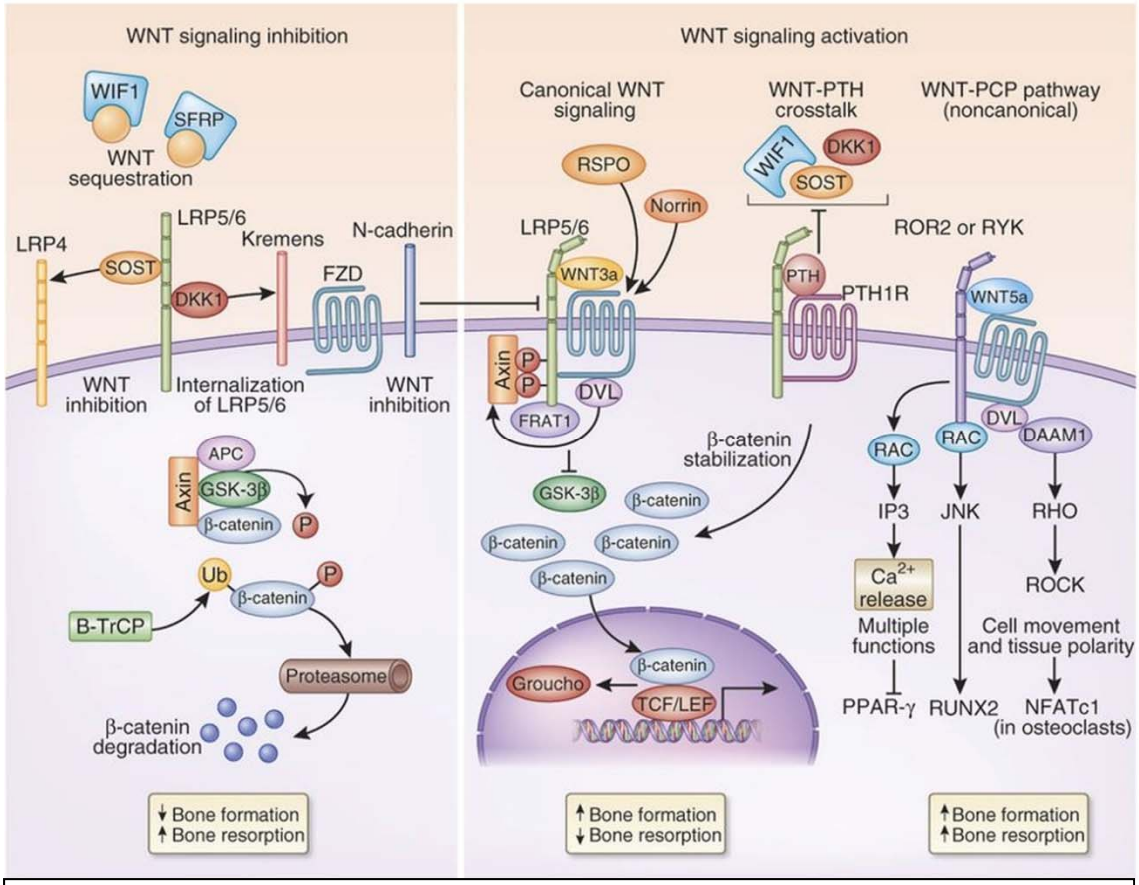


Figure 5. Wnt signaling pathways in bone. Wnt signaling is inhibited by soluble factors including Sost, Dkk1 and Sfrp, among others. During inhibition of Wnt, the GSK-3β/APC/Axin complex phosphorylates β-catenin, leading to proteasome-mediated degradation of β-catenin. When Wnt signaling is activated, Lrp5/Axin/Fzd complex inhibits GSK-3β and β-catenin accumulates in the cytoplasm. From there, β-catenin is utilized for gap junction formation, integrin complexes and as a transcription factor in the nucleus (shown). Figure from [5].

characterized primary ligands beyond the Wnt family, these human genetic studies implicated Wnt signaling as a major regulator of bone metabolism.

**Wnt signaling participates in mechanotransduction**

Shortly after the discoveries regarding LRP5's role in regulating human skeletal properties, mouse models were developed to model the diseases in mice and open up experimental options not possible in human patients. Mice with loss-of-function mutations in Lrp5 (i.e., "knockout") recapitulate the low bone mass phenotype observed in human OPPG patients (Figure 6A). These mice have low BMD, compromised

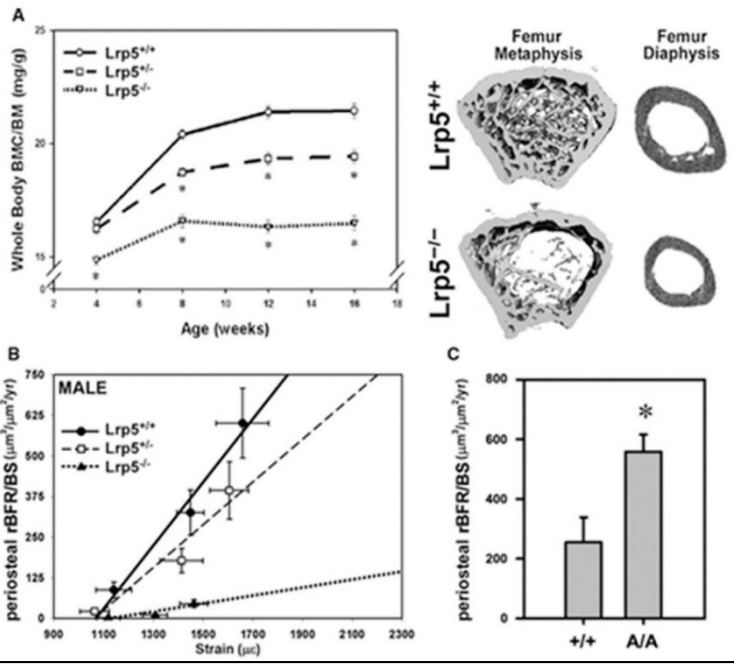


Figure 6. Lrp5 is critical for the response to mechanical load in bone. Lrp5 KO mice have reduced bone mineral content (A) and reduced bone formation in response to loading (B). Lrp5 HBM mice are more sensitive to mechanical stimulus (C). Figure from [3].

trabecular mass and architecture, reduced cortical bone size, and impaired biomechanical properties [46]. Those observations prompted investigation into the role of Wnt signaling in mechanotransduction, the first experiments of which began by looking at mechanoresponsiveness in Lrp5$^{-/-}$ mice. *In vivo* mechanical loading experiments, using the rodent ulnar loading model, were first performed to assess the ability of Lrp5$^{-/-}$ mice to respond anabolically to a simulated vigorous exercise session. In both male and female Lrp5$^{-/-}$ mice, load-induced bone formation was significantly impaired compared to control (wild-type; WT) mice [46] (Figure 6B). That conclusion was later confirmed by another group in an independently generated Lrp5 knockout model, using a different loading modality (tibia loading) [47]. Thus the experimental data are consistent in implicating Wnt signaling through Lrp5 as a crucial process for skeletal mechanotransduction. i.e., without Lrp5 receptors, bone tissue cannot adapt properly to mechanical inputs. Those observations might explain a portion of the low bone mass phenotype among OPPG patients, i.e., that

these individuals are unable to respond to otherwise stimulatory mechanical signals, and consequently, bone properties never reach their appropriate size and strength.

While the Lrp5 knockout models are useful for exploring the role of the Wnt/Lrp5 axis in bone metabolism and mechanotransduction, the field saw a developing interest in understanding whether the gain-of-function mutations in LRP5 found in several families with HBM might also confer improved mechanical signaling properties to the cell. Different knock-in mouse lines, harboring a variety of HBM-causing missense mutations in Lrp5 were developed to study the HBM phenotype. Like the human patients that these mutations were modeled after, the HBM knock-in mice exhibited high BMD, dramatically increased trabecular and cortical bone mass, and improved biomechanical properties [48]. More importantly, however, the gain-of-function mutant mice were more responsive to tibial loading than their WT littermates (Figure 6C) [49]. In summary, mice with either loss- or gain-of-function mutations in Lrp5 exhibit altered load-induced bone formation, suggesting that Lrp5 plays a major role in mechanotransduction signaling in bone.

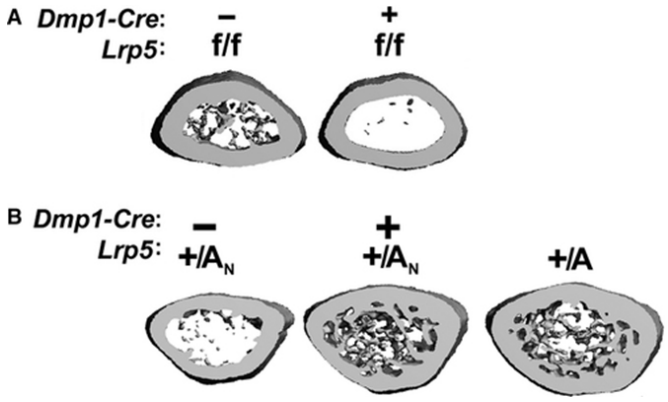


Figure 7. Lrp5 mutations in bone alter bone mass. (A) Deletion of Lrp5 in osteocytes reduces bone mass, whereas mutation in Lrp5 resulting in increased Lrp5 function (B) increases bone mass. Figure from [3].

**Osteocytes are the cell type of action for Wnt-mediated modulation of bone mass**

While both the gain-of-function knock-ins, and the loss-of-function knockout, all model the phenotypes observed human patients with analogous LRP5 mutations (i.e., the mice

and humans have altered Lrp5 expression globally), those mouse models do not reveal the specific cell type(s) of action that account for the Wnt-driven skeletal phenotypes. To address this issue, cell-selective deletion of Lrp5 or expression of Lrp5-HBM alleles in specific cell types can reveal the relative contributions of these cell types to the overall phenotype. Mice with floxed Lrp5 alleles ($Lrp5^{f/f}$), where recombination of the LoxP sites results in a null allele, have a normal bone mass in the absence of Cre recombinase. However, when crossed to mice that express Cre in osteocytes (Dmp1-Cre), the mice develop an early-onset osteopenic phenotype that mimics the global $Lrp5^{-/-}$ model (Figure 7A) [48]. Likewise, mice engineered with a Cre-inducible heterozygous gain-of-function missense mutation in Lrp5, where recombination of a floxed Neo cassette in one of the introns releases the HBM allele from its dormant state, have normal bone mass in the absence of Cre recombinase. However, when crossed to mice that express Cre in osteocytes (Dmp1-Cre), the mice develop an early-onset hyperostosis phenotype that mimics the global Lrp5-HBM model (Figure 7B) [48]. Thus, the osteocyte-selective deletion of Lrp5 and expression of Lrp5-HBM both recapitulate the global knockout and knock-in models, respectively, suggesting that mutation of Lrp5 in the osteocyte population (or at least in the $^{10kb}$Dmp1-expressing population) is sufficient to recapitulate the bone phenotype of body-wide mutation. These data implicate the osteocyte as the cell type of action for Wnt/Lrp5-mediated signaling in the modulation of bone mass.

**Osteocytes are the cell type of action for Wnt-mediated mechanotransduction**

Given the discovery that Lrp5 signaling in the osteocyte population accounts for the skeletal effects of this receptor, additional work was performed to determine whether Wnt/Lrp5-mediated mechanotransduction was localized to the osteocyte. As described

above, crossing Dmp1-Cre mice to $Lrp5^{f/f}$ mice deletes Lrp5 selectively in the osteocyte population. When subjected to ulnar loading, these mice have a severe deficit in load-induced bone gain [50], much like the global $Lrp5^{-/-}$ mice (Figure 8) [46]. Because the osteocyte is a key cell type for Wnt/Lrp5-mediated mechanotransduction, the obvious next step was to look for cellular mechanisms that might control Lrp5 signaling specifically in osteocytes, potentially explaining the normal mode of action for the Lrp5 receptor in a typical mechanical signaling event. This work was focused on Wnt/Lrp5 modulators that were enriched in osteocytes, and the most obvious molecule is sclerostin. In the skeleton, sclerostin expression is localized largely to the osteocyte population, to the exclusion of other skeletal cells [51]. Moreover, loss of sclerostin either by mutations in the SOST coding sequence [52], or by deletion of downstream SOST enhancer regions [53], results in very high bone mass. Those two attributes, in addition to the observation that sclerostin is a high-affinity Lrp5 antagonist [54], has fueled inquiries into whether sclerostin is a key mediator of Lrp5-mediated mechanotransduction. Sclerostin transcript and protein levels are dramatically reduced by mechanical loading, and the degree of down-regulation is closely associated with strain magnitude [55]. Thus, a load-induced reduction in local sclerostin levels appears to be a reasonable explanation as to how Lrp5 achieves activation during loading. In that context, mechanical stimulation induces a down-regulation of sclerostin protein, which releases Lrp5 from inhibition, and promotes Wnt local Wnt signaling through Lrp5. If this model is true, it would require that sclerostin must undergo downregulation in order for mechanotransduction to occur. Testing this hypothesis directly with a functional study is challenging but not impossible, in that it would require applying mechanical loading to a mouse model in which

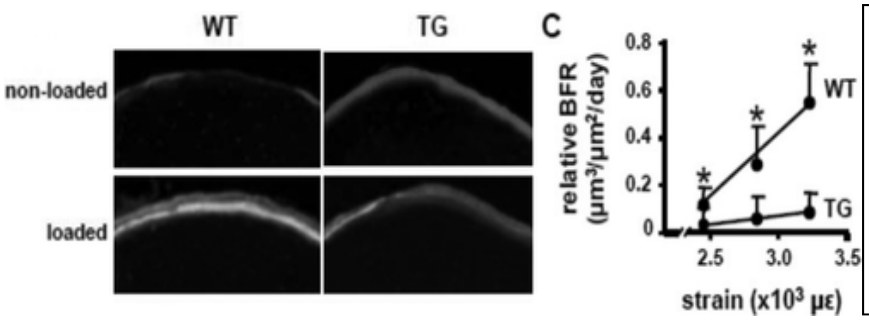


Figure 8. Sost prevents loading response in bone. Mice expressing the Dmp1-hSost transgene do not respond to mechanical load. Figure from [3].

sclerostin levels could be maintained at a high level, even in the presence of a mechanical stimulus (which normally causes Sost downregulation). Those experimental conditions were achieved by using the Dmp1-hSOST transgenic mouse model. This mouse harbors a transgene comprising a human SOST cDNA under the control of the mouse Dmp1 promoter [56]. The Dmp1 promoter is load-responsive in the positive direction, i.e., Dmp1 expression is increased in response to a mechanical stimulus [57]. In the Dmp1-hSOST transgenic mouse, mechanical loading induces the predicted downregulation of endogenous Sost expression (as would occur in a WT mouse), but at the same time induces an upregulation of transgenic hSOST expression, due to a load-induced increase in Dmp1 promoter activity. Therefore this mouse can maintain high levels of sclerostin protein even in the context of mechanical loading. When subjected to ulnar loading, the Dmp1-hSOST exhibits a nearly complete lack of mechanoresponsiveness (Figure 8), which phenocopies the Lrp5-null mechanoresponsiveness [56]. In summary, numerous functional studies suggest that osteocyte Wnt/Lrp5 signaling is crucial for skeletal mechanotransduction, and the process appears to be regulated by the secreted Lrp5 antagonist sclerostin.

**Wnt-mediated mechanotransduction during mechanodeprivation**

Although portions of the extracellular membrane components of Wnt signaling, such as Sost and Lrp5, have been explored in the mechanotransuctive response, the intracellular

downstream signaling molecules, such as β-catenin, have a more poorly defined role in bone. β-catenin is a downstream mediator of canonical Wnt, and activation of Lrp5 leads to stabilization of β-catenin and changes in gene expression. As mentioned above, Lrp5 and Sost are involved in the load-induced anabolic bone response. These genes are also involved in modulating reductions in bone mass that accompany disuse. For example, the expression of High Bone Mass (HBM)-causing missense mutations in Lrp5 or genetic deletion of Sost leads to an osteoprotective phenotype when mechanical stimulation is removed by disuse models (tail suspension or botox injection). However, it is unclear what downstream molecular mechanisms are altered in this response, or if increased levels of β-catenin would generate the same osteoprotective phenotype. Recent studies have evaluated the role of β-catenin in osteocytes but have not evaluated its role in disuse mechanotransduction. We and others have reported that deletion of β-catenin in osteocytes results in decreased response to enhanced loading [58, 59], and the Bonewald lab has reported that haploinsuffiency of β-catenin prevents bone loss during disuse [60], but the potential osteoprotective effects of β-catenin stabilization on disuse-induced bone wasting are not known.

More recently, sclerostin-mediated antagonism of Lrp5 appears to require a "facilitator" protein, without which the full inhibitory effects of sclerostin are not achieved. The facilitator protein has been identified as Lrp4 [1], another LDL-like family member that has important functions in neuromuscular junction architecture [61]. Lrp4 antagonizes Wnt activation by binding inhibitors such as Sost, Wise (Sostdc1), and potentially Dkk1. A new form of sclerosteosis (*SOST2*), a human high bone mass disease, has been identified in which mutations in Lrp4 lead to bone overgrowth in

patients [1]. This same group identified Lrp4 as a novel Sost binding partner by tandem affinity purification. To date, mouse models of Lrp4 have been limited because global deletion of Lrp4 is neonate-lethal due to lack of neuromuscular junction formation [62, 63]. However, when deletion was limited to osteoblasts and osteocytes using conditional knockout mice [62], or when Lrp4 antibody was administered to wild-type rats [63], bone mass was increased, similar to the phenotype observed in sclerosteosis patients. A mouse model mimicking the human R1170Q mutation was recently reported [64], and displayed increased bone mass, although the cellular mechanisms underlying the phenotype were not addressed (Figure 9). Despite these recent findings, the role of Lrp4 signaling in bone mechanotransduction has not been addressed, and this novel receptor remains poorly characterized, particularly with regard to its *in vivo* biology. Because Lrp4 acts as a putative sclerostin facilitator, it may play a critical role in mechanotransduction signaling in bone; if so, it might represent a possible therapeutic target for improving bone properties. While genetic deletion of Sost leads to an osteoprotective phenotype, in is unclear if loss of Lrp4 function in bone prevents the bone-wasting effects seen during disuse.

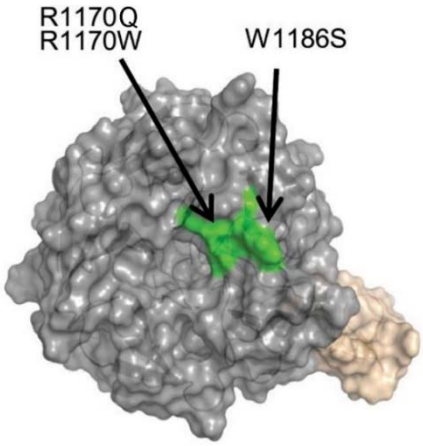


Figure 9. Mutations in the 3rd beta-propeller central domain increase bone mass in patients with sclerosteosis. Three mutations in the central domain of Lrp4 3rd beta-propeller results in high bone mass in patients. This is believed to be a binding pocket for Wnt inhibitor Sost. Figure adapted from [1].

In summary, portions of the Wnt signaling cascade have been implicated in the mechanotransductive response in bone. However, many questions remain about the

involvement of other components of Wnt signaling (Lrp4), and downstream Wnt modulators (β-catenin). Understanding the function of these various components will lead to the discovery of potential anabolic bone therapies that may work prevent bone-wasting in disease or disuse states, particularly in combination with non-pharmacologic therapies such as exercise. Here, I aim to further understand the role of Wnt pathway components in the mechanotransductive response in bone cells. First, I used a constitutively-active β-catenin mouse model to determine if artificial elevation of β-catenin in the osteocyte population protects bone tissue from disuse-induced bone wasting. Next, I evaluated the role of Lrp4 in bone homeostasis and mechanotransduction by generating a new mouse model that is orthologous to the HBM patients carrying the R1170W point mutation, and conducted experiments to determine the mechanism of action of Lrp4, as well as characterize Lrp4 as a possible therapeutic bone target.

Here, I hypothesize that two components of the Wnt signaling pathway, β-catenin and Lrp4, are critical for the osteocyte mechanotransduction response. Specifically, in the absence of normally functioning β-catenin or Lrp4, mechanodepravation-induced bone loss will be reduced.

Aim 1: Determine the susceptibility to disuse-induced bone loss following constitutive activation of β-catenin in osteocytes. Extracellular and membrane-bound components of canonical Wnt signaling appear to affect disuse- induced bone loss. I will generate mice with mutations in the intracellular Wnt mediator β-catenin, to understand whether this canonical node can be targeted to prevent bone wasting from disuse. I will generate mice with tamoxifen-inducible gain-of-function (floxed exon 3) mutations in β-catenin in late-stage osteoblasts/osteocytes using the 10KbDmp1-CreERt2 driver, and assess the degree

of bone loss resulting from tail suspension and Botox injection. I will monitor bone loss radiographically and histologically, and look for changes in transcriptome-wide RNA expression using RNAseq from bone-derived transcripts [65] that might highlight novel targets for preventing bone loss from disuse.

Aim 2: Determine the role of Lrp4 3rd beta-propeller central domain in sclerostin action in bone homeostasis and mechanodeprevation. Mutations in patients within the central domain of the Lrp4 3rd β-propeller result in high bone mass disease. I will generate a mouse model with the R1170W mutation in Lrp4 to mimic patients and recapitulate this phenotype in a model for experimental manipulation. I will then expose this model to altered levels of circulating sclerostin by genetic manipulation or pharmacological methods. Finally, I will determine the necessity of sclerostin binding to Lrp4 in disuse.

## ***Chapter 2: Materials and Methods***

### Generation of mouse models

*β-catenin Constitutively Active mouse models*

All mice used in the experiments harbored one floxed gain-of function β-catenin allele (exon 3 flox, hereafter referred to as constitutively active, or "*CA*") and one floxed loss-of-function β-catenin allele (exon 1-6 flox, hereafter referred to as loss-of-function, or "*LOF*"). Both gain-of function and loss-of-function β-catenin alleles have been described previously [66, 67]. Briefly, $\beta cat^{CA}$ mice contain LoxP sites flanking exon 3, which houses the code for the Gsk-3β phosphorylation site (required for degradation) of the β-catenin protein. $\beta cat^{LOF}$ mice harbor LoxP sites in introns 1 and 6 of the βcat (Ctnnb1) gene, which results in a null allele upon recombination of the LoxP sites. In the combined $\beta cat^{CA/LOF}$ mouse model that I bred, both alleles behave as wild-type prior to recombination. After Cre-mediated recombination, the mice are essentially heterozygous for the CA allele, as the LOF allele becomes null. I chose this approach to produce only the degradation-resistant protein in osteocytes, but to do so in a haplo-insufficient context to avoid very high levels of active β-catenin within the cell. $^{10kb}$Dmp1-CreERt2 transgenic mice have been described previously [68]. These mice harbor a cDNA for the Cre recombinase–mutant estrogen receptor fusion protein that results in Cre sequestration in the cytosol (away from the chromatin) until the selective ligand tamoxifen is encountered [69]. The CreERt2 gene was driven by a 10 kb fragment of the Dentin Matrix Protein-1 (Dmp1) promoter, which provides osteocyte and late osteoblast selectivity of expression [70]. $\beta cat^{+/LOF}$ mice were bred to 10 kbDmp1-CreERt2 x $\beta cat^{+/CA}$ mice to generate littermate $\beta cat^{CA/LOF}$ mice that were either transgenic

(hemizygous for CreERt2) or nontransgenic (CreERt2-negative). Male mice were selected for the muscle paralysis experiments, and female mice were selected for tail suspension experiments. Experimental mice were same-sex housed in cages of three to five (independent of Cre genotype) and given standard mouse chow and water ad libitum. All animal procedures were performed in accordance with relevant federal guidelines and conformed to the Guide for the Care and Use of Laboratory Animals (8th Edition). The Indiana University animal facility is an AAALAC-accredited facility.

*Cre induction*

To induce adult-onset recombination of the floxed βcat alleles, 12-week old mice were treated with 20 mg/kg tamoxifen free base (M&P Biomedicals, Santa Ana, CA). Tamoxifen powder was dissolved in dimethyl formamide (DMF) at a concentration of 100 mg/mL and then suspended in ~150 μL of corn oil for IP injection. Mice that received vehicle treatment (no Cre induction) were injected with an equivalent volume of DMF alone suspended in 150 μL of corn oil. Mice were treated with single injections of tamoxifen or vehicle 3 days prior to the first day of disuse. Details for the experimental schedule are shown in Figure 10.

*Lrp4 R1170W knock-in mice*

To generate a new knock-in model of a human patient with an Lrp4 mutation who presented with a sclerosteosis-like phenotype [1], the orthologous mutation was generated in mice using a Crispr/cas9 approach. Briefly, a 135bp donor oligo was knocked into the 3' half of Lrp4 exon 25 and adjacent intron. The donor oligo contained a c.3508C→T mutation (plus several local nonsense mutations to facilitate genotyping)

that results in an Arg1170Trp substitution (referred to as $Lrp4^{KI}$). The Lrp4-R1170W knock-in mice were on a fixed C57Bl/6J background.

*Dmp1-hSost mice*

The 8kbDmp1-hSOST transgenic mouse has been described previously [56]. Briefly, a 12-kb DNA fragment containing 8 kb of the 5′-flanking region, the first exon, the first intron, and 17 bp of exon 2 of the murine Dmp1 gene was used to drive expression of a human SOST cDNA. The Dmp1-hSOST mice were on a fixed C57Bl/6J background.

**Dual-energy x-ray absorptiometry (DEXA)**

For β-catenin constitutive activation studies, whole-body DEXA scans were collected on isofluorane-anesthatized mice using a PIXImus II (GE Lunar) densitometer. All mice were scanned 3 days prior to disuse, and again after 4 weeks of disuse, immediately before euthanasia. From the whole-body scans, areal bone mineral density (BMD) and bone mineral content (BMC) were calculated for the right and left hindlimbs using the Lunar ROI tools.

For Lrp4KI studies, whole-body DEXA scans were collected on isolfuorane-anesthetized mice using a Faxitron UltraFocusDXA x-ray densitometer (Faxitron Bioptics, Inc., Tucson, AZ). All mice were scanned between the ages of 4 to 18 weeks (longitudinal studies) or 3 days prior to the start of the experimental period and again immediately before euthanasia (disuse and antibody studies). From the whole-body scans, areal bone mineral density (BMD) and bone mineral content (BMC) were calculated for the whole body (head and tail excluded) or limbs, depending on the study, using the Faxitron ROI tools.

**Micro-computed tomography (μCT)**

After sacrifice, the proximal half of formalin-fixed tibiae were scanned, reconstructed, and analyzed on a Scanco μCT-35 desktop microcomputed tomographer (Scanco Medical AG, Brüttisellen Switzerland) as previously described [71]. Briefly, samples were scanned at 10-μm resolution (femur, tibia and vertebra) or 20-μm resolution (skull), 50-kV peak tube potential and 151-ms integration time. Standard output parameters related to cancellous and cortical bone mass, geometry, and architecture were measured [72].

**Hindlimb suspension**

For β-catenin constitutive activation studies, eighty 12-week-old female mice were used for the hindlimb suspension experiments, comprising 40 mice of each genotype (i.e., 40 Cre+; $\beta cat^{CA/LOF}$ and 40 Cre-; $\beta cat^{CA/LOF}$). Each genotype was further divided into control and hindlimb-suspended mice with half of each of those subgroups receiving tamoxifen and half receiving vehicle (n = 10/group). All mice were individually housed following Cre induction/vehicle injection and a tail harness was used to suspend the experimental mice as previously described [71]. Control mice were permitted unencumbered normal movement in their cages. Mice received intraperitoneal injections of alizarin (20 mg/mL) 6 days prior to sacrifice and calcein (10 mg/kg) 3 days prior to sacrifice. Mice were suspended for a total of 4 weeks, and euthanasia was performed at the end of the $4^{th}$ week of suspension.

**Botulinum toxin (Botox)-induced muscular paralysis**

For β-catenin constitutive activation studies, eighty 12-week-old male mice were used for the Botox experiments, comprising 40 mice of each genotype (i.e., 40 Cre+; $\beta cat^{CA/LOF}$

and 40 Cre-; $\beta cat^{CA/LOF}$). Each genotype was further divided into control (saline-injected) and Botox-treated mice, with half of each of those subgroups receiving tamoxifen and half receiving vehicle (n = 10/group). For Lrp4KI studies, forty 12-week old male mice were used for the Botox experiment, comprised of 20 mice of each genotype. Each genotype ($Lrp4^{+/+}$ or $Lrp4^{KI/KI}$) was further divided into control or Botox-treated mice. The right hindlimb musculature (quadriceps, triceps surae, tibialis anterior, hamstrings) was injected with 20 μL of Botulinum Toxin A (Botox; Allergan Inc., Irvine, CA), while the left hindlimb musculature was left alone and served as an internal control. Control mice received 20 μL injections of saline in the right hindlimb in an identical fashion as the Botox-treated mice. The injections (both Botox and saline) were repeated one week later to ensure paralysis in the Botox-treated group [71]. Botox efficacy was qualitatively evaluated for each mouse every 3-4 days, based on the inability of the treated mice to use the limb in normal cage locomotion.

**Protein extraction and Western Blotting**

*Protein extraction from mouse bones*

Immediately after sacrifice, mouse femur, tibia and fibula were dissected, stripped of soft tissue, flushed to remove bone marrow. The remaining cortical bone tissue was immediately snap frozen in liquid nitrogen and pulverized to a fine powder in a mortar and pestle. 800 uL of 4X SDS-PAGE sample buffer was added directly to the mortar containing the bone powder, which immediately froze. The extract was thawed, collected, heated at 95ºC for 5 min, centrifuged at 14,000 x g for 10 min, and the supernatant was retained to run directly on gels.

*Gel electrophoresis and transfer to nitrocellulose*

Approximately 20 μg of protein from each sample was run on a 4-12% polyacrylamide gradient gel (GenScript) along with pre-stained molecular weight markers (Bio-Rad). Separated proteins were transferred to nitrocellulose overnight, after which the membranes were stained with PonceauS to visualize total protein and qualitatively evaluate protein loading consistency. Membranes were blocked for 2 hrs in 5% powdered milk in TBST (wash buffer) then incubated with primary antibodies (diluted in 5% milk/TBST) at 4ºC overnight, washed 6X in TBST, then incubated with species-appropriate HRP-conjugated 2º antibody for 1 hr at R/T. After a final 6X wash in TBST, the nitrocellulose was rinsed in deionized water and bound HRP was reacted with ECL reagent for 5 min (Amersham, ECL Prime Reagent). Blots were imaged using an iBrightCL1000 (Invitrogen).

*Antibodies*

Mouse anti-β-catenin (Novus Biologicals) diluted 1:2000; mouse anti-Lrp4 (ab201923, Abcam) diluted 1:5000; goat polyclonal anti-sclerostin (AF1589, Sigma) diluted 1:2000; mouse monoclonal anti-vinculin (vin11-5, Sigma) diluted 1:5000; HRP donkey anti-goat IgG antibody (Jackson) 1:10,000 or goat anti-mouse IgG antibody (Jackson) 1:10,000.

**Quantitative cortical bone histomorphometry**

Mice received injections of demeclocycline (90 mg/kg), alizarin complexone (20 mg/mL) and calcein (10 mg/kg) at timepoints outlined in individual experiments. Mice were sacrificed 4 weeks after the initiation of disuse. After μCT scanning, the fixed tibiae and femurs were dehydrated in graded ethanols, cleared in xylene, and embedded in methylmethacrylate. Thick sections were collected at the tibial and femoral midshafts

using a diamond-embedded wafering saw. Sections were ground and polished to ~30 μm, mounted and coverslipped, then digitally imaged on a fluorescent microscope. Periosteal and endocortical bone formation parameters were calculated at the midshaft by measuring the extent of unlabeled perimeter (nL.Pm), single-labeled perimeter (sL.Pm), double-labeled perimeter (dL.Pm), and the area between the double labeling (dL.Ar) with Image-Pro Plus software (MediaCybernetics Inc., Gaithersburg, MD). The derived histomorphometric parameters mineralizing surface (MS/BS), mineral apposition rate (MAR), and bone formation rate (BFR/BS) were calculated using standard procedures described elsewhere [73]. Relative bone formation parameters were calculated by subtracting the disuse (right) limb value from the control (left) limb value for each mouse.

**dd-PCR assay for genomic recombination of the conditional β-catenin alleles**

Droplet digital PCR (ddPCR) was performed as previously described [74]. Briefly, epiphyseal ends of bone were removed from cleaned long bones, decalcified in EDTA for 48 hours with gentle rocking and the bone marrow removed by extensive mechanical abrasion/washing with a swab and PBS. DNA was extracted from bone pieces using the DNeasy Blood and Tissue Kit (Qiagen) and 30 ng of cortical bone DNA was used in subsequent PCR reactions. Supermix for Probes mastermix (BioRad, Hercules, CA) was used following the manufacturer's recommendations. PCR was performed using Eppendorf EP gradient S machines, nanodroplets were created using an automatic droplet generator, amplimer containing droplets were counted with a QX200 sample reader, and data were analyzed using Quantasoft software (all instrumentation from BioRad). All reactions were run in duplicate. The primer pairs and probes described below were

purchased from IDT (Coralville, IA) and were used to amplify and quantify the number conditional and recombined alleles. At least 1300 amplimer-containing droplets per sample were created in order to measure Cre-mediated recombination. PCR primers. For the LOF allele, three PCR primers (loxP-f: tgaaggcatgcctgcagataacttc, cond-r: ctaggctatgtgccccgaca, rec-r: cccttcaatgcttagcaccgt) were used to generate 2 unique amplicons – 223bp for the conditional allele and 163bp for the recombined mutant allele. Fluorescent probes were designed to complement each amplicon (conditional: 5HEX/agagcttcctgacaccgtggct /3IABkFQ, recombined: 56-FAM/ cgcgcacacacacacaggctc /3IABkFQ). PCR was performed (95°C/10min; 94°C/30sec; 60°C/60sec; 72°C/30sec; 40 cycles; 98°C/10min; 12°C hold) with cycling ramp time slowed to 1.2sec/°C. For the CA allele, thee PCR primers (f: TATCACGAGGCCCTTTCGTC, cond-r: cctgaagaagccatctacgaca, rec-r: tcattgcatactgcccgtca) were used to generate 2 unique amplicons – 327bp for the conditional allele and 273bp for the recombined mutant allele. Fluorescent probes were designed to complement each amplicon (conditional: 5HEX/ accctcacctgctctccttggct /3IABkFQ, recombined: 56-FAM/ catgtgggactccgctaccct /3IABkFQ) (PCR was performed (95°C/10min; 94°C/30sec; 60°C/60sec; 72°C/30sec; 40 cycles; 98°C/10min; 12°C hold) with cycling ramp time slowed to 1.2sec/°C. For both alleles, template-less water controls were run in every assay to ensure consistency and identify any background signal.

**RNA sequencing of osteocyte-enriched cortical bone lysates in tail suspended mice**

Female Cre+ and Cre- $\beta cat^{CA/LOF}$ (n=4-6/group) mice were used for transcriptional analysis. At 12 weeks of age, Cre-mediated recombination of the βcat alleles was induced with tamoxifen as described above. Three days after Cre induction, mice were

tail suspended (n=4-6) for 3 days or left alone as ground controls. On the 4th day, mice were euthanized and the tibia and femur cortical tubes (without marrow, periosteum, or epiphyses) were prepared for RNA extraction as previously described [75]. Total RNA was purified using a Trizol/Qiagen RNeasy Kit prep. RNA quality was assessed using a bioanalyzer (Agilent Technologies, Santa Clara, CA, USA). cDNA libraries were generated from Poly(A)+-enriched RNA using the Illumina TruSeq RNA Library Prep kit v2 (Illumina Inc., Hayward, CA, USA) and the libraries were sequenced using Illumina NextSeq 550 sequencer (Illumina Inc., Hayward, CA, USA). RNAseq data (n=3/group) quality was checked using FastQC (version 0.11.5) software [http://www.bioinformatics.bbsrc.ac.uk/projects/fastqc]. Sequence reads were mapped to the mouse reference genome (mm10) using STAR (version 2.6) [76]. After read mapping, "featureCounts" from Rsubread package (version 1.30.5)[77] was used to perform summarization of reads mapped to RefSeq genes, and gene-wise read counts were generated. Genes were filtered from downstream analysis if they did not have CPM (counts per million) value of at least 1 in at least three libraries. The data was normalized using TMM normalization method [78]. Differentially expressed genes were identified using edgeR (version 3.22.3) [79]. A gene was considered significantly differentially expressed when its false discovery rate (FDR) corrected p-value was less than 0.05 and fold change was greater than 2. Heatmaps were generated using heatmap.2 function in R package 'gplots'.

**Sclerostin inhibition *in vivo***

Eight-week-old female mice ($Lrp4^{+/+}$ or $Lrp4^{KI/KI}$) were randomized to receive twice-weekly subcutaneous injections of either sclerostin neutralizing antibody (Scl-mAb) at 25

mg/kg (37) or vehicle control for the next 4 weeks (n = 8 mice per genotype and treatment group). Scl-mAb doses were adjusted weekly on the basis of body mass measurement. Animals were euthanized by $CO_2$ inhalation when 12 weeks old.

**Biomechanical measurements of whole-bone strength**

The left femur was collected from each euthanized mouse, wrapped in saline-soaked gauze, and frozen at −20°C until the day of testing. Once femurs had been collected from all mice, they were equilibrated at room temperature in a saline bath for 3 hours before mechanical testing. Measures of whole-bone strength were obtained on femurs positioned posterior side down across two lower supports (spaced 9 mm apart) of a three-point bending apparatus. The fixtures were mounted in the frame of a TestResources R System test instrument, which has a force resolution of 0.01 N [48]. Each femur was loaded to failure in monotonic compression using a crosshead speed of 0.2 mm/s, during which force and displacement measurements were collected every 0.01 s. From the force versus displacement curves, ultimate force, yield force, stiffness, and energy to failure were calculated using standard equations [80].

**Muscle function testing**

*In vivo* muscle function in Lrp4 mutant mice was evaluated using the 1305A Whole Mouse/Rat Test System (Aurora Scientific Inc., Aurora, ON, Canada) [81] as described previously. Briefly, electrodes were inserted subcutaneously near the tibial nerve in anesthetized mice, which were positioned in the instrument to allow ankle dorsiflexion. Electrode placement and stimulation current were adjusted to achieve the maximum twitch response and then increased to ~35 mA for plantarflexion to ensure supramaximal stimulation of the muscle fibers. The maximum isometric torque (N/m) was recorded for

stimulation frequencies between 25 and 300 Hz, with a pulse width of 0.2 ms and strain duration of 200 ms. Data were recorded using the Dynamic Muscle Control/Data Acquisition and Dynamic Muscle Control Data Analysis programs (Aurora Scientific Inc.).

**Statistical analysis**

Statistical analyses were conducted with SigmaPlot. Statistical details of each experiment can be found in the figure legends. Statistical significance was taken at $p<0.05$. Two-tailed distributions were used for all analyses. Data are presented as means ± SEM.

## *Chapter 3: Constitutive activation of β-catenin in osteocytes protects bones from disuse-associated bone wasting.*

### Recombination of β-catenin in bone following tamoxifen injection

I first sought to validate the experimental mouse model by assessing whether the tamoxifen-inducible Cre strategy I employed was efficient at recombining the floxed constitutively active (CA) β-catenin allele. Specifically, I tested at the protein level whether tamoxifen treatment induced the CA allele, and conversely, whether unprovoked recombination of the CA allele occurred in the absence of tamoxifen. To this end, β-cat$^{CA/LOF}$ mice that were positive or negative for CreERt2 were raised to 10 weeks of age, treated with a single dose of tamoxifen, and sacrificed 3 days later. Protein was extracted from long bone cortices, subjected to SDS-PAGE, transferred to nitrocellulose, and blotted for β-catenin (Figure 10). Only mice that were both Cre-positive and exposed to tamoxifen produced a significant lower molecular weight band, which is consistent with an internally truncated β-catenin protein that is 8.5kD lighter when lacking the amino acid sequence of exon 3. Samples were collected just 3 days after a single dose of

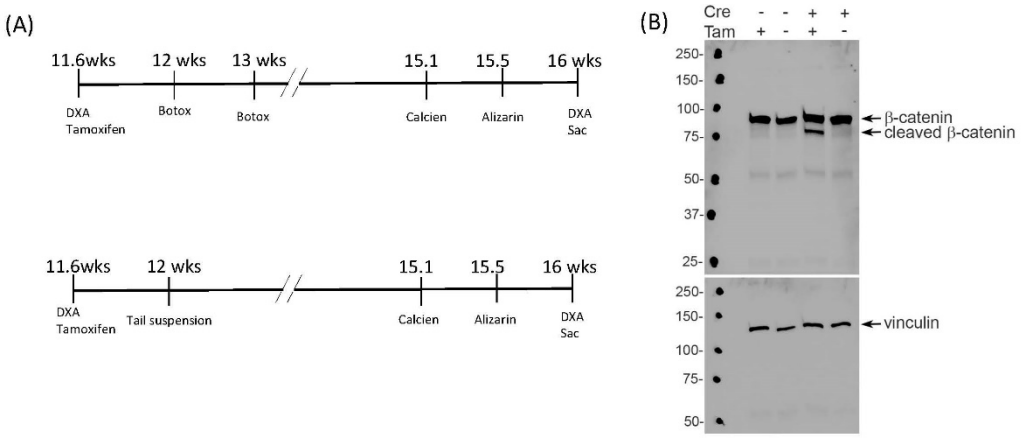


Figure 10. Constitutive activation of β-catenin in bone. A) Timeline of tail suspension and Botox experiments. B) Western blot of osteocyte-enriched bone from Dmp1-CreERt2-positive (Cre: +) or Dmp1-CreERt2-negative (Cre: -) mice treated with tamoxifen (Tam: +) or corn oil (Tam: -) for 3 days.

tamoxifen, and the larger molecular weight band in these samples may be attributable to either residual B-catenin, incomplete recombination or a combination of both factors.

To assess whether the rates of recombination for the constitutively active (CA) and loss-of-function (LOF) alleles were similar, cortical bone genomic DNA was extracted from transgenic (TG) and non-transgenic (NTG) $\beta cat^{CA/LOF}$ mice treated with tamoxifen. ddPCR was performed to generate 1,500 amplimer-containing droplets/sample in 3 animals with each genotype. Primer and probe sets were designed to distinguish recombined and non-recombined CA and LOF alleles. Each ddPCR assay was performed in duplicate. LOF allele recombination rate was 15±3.6% for the βcat LOF allele and 11±2.9% for the βcat CA allele in TG tamoxifen treated mice. The different rates of recombination did not differ significantly between the LOF and the CA allele ($p=0.13$) and there was no recombination for either allele in the non-transgenic mice. Thus activation of the CA allele occurred at comparable rates as inactivation of the LOF allele in the experimental assays. However, ddPCR cannot measure the frequency with which recombination of each allele occurred in the same cell, nor can it distinguish recombination occurred in gDNA recovered from osteocytes or from other cell types (e.g., endothelial cells) in the cortical bone extracts. This latter point is important given the recent report of numerous vascular channels in the mouse femoral cortex [82], which might easily escape removal during centrifugation and periosteal stripping.

**Tail Suspension Induced Bone Wasting**

To evaluate the bone-wasting effects of a fluid-shift disuse model in mice that have impaired ability to degrade β-catenin in osteocytes, I measured the effects of tail suspension on hindlimb bone mass and density in β-catenin stabilized and control mice.

During the experimental period, recombination of the β-cat$^{CA/LOF}$ alleles in ground control mice resulted in an 8.7% increase in tibial BMD whereas uninduced (corn-oil treated) ground control mice exhibited a 3% increase in tibial BMD mice (Figure 11A). Tail suspension was associated with an 8% loss in tibial BMD among uninduced mice, whereas activation of the β-cat CA allele in tail suspended mice resulted in no change (2.5% increase, *NS*) in tibial BMD, though the activated tail-suspended mice failed to gain as much BMD as their activated ground control littermates. To account for the potential confounding effects of tamoxifen on the osteoprotective effects of β-catenin stabilization during disuse, I conducted additional but identical tail suspension experiments using Cre-negative mice. The control experiments revealed that tamoxifen alone resulted in an 8.3% increase in tibial BMD (Figure 11C), whereas the corn oil-treated ground control mice exhibited a 4% increase in tibial BMD. While this tamoxifen-induced change in ground control mice is similar to that observed among Cre-positive mice (a 5.7% increase over oil-treated among the Cre-positive group vs. 4.3% increase over oil-treated mice among the Cre-negative group), the osteoprotective effects of tamoxifen treatment were completely absent when Cre was not present (and by inference, absent β-catenin activation) as revealed by an 8.5% decrease in tibial BMD among tamoxifen-treated tail-suspended mice not expressing Cre-recombinase in osteocytes (versus a 2.5% increase in induced mice following tail suspension). Tibial bone mineral content (BMC) followed a similar pattern of bone wasting during disuse, and rescue in induced mice (Figure 11B); tail suspension was significantly lower in induced mice, although not to the extent of non-activated mice and is likely due to the effect of tamoxifen and/or B-catenin activation in activated ground control mice. One exception to

the pattern was a stronger effect of β-catenin activation in ground control mice, independent of tamoxifen. In summary, induction of constitutively active β-catenin alleles in Dmp1-expressing cells results in protection from tail-suspension induced bone loss of whole bone BMD and BMC, which is not attributable to direct skeletal effects of tamoxifen treatment.

Following 4 weeks of tail suspension, tibiae were evaluated for compartment-specific changes in bone mass, architecture, and dynamic formation indices. As expected, in non-activated mice, proximal tibia cancellous bone volume fraction (BV/TV) was reduced significantly by tail suspension (24.2% reduction, $p<0.05$; Figure 12A). Activation of β-catenin in ground control mice induced a slight but non-significant increase in BV/TV (12.7% increase, *NS*), which was not significantly affected by tail suspension (5.8% increase, *NS*). In contrast, the parallel experiment conducted in Cre-negative mice revealed a significant loss of BV/TV in tamoxifen treated mice (Figure 12E), which suggests that the bone-sparing effects of β-catenin activation seen in the tail-suspended Cre-positive mice was not a result of tamoxifen. Other μCT parameters (Tb.N, Tb.BMC) showed similar effects as noted for BV/TV, with the exception of trabecular thickness (Tb.Th), which was not rescued in induced tail-suspended mice. In summary, induction of constitutively active β-catenin alleles in Dmp1-expressing cells results in protection from tail-suspension induced deterioration of trabecular bone structural parameters, most of which is not attributable to direct skeletal effects of tamoxifen treatment.

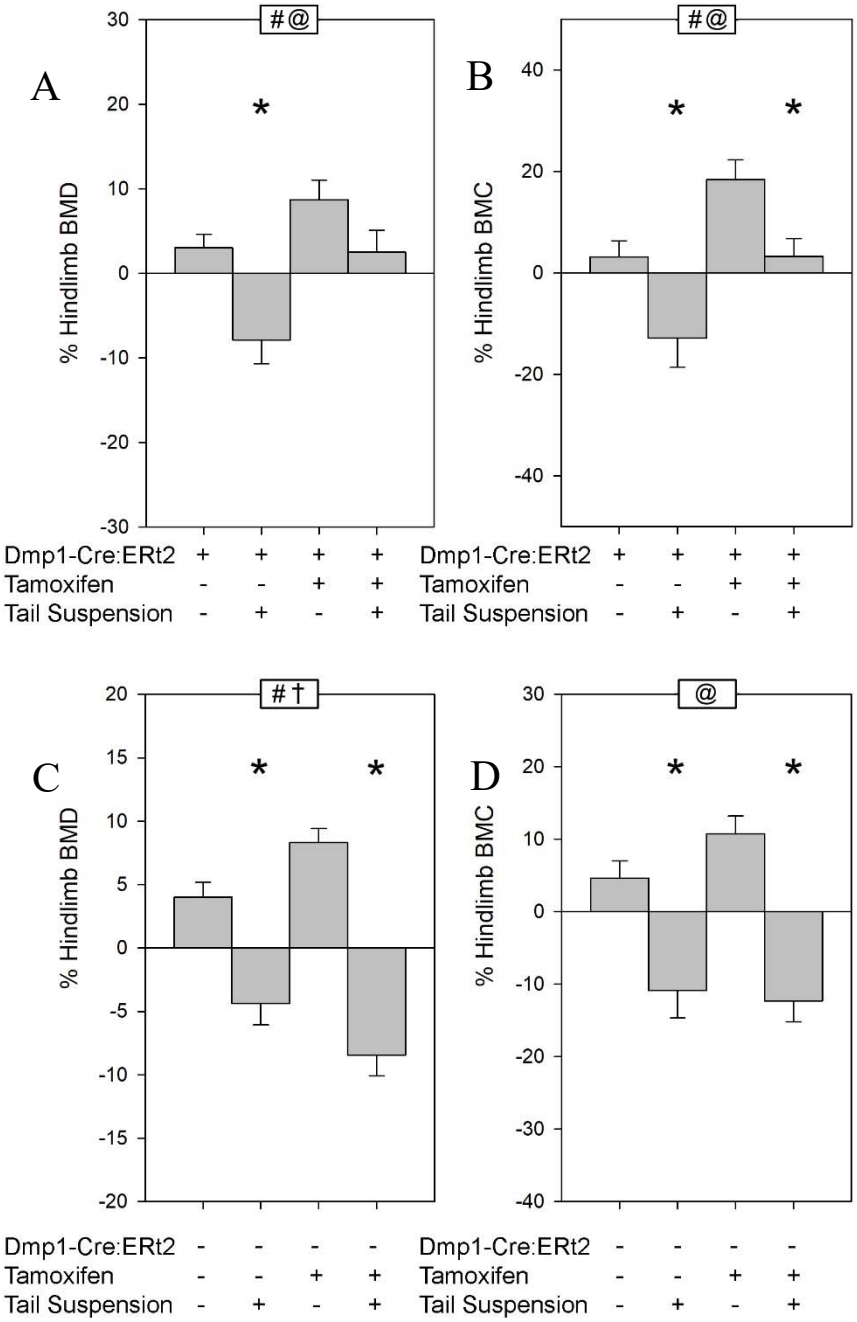


Figure 11. Mice with constitutive activation of β-catenin are protected from mechanodeprivation-induced bone loss during 4 weeks of tail suspension. Percent change in tibial bone mineral (A,C) density and (B,D) content, calculated from DXA scans collected just prior to the start of the experiment and again at sacrifice following 4 weeks of tail suspension for Cre-positive and Cre-negative mice. N=10/group Data were tested using 2-way ANOVA with Tamoxifen/oil and the tail suspension as main effects. Inset at the top of each graph indicates significance of the main effects and interaction (#=Tamoxifen/Oil $p<0.05$; @=Tail suspension $p<0.05$; †=interaction $p<0.05$). When at least one term was significant, Fisher's PLSD post-hoc tests were conducted between ground control and tail suspended mice and are indicated as *$p<0.05$.

Dynamic cortical bone formation parameters were measured over the experimental period using fluorochrome labels administered throughout the treatment period. Bone formation parameters on both endocortical and periosteal surfaces were minimal in uninduced mice subjected to tail suspension (Figure 13A and B). Activation of β-catenin had an effect on bone formation at the periosteal (2-fold increase, $p<0.05$) but not endocortical surface in ground control mice, which could be fully explained by tamoxifen effects (Figure 13D). However, as reported for the DXA measurements, tamoxifen treatment alone had no protective effects on tail-suspension-induced suppression of bone formation parameters. In summary, induction of constitutively active β-catenin alleles in Dmp1-expressing cells results in protection from tail-suspension induced reduction in endocortical and periosteal bone formation rates, which is not attributable to direct skeletal effects of tamoxifen treatment.

**Botulinum Toxin (Botox)-Induced Bone Wasting**

After learning that activating β-catenin alleles in Dmp1-expressing cells conferred protection from the bone-wasting effects of tail suspension, I employed a second model of bone wasting to evaluate whether degradation-resistant β-catenin had broader efficacy for disuse in general. I measured the bone-wasting effects of muscle paralysis-induced disuse, using intramuscular injection of botulinum toxin (Botox) in Dmp1-CreERt2 × $\beta cat^{CA/LOF}$ mice and used the contralateral uninjected limb as a control. During the experimental period, recombination of the β-$cat^{CA/LOF}$ alleles in saline-injected control mice resulted in a 9.1% increase in tibial BMD in the treated limb, whereas uninduced saline injected control mice exhibited a 1.8% (*NS*) increase in tibial BMD (Figure 14A). Botox injection was associated with a 10.8% loss in tibial BMD among uninduced (corn

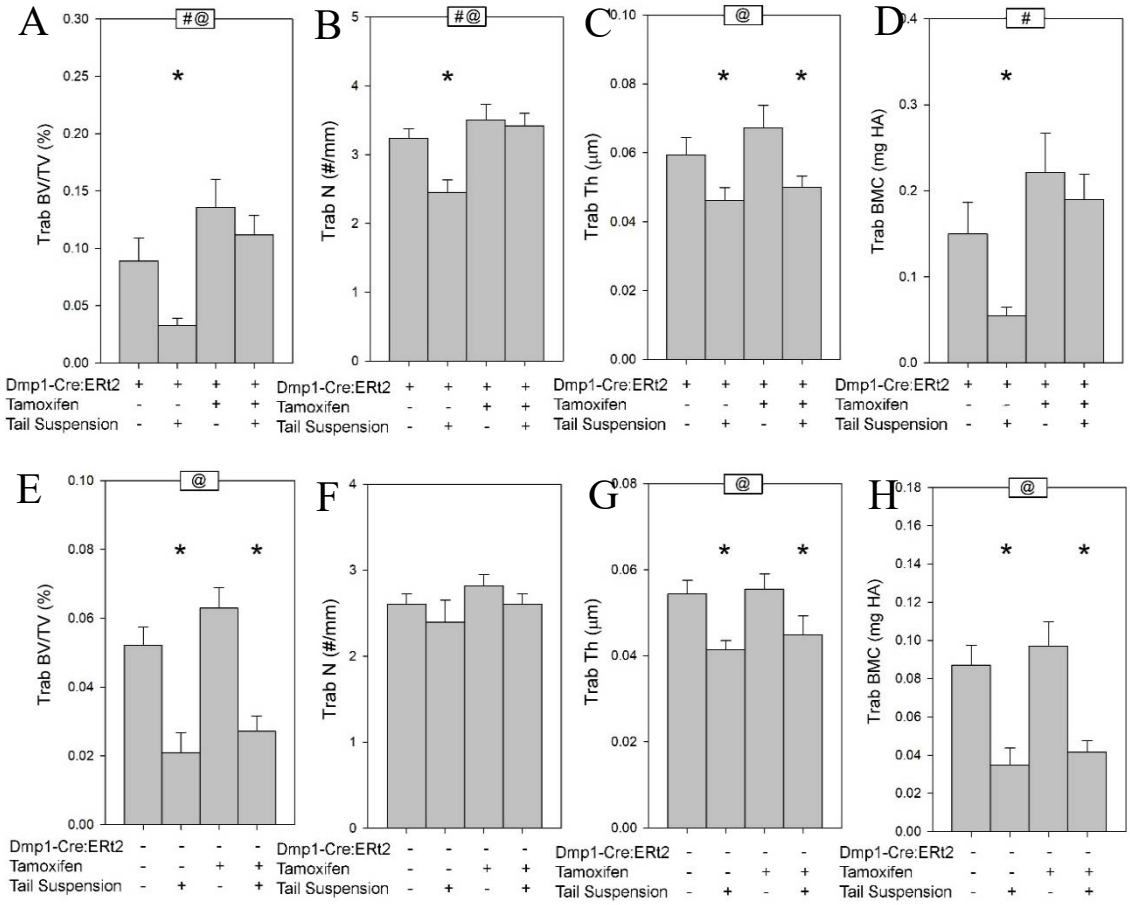


Figure 12. μCT measurements of cancellous bone properties in the tibiae of ground control and tail suspended Cre-positive and Cre-negative βcat CA mice. (A,E) Bone volume fraction, (B,F) trabecular number, (C,G) trabecular thickness, and (D,H) trabecular bone mineral content were measured in the proximal tibia. N=8-10/group Data were tested using 2-way ANOVA with Tamoxifen/oil and the tail suspension as main effects. Inset at the top of each graph indicates significance of the main effects and interaction (#=Tamoxifen/Oil $p<0.05$; @=Tail suspension $p<0.05$; †=interaction $p<0.05$). When at least one term was significant, Fisher's PLSD post-hoc tests were conducted between ground control and tail suspended mice and are indicated as *$p<0.05$.

oil treated) mice, whereas activation of the β-cat CA allele in mice treated with Botox resulted in a slight loss (-5.6%, *NS*) in tibial BMD. To account for the potential confounding effects of tamoxifen, I conducted identical Botox experiments in Cre-negative mice. Tamoxifen alone resulted in a 3.9% increase (*NS*) in tibial BMD (Figure 14C), whereas the corn-oil treated saline control mice exhibited a 0.4% reduction (*NS*) in tibial BMD. The tamoxifen-induced change in Cre-negative ground control mice is about

half of the effect seen Cre-positive ground control mice, suggesting that induction of the β-cat CA allele has positive effects on BMD in ground control mice. However, as reported for the tail suspension studies, the osteoprotective effects of tamoxifen treatment alone on Botox-induced bone loss were completely absent (14% decrease in tibial BMD in tamoxifen-treated vs. 15.7% decrease in corn oil treated), again, suggesting that the

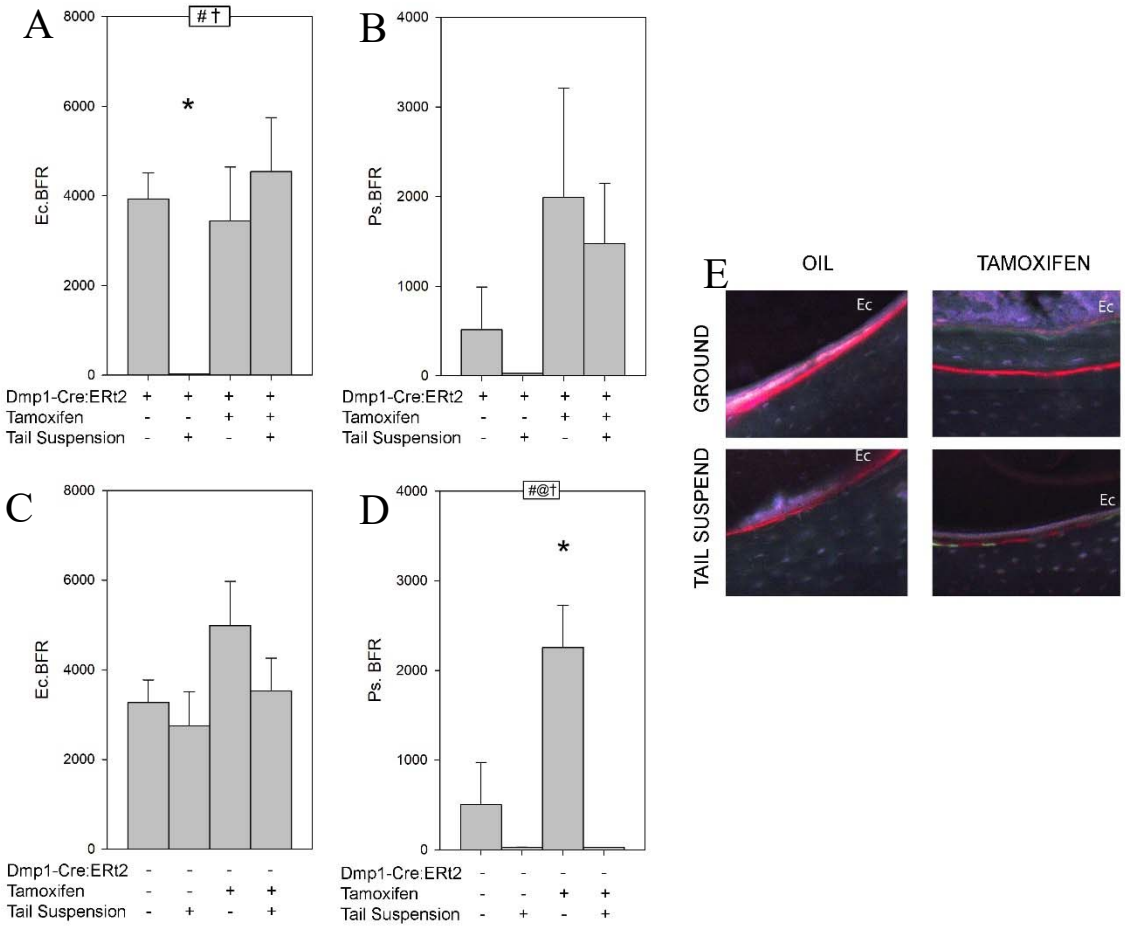


Figure 13. Dynamic histomorphometry of Cre-positive and Cre-negative βcat CA mice following tail suspension. Fluorochrome labels were administered 3 days apart and measured for single label length, double label length and double label area on endosteal and periosteal bone surfaces. Endosteal bone formation rate (A,C), as well as periosteal bone formation rate (B,D) were calculated. (E) Representative images of the endocortical surface of Cre-positive mice. Mice were given fluorochrome labels (red and green) 5 and 3 days prior to the end of the disuse period. N=3/6/group. Data were tested using 2-way ANOVA with Tamoxifen/oil and the tail suspension as main effects. Inset at the top of each graph indicates significance of the main effects and interaction (#=Tamoxifen/Oil $p<0.05$; @=Tail suspension $p<0.05$; †=interaction $p<0.05$). When at least one term was significant, Fisher's PLSD post-hoc tests were conducted between ground control and tail suspended mice and are indicated as *$p<0.05$.

protection from botox-induced bone loss was attributable to activation of β-cat CA. Tibial bone mineral content (BMC) followed a similar pattern of bone wasting during disuse, and rescue in induced mice (Figure 14B). In summary, induction of constitutively active β-catenin alleles in Dmp1-expressing cells results in protection from paralysis-induced loss of whole bone BMD and BMC, which is not attributable to direct skeletal effects of tamoxifen treatment.

Following 4 weeks of muscle paralysis induced by treatment with Botox, tibia were evaluated for compartment-specific changes in bone mass and architecture indices. As expected, in uninduced mice, proximal tibia cancellous bone volume fraction (BV/TV) was reduced significantly by Botox injection (43% reduction, $p<0.01$; Figure 15A), relative to the contralateral control limb. Activation of β-catenin in saline-injected control mice induced a slight but nonsignificant decrease in BV/TV (8% decrease, P=0.813), which was not significantly affected by Botox treatment (12.8% decrease, P=.480). In contrast, the parallel experiment conducted in Cre-negative mice revealed a significant loss of BV/TV in tamoxifen treated mice that also received Botox injection (Figure 15E), which suggests that the bone-sparing effects of β-catenin activation seen in the Botox-injected Cre-positive mice was not a result of tamoxifen effects. Tb.BMC showed similar effects as noted for BV/TV, with the exception of trabecular thickness (Tb.Th), which was not rescued in induced Botox mice, and Tb.N, which was not different among groups. In summary, induction of constitutively active β-catenin in Dmp1-expressing cells results in protection from muscle-paralysis induced deterioration of trabecular bone structural parameters, most of which is not attributable to direct skeletal effects of tamoxifen treatment.

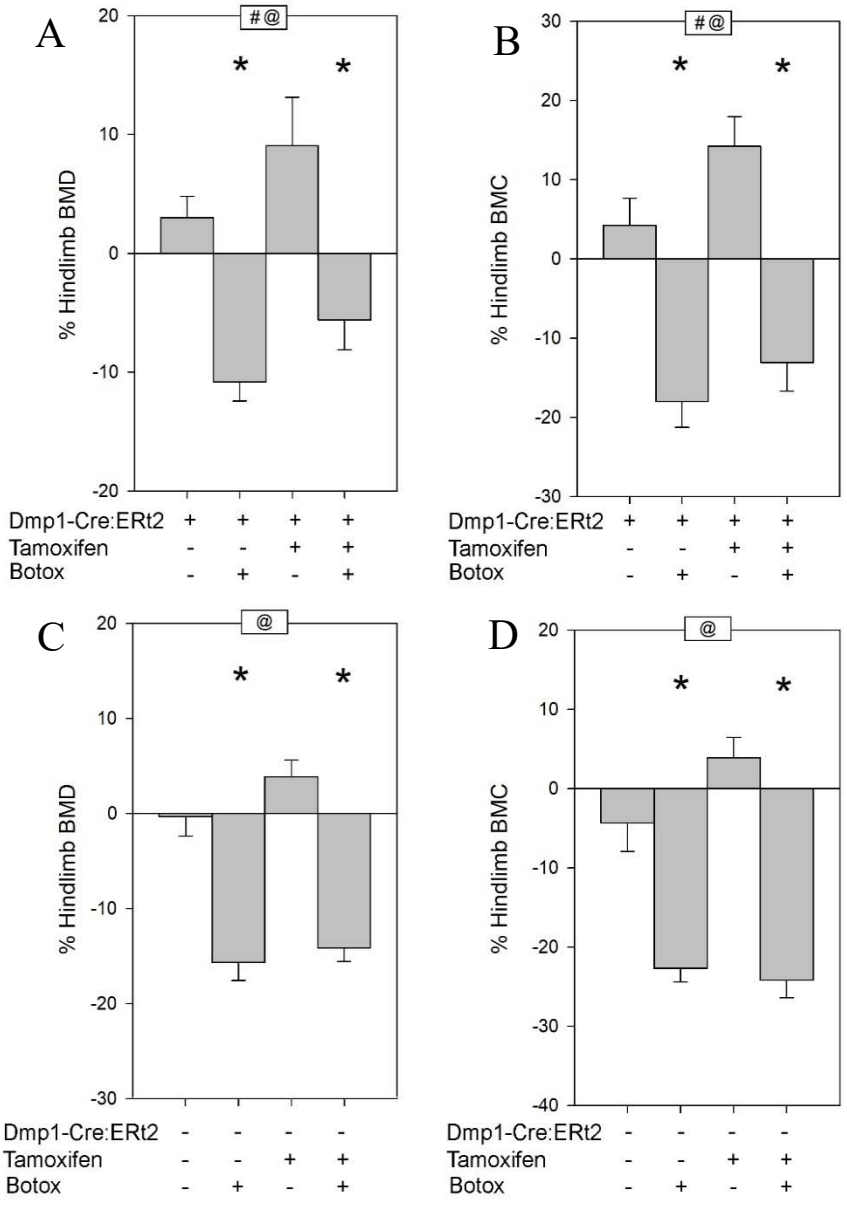


Figure 14. Mice with constitutive activation of β-catenin are not protected from mechanodeprivation-induced bone loss during 4 weeks of muscle paralysis disuse. Percent change in right tibial (A,C) bone mineral density and (B,D) content calculated from DEXA scans collected just prior to the start of the experiment and again at sacrifice following 4 weeks Botox in βcat CA Cre-positive and Cre-negative mice. N=10/group Data were tested using 2-way ANOVA with Tamoxifen/oil and the Botox injection as main effects. Inset at the top of each graph indicates significance of the main effects and interaction (#=Tamoxifen/Oil $p<0.05$; @=Botox $p<0.05$; †=interaction $p<0.05$). When at least one term was significant, Fisher's PLSD post-hoc tests were conducted between saline and botox injected mice and are indicated as *$p<0.05$.

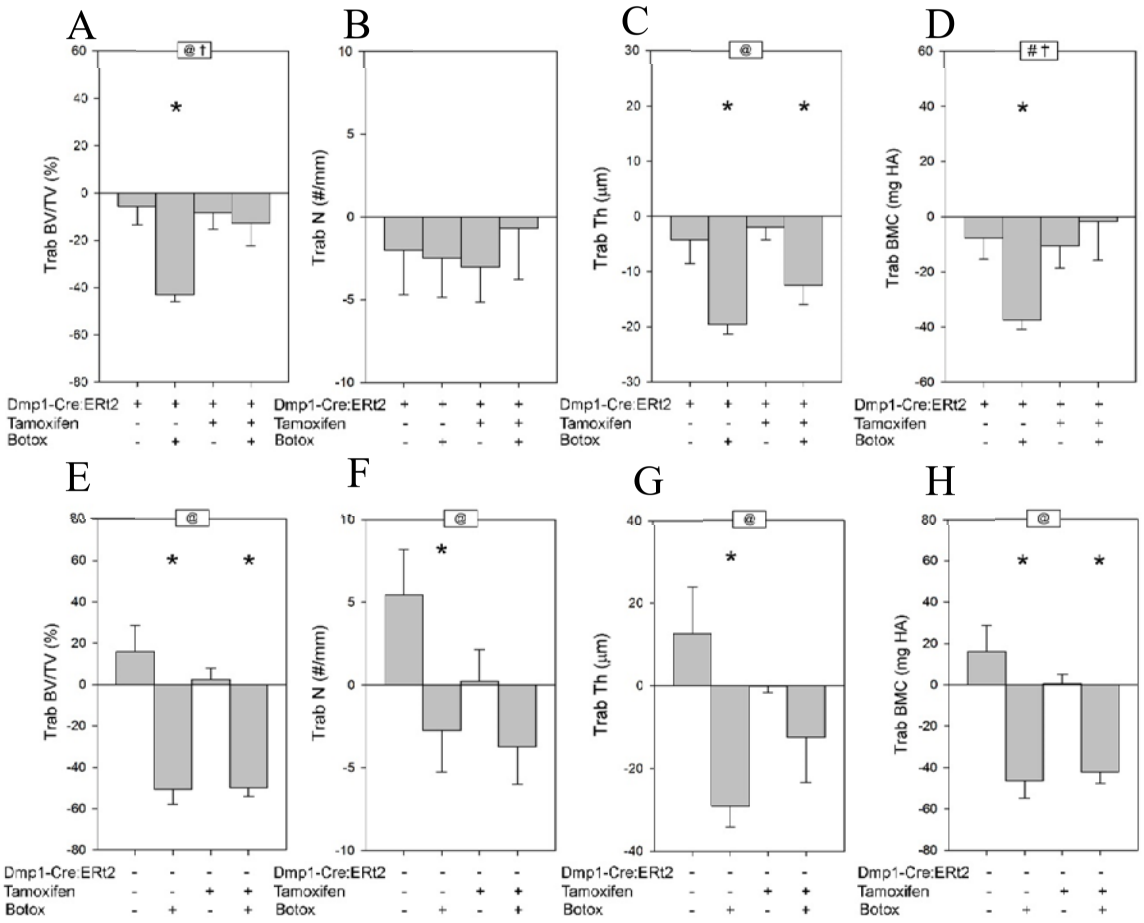


Figure 15. μCT measurements of cancellous bone properties in the tibiae of saline-injected control and Botox in βcat CA Cre-positive and Cre-negative mice. (A,E) Bone volume fraction, (B,F) trabecular number, (C,G) trabecular thickness, and (D,H) trabecular bone mineral content were measured in the proximal tibia. Right limb values were compared pair-wise to the contralateral (left leg) non-injected control. N=10/group Data were tested using 2-way ANOVA with Tamoxifen/oil and the Botox injection as main effects. Inset at the top of each graph indicates significance of the main effects and interaction (#=Tamoxifen/Oil $p<0.05$; @=Botox $p<0.05$; †=interaction $p<0.05$). When at least one term was significant, Fisher's PLSD post-hoc tests were conducted between saline and Botox injected mice and are indicated as *$p<0.05$.

**Gene Expression in Osteocyte-Enriched Lysates**

Differential gene expression analysis using RNAseq identified 396 genes up- and 222 genes down-regulated in mice with stabilized β-catenin following tail suspension compared to stabilized β-catenin ground controls (Figure 16A). Eighty-one genes were up- and 27 genes were down-regulated in tail-suspended uninduced mice compared to induced ground controls (Figure 16B). Sixty-nine of these genes including *Calcr* (up), *Apod* (up) and *Ostn* (down) were commonly changed in both stabilized β-catenin mice and non-stabilized mice in response to tail suspension (Figure 16). Thirty-five genes including *Wnt11, Gli1, Nell1, Gdf5* and *Pgf* were significantly differentially regulated between tail-suspended β-catenin stabilized mice and tail suspended non-stabilized mice (Figure 16C). Many of these genes were also differentially regulated between stabilized and non-stabilized ground controls (Figure 16C), suggesting that these genes are likely β-catenin targets. These genes might play a role in the β-catenin-mediated osteoprotective effects of disuse-induced bone wasting.

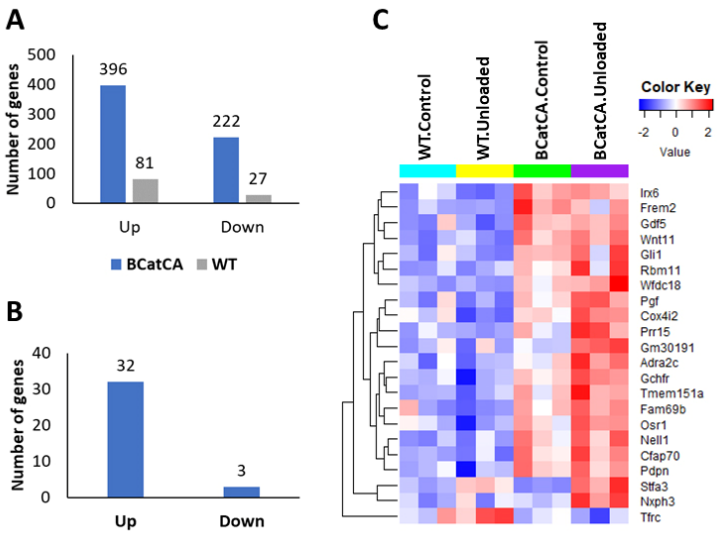


Figure 16. RNAseq of bones from βcatCA mice A) Number of genes up- and down-regulated in tail suspended stabilized β-catenin (βcat CA) mice and uninduced (control) mice compared to respective ground controls. B) Number of genes up- and down-regulated in tail suspended βcat CA mice compared to tail suspended uninduced mice. C) Heatmap showing the expression profiles of protein coding genes differentially expressed between tail suspended βcat CA mice and tail suspended WT mice. N=3

## *Chapter 4: The R1170W mutation in Lrp4 increases bone mass via loss of facilitator function with sclerostin*

### Mice with the Lrp4 R1170W mutation exhibit increased bone mass

To better understand the cellular mechanisms driving the high bone mass (HBM) phenotype in SOST2 patients, I generated an orthogonal mouse model to one of the families (LRP4 R1170W) using a CRISPR/Cas9 approach (Figure 17A). A C→T point mutation was knocked into the first position of the codon for aa.1170 (confirmed by Sanger sequencing, Figure 17B), which resulted in the predicted Arg→Trp amino acid substitution. Western blotting for Lrp4 indicated that the missense mutation had no effect on protein expression in cortical bone (Figure 17C).

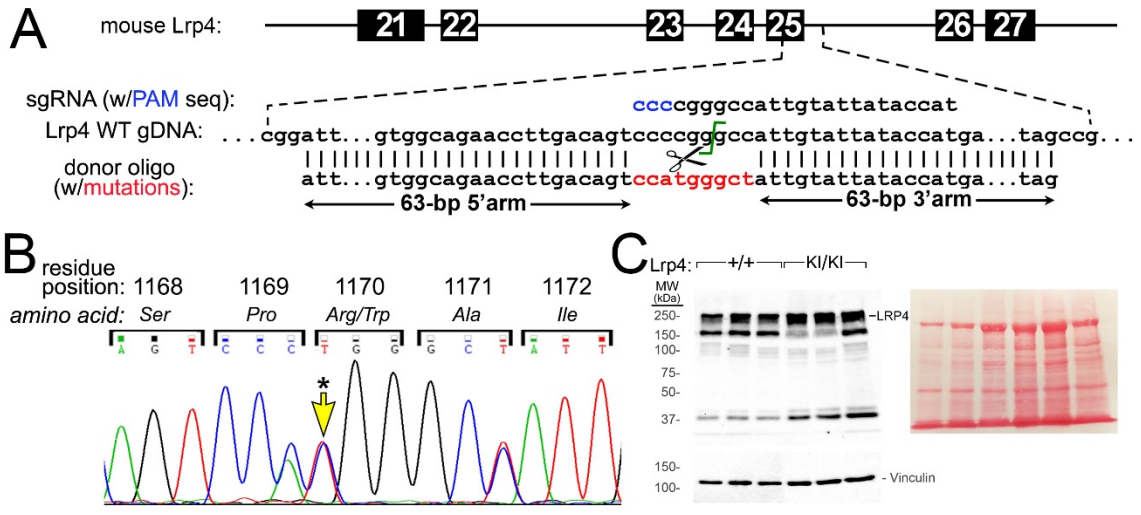


Figure 17. Generation of Lrp4 R1170W knockin mouse model. A) Mouse Lrp4 genomic DNA schematic, showing the exon 25/intron 25 targeting area. A CRISPR/Cas9 approach was used to replace a 135bp sequence with a donor oligo containing a C→T mutation at position 1 of aa1170, as well as two silent mutations in the flanking codons to facilitate genotyping. B) PCR products from exon 25 were sequenced to confirm mutations. A representative Sanger electropherogram from a heterozygous knockin mouse shows equal expression of the 3 individual base substitutions in the three consecutive codons. C) Western blot of cortical bone tissue protein extract from 6-8 week old Lrp4 WT and $Lrp4^{KI}$ mice, immunoreacted for Lrp4 (~240kDa), indicating comparable Lrp4 protein expression levels in $Lrp4^{KI}$ vs. Lrp4 WT mice. Lane loading equivalency was assessed by stripping and reprobing for the focal adhesion protein vinculin (lower panel) and via Ponceau-S staining of the membrane for total protein prior to blotting (right panel).

I next sought to determine whether the Lrp4-R1170W knockin male and female mice (hereafter referred to as $Lrp4^{KI}$) recapitulate the skeletal phenotype reported for SOST2 patients with centrally located 3rd β-propeller missense mutations (R1170W, R1170Q, W1186S). The $Lrp4^{KI}$ colony was expanded, along with wild-type and heterozygous littermates, and subjected to a battery of skeletal phenotyping endpoints. The mutation did not affect body mass or femur length, but $Lrp4^{KI}$ mice displayed significant increases in DXA-derived whole body bone mineral density (BMD) and content (BMC) as early as 6 weeks of age (Figure 18A, Tables 1 and 2). At 18 weeks of age, μCT-derived femur and vertebral cortical and cancellous bone mass were significantly increased in $Lrp4^{KI}$ as compared to both WT and heterozygous littermates (Figure 18D-G). pQCT-derived cortical BMC and trabecular BMD in the proximal tibia of 8-week-old $Lrp4^{KI}$ mice were also significantly elevated (Figure 18H-J). Three-point bending tests conducted on femora from 18 week old mice revealed improved biomechanical properties in $Lrp4^{KI}$ mice, including significantly increased ultimate force and energy absorption (Figure 18K-M).

Patients with SOST2 display calvarial sclerosis, which is recapitulated in $Lrp4^{KI}$ mice, though much more robustly in male mice compared to female mice (Figure 18N-P, Table 2). It was previously reported that stenosis of cranial nerve foramina in the basicranium of Lrp5-HBM and Sost knockout mouse models [71], which, at least in sclerosteosis patients, can lead to cranial nerve deficits. However, foramen ovale area was not significantly affected by the $Lrp4^{KI}$ mutation (Figure 18N-P). Although not reported in SOST2 patients, I also found dental anomalies in $Lrp4^{KI}$ mice, including

supernumerary incisors and molars, with altered cusp morphology (Figure 19). In summary, Lrp4$^{KI}$ mice recapitulate the human HBM phenotype associated with SOST2.

**Lrp4$^{KI}$ mice have increased bone formation, sclerostin expression, and mildly impaired muscle function**

Understanding of the mechanism of action (increased osteoanabolism or decreased osteocatabolism) for the observed HBM phenotype in Lrp4$^{KI}$ mice can guide translational applications for Lrp4 targeting. To address cellular activity, I performed quantitative cortical bone histomorphometry on Lrp4$^{KI}$ and WT control mice. In skeletally mature (16-17 weeks of age) mice, mineralizing surface and bone formation rate were increased on the endocortical surface (Figure 20A-G). No changes in the resorption marker CTx were detected in 8 wk-old wild-type or Lrp4$^{KI}$ mice (Figure 21H). Taken together those observations suggest that the increased bone mass observed in Lrp4$^{KI}$ mice is due to increased bone formation, positioning Lrp4 as a target for anabolic action in bone.

Lrp4 has been proposed to serve as a sequestering protein for sclerostin, where it might serve as a "molecular net" to keep sclerostin levels high in the perimembrane region of bone cells [83]. Serum levels of sclerostin were significantly greater in Lrp4$^{KI}$ mice than in WT and heterozygous mice (Figure 20I), which is consistent with patient data [1] and supports the premise that mutant Lrp4 has impaired ability to retain sclerostin at the cell surface. However, cortical bone tissue lysates from Lrp4$^{KI}$ mice yielded greater levels of sclerostin than lysates from WT mice (Figure 20H), which runs counter to the proposal that osteocytes with mutant Lrp4 are less efficient at retaining sclerostin locally.

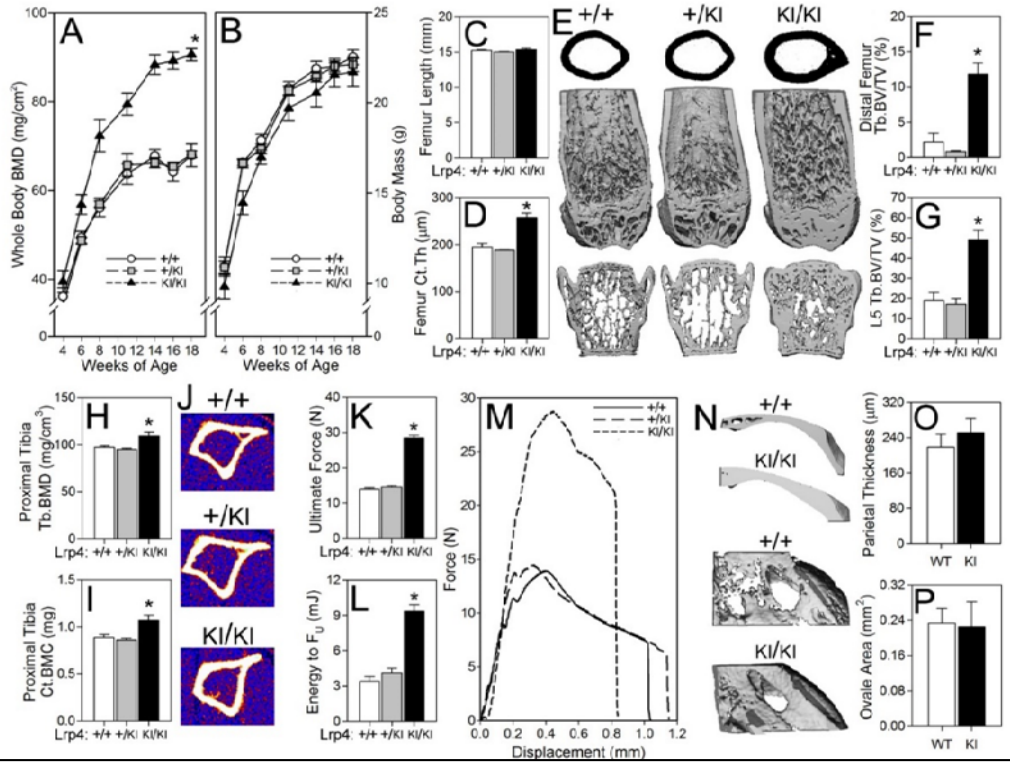


Figure 18. Lrp4$^{KI}$ mice have a high bone mass phenotype. (A) Whole body bone mineral density (BMD) was significantly elevated in female Lrp4$^{KI}$ mice vs. WT (+/+) and heterozygous (+/KI) littermates, despite (B) normal body mass. (D-G) Trabecular bone volume fraction (Tb.BV/TV) in the distal femur and 5$^{th}$ lumbar vertebra (L5), and cortical thickness (Ct.Th) in the mid-diaphyseal femur, were significantly increased in 18-wk old female Lrp4$^{KI}$ mice compared to WT (+/+) and heterozygous (+/KI) littermates, despite (C) normal femur length. (E) The center panel depicts μCT reconstructions from the midshaft femur (upper) distal femur (middle) and vertebral body (lower) from representative +/+ and KI/KI mice. (H-J) Peripheral quantitative computed tomography (pQCT) measurements through the proximal tibia of 8 week old female +/+, +/KI, and KI/KI mice reveal an increase in trabecular BMD and cortical BMC among KI/KI mice. (K-M) Mechanical testing of femora from 18-wk old female +/+, +/KI and KI/KI mice reveal increased ultimate force and energy to ultimate force ($F_U$) among knockin mice. (N-P) Parietal thickness and planar area of foramen ovale in 18-wk old female +/+ and KI/KI female crania were not affected by the mutation. Male data are presented in Table S2. For panels A and B, *p<0.05 for comparison to +/+ by repeated measures ANOVA; for panels C-P, *p<0.05 for comparison to +/+ mice, using one-way ANOVA followed by Fisher's PLSD post hoc tests. *n*=10/group

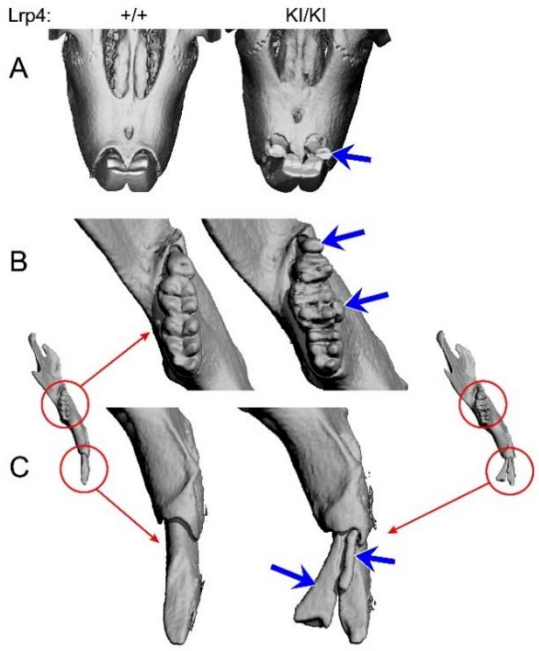


Figure 19. Lrp4$^{KI}$ mice display supernumerary teeth and altered molar cusp patterns. Top panel: μCT reconstructions from the occlusal view of the maxillary incisors illustrating a set of secondary incisors (blue arrow) distolingual to the primary set in the Lrp4$^{KI}$ mice. Middle/lower panel: close-up view of the mandibular dentition reveal extra incisors of varying development, and additional molar teeth on the distal end and lingual edge of the tooth row (blue arrows). The molars also exhibit altered cusp pattern compared to those seen in the WT mice.

Lrp4 is critical for neuromuscular junction (NMJ) formation and muscle function, where it serves as a receptor for motoneuron-derived Agrin, triggering interaction with MuSK [84]. Mutations in the 3$^{rd}$ β-propeller of Lrp4 can affect Agrin and MuSK binding [85], so I performed in vivo muscle force testing in 8 week old female WT and Lrp4$^{KI}$ mice to determine whether muscle function was affected by the R1170W missense mutation. Time to maximum torque and half relaxation time were not different between WT and Lrp4$^{KI}$ mice, but maximum torque was significantly lower in Lrp4$^{KI}$ mice (Figure 20J-M). However, a change in muscle function does not explain the HBM phenotype in Lrp4$^{KI}$ mice since the mutation was associated with reduced rather than enhanced muscle forces on the skeleton. In summary, Lrp4$^{KI}$ mice have HBM due to increased anabolic activity, despite increased local and systemic sclerostin and compromised muscle function.

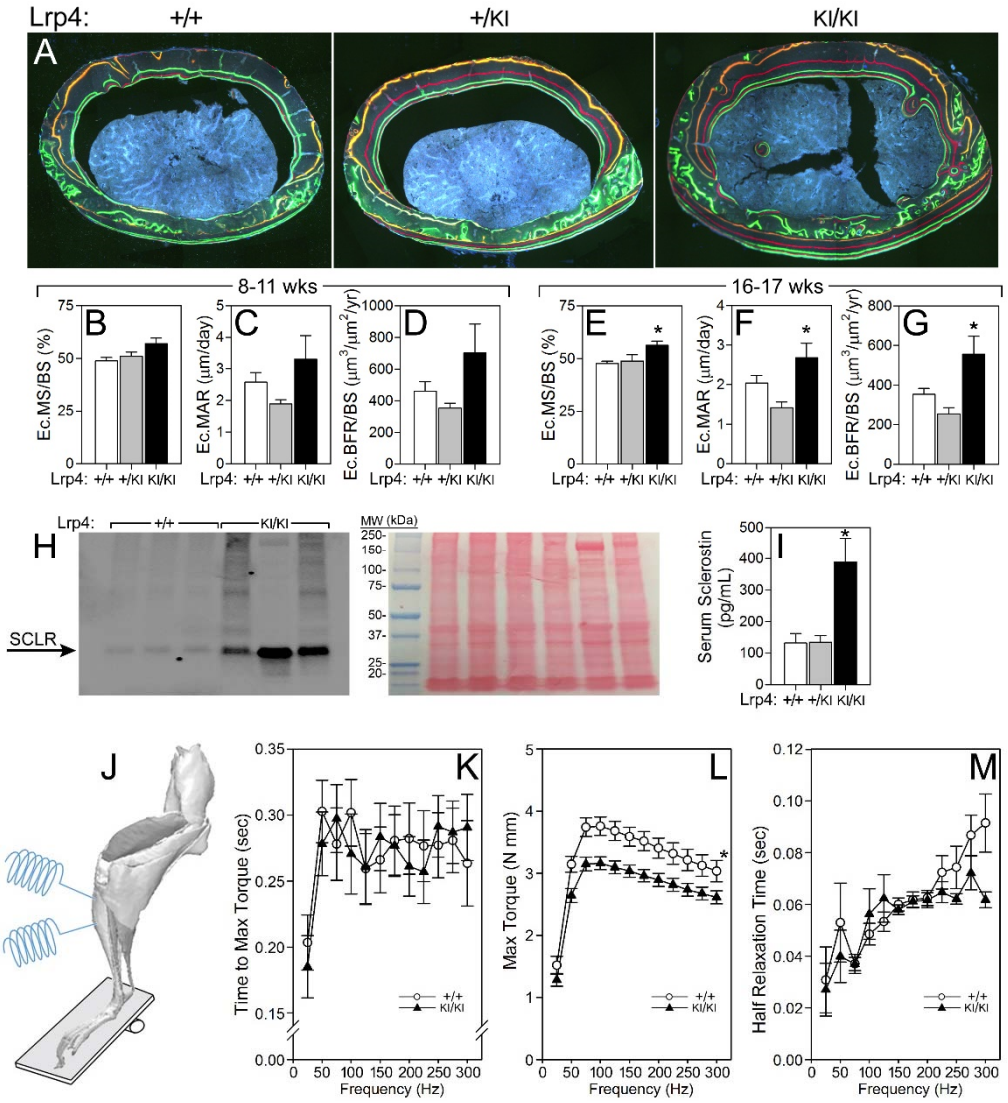


Figure 20. Lrp4$^{KI}$ mice have increased bone formation, increased circulating and local sclerostin, and reduced skeletal muscle function. A) Quantitative endocortical bone histomorphometry of the midshaft femur of 18 week old +/+, +/KI and KI/KI female mice, measured using labels injected at 8 (orange) and 11 (red) weeks of age (B-D), and again using labels injected at 16 (green) and 17 (red) weeks of age (E-G), indicate a significant increase in the bone formation parameters mineralizing surface (MS/BS), mineral apposition rate (MAR), and bone formation rate (BFR/BS) at the later time point. (H) Western blot of cortical bone tissue protein extract from 6-8 week old Lrp4 WT and Lrp4$^{KI}$ mice, immunoreacted for sclerostin (~30 kDa), indicating increased sclerostin protein expression levels in Lrp4$^{KI}$ vs. Lrp4 WT mice. Lane loading equivalency was assessed by Ponceau-S staining of the membrane for total protein prior to blotting (right panel). (I) Serum sclerostin was also significantly elevated in the circulation of Lrp4 KI mice, compared to +/+ and +/KI mice. (J) *In vivo* muscle function of the anterior compartment musculature (left panel) in 10-wk old female mice revealed a deficiency in maximum torque (K), but not the time to maximum torque (L) or half muscle relaxation time (M), among Lrp4KI mice, compared to WT mice. For panels B-I, $p<0.05$ for comparison to +/+ mice, using one-way ANOVA followed by Fisher's PLSD post hoc tests; for panels in K-M, *$p<0.05$ for comparison to +/+ mice by repeated measures ANOVA. n=6/group (B-G); 3-8/group (H-I); and 9-10/group (K-M).

**Overexpression of Sost in bone tissue causes osteopenia in WT but not Lrp4$^{KI}$ mice**

Some reports suggest that Lrp4 acts as a facilitator of sclerostin inhibition of Lrp5/6, a proposition that is supported by direct interaction between the Lrp4 3$^{rd}$ β-propeller and sclerostin, and by suppression of sclerostin-mediated Wnt inhibition by Lrp4 knockdown [1]. To determine whether compromise of the sclerostin–Lrp4 interaction can account for the HBM phenotype of Lrp4KI, I bred Lrp4KI mice with transgenic mice that overexpress human Sost in osteocytes (8kbDmp1-hSost). As expected, whole body BMD and BMC were decreased in Lrp4 WT mice overexpressing Sost, but Lrp4KI mice were unaffected by Sost overexpression (Figure 21A, Tables 3 and 4). Lrp4KI mice were protected from the osteopenic effects of Sost overexpression in the cancellous compartment of both the femur and spine (Figure 21B-D), but the protective effects in the cortical compartment could not be evaluated because Lrp4 WT mice did not manifest a Sost transgene effect, when evaluated by microCT (Figure 21E) or bone formation parameters (Figure 21F,G,I). The resorption marker CTx was not affected by the Sost transgene in either Lrp4 genotype (Figure 21H). In summary, the otherwise bone-suppressive effects of excessive sclerostin in bone were absent in Lrp4KI mice, suggesting that the R1170W mutation confers resistance to the inhibitory effects of sclerostin.

Table 1. Radiographic and biomechanical analysis of female Lrp4 WT, HET and KI mice

| | **Wild-type (WT)** | **R1170W/+ (HET)** | **R1170W/R1170W (KI)** |
|---|---|---|---|
| Whole Body BMC (18 wk; g) | 0.49 ± 0.1 | 0.47 ± 0.1 | 0.77 ± 0.1 |
| Body Weight (18 wk; g) | 22.5 ± 1.3 | 22.1 ± 1.0 | 21.6 ± 2.2 |
| Femur length (mm) | 15.2 ± 0.5 | 15.0 ± 0.2 | 15.3 ± 0.5 |
| **Femur µCT** | | | |
| Tb.N (1/mm) | 2.16 ± 0.35 | 1.88 ± 0.30 * | 2.84 ± 0.29 * |
| Tb.Th (mm) | 0.04 ± 0.01 | 0.04 ± 0.01 | 0.08 ± 0.01 * |
| Tb.Sp (mm) | 0.47 ± 0.08 | 0.55 ± 0.09 * | 0.34 ± 0.05 * |
| Tb.BMD (mg/cm$^3$) | 868 ± 40 | 879 ± 37 | 924 ± 34 * |
| Tb.BMC (mg) | 0.06 ± 0.12 | 0.02 ± 0.01 | 0.41 ± 0.18 * |
| Ct.BMD (mg/cm$^3$) | 1.08 ± 0.02 | 1.08 ± 0.01 | 1.09 ± 0.01 * |
| Ct.BMC (mg) | 2.59 ± 0.42 | 2.60 ± 0.09 | 3.97 ± 0.70 * |
| **5$^{th}$ Lumbar µCT** | | | |
| Tb.N (1/mm) | 3.79 ± 0.8 | 3.69 ± 1.0 | 5.93 ± 1.1 * |
| Tb.Th (mm) | 0.05 ± 0.01 | 0.05 ± 0.01 | 0.08 ± 0.02 * |
| Tb.Sp (mm) | 0.26 ± 0.04 | 0.27 ± 0.05 | 0.17 ± .05 * |
| Tb.BMD (mg/cm$^3$) | 871 ± 10 | 878 ± 15 | 871 ± 19 |
| Tb.BMC (mg) | 0.28 ± 0.19 | 0.26 ± 0.14 | 0.79 ± 0.27 * |
| **Femur 3 point bending** | | | |
| Stiffness (N/mm) | 70.2 ± 12.2 | 67.9 ± 21.9 | 108.6 ± 2.6 * |
| Energy to $F_U$ (mJ) | 3.38 ± 1.3 | 4.10 ± 1.3 | 9.35 ± 1.6 * |
| Energy to $F_F$ (mJ) | 10.1 ± 2.6 | 9.6 ± 2.9 | 15.3 ± 4.7 * |

*$p<0.05$ for comparison to WT mice, using one-way ANOVA followed by Fisher's PLSD post hoc tests.

Table 2. Radiographic and biomechanical analysis of male Lrp4 WT, HET and KI mice

| | **Wild-type (WT)** | **R1170W/+ (HET)** | **R1170W/R1170W (KI)** |
|---|---|---|---|
| Whole Body BMD (18 wk; g/cm$^2$) | 70.1 ± 7.3 | 75.0 ± 8.0 | 91.6 ± 12.6* |
| Whole Body BMC (18 wk; g) | 0.54 ± 0.1 | 0.57 ± 0.1 | 0.76 ± 0.2* |
| Body Weight (18 wk; g) | 28.3 ± 0.8 | 27.68 ± 3.2 | 26.34 ± 2.2 |
| Femur length (mm) | 15.4 ± 0.5 | 15.1 ± 0.2 | 15.2 ± 0.2 |
| **Femur µCT** | | | |
| Tb.BV/TV (unitless) | 0.046 ± 0.02 | 0.046 ± 0.02 | 0.166 ± 0.05* |
| Tb.N (1/mm) | 3.193 ± 0.34 | 2.960 ± 0.27 | 3.722 ± 0.31* |
| Tb.Th (mm) | 0.05 ± 0.00 | 0.05 ± 0.01 | 0.07 ± 0.01* |
| Tb.Sp (mm) | 0.31 ± 0.03 | 0.34 ± 0.03 | 0.25 ± 0.03* |
| Tb.BMD (mg/cm$^3$) | 887.3 ± 8.7 | 887.1 ± 21.6 | 901.5 ± 15.0* |
| Tb.BMC (mg) | 0.16 ± 0.10 | 0.17 ± 0.08 | 0.67 ± 0.23* |
| Ct.BMD (mg/cm$^3$) | 1.06 ± 0.01 | 1.06 ± 0.00 | 1.07 ± 0.01* |
| Ct.BMC (mg) | 2.43 ± 0.23 | 2.57 ± 0.21 | 3.79 ± 0.28* |
| Ct.Th (mm) | 0.188 ± 0.01 | 0.195 ± 0.01 | 0.259 ± 0.02* |
| **5$^{th}$ Lumbar µCT** | | | |
| Tb.BV/TV (unitless) | 0.20 ± 0.03 | 0.18 ± 0.03 | 0.37 ± 0.15* |
| Tb.N (1/mm) | 4.75 ± 0.22 | 4.45 ± 0.23* | 5.63 ± 1.15* |
| Tb.Th (mm) | 0.47 ± 0.01 | 0.048 ± 0.00 | 0.06 ± 0.02* |
| Tb.Sp (mm) | 0.20 ± 0.01 | 0.21 ± 0.013* | 0.18 ± 0.06* |
| Tb.BMD (mg/cm$^3$) | 881.7 ± 6.3 | 882.5 ± 9.5 | 870.9 ± 23.5 |
| Tb.BMC (mg) | 0.342 ± 0.07 | 0.289 ± 0.07 | 0.586 ± 0.24* |
| **Femur 3 point bending** | | | |
| Ultimate Force (N) | 15.7 ± 2.9 | 16.9 ± 2.7 | 32.2 ± 4.4* |
| Stiffness (N/mm) | 56.9 ± 18.7 | 79.9 ± 20.8* | 102.7 ± 51.2* |
| Energy to $F_U$ (mJ) | 4.94 ± 1.5 | 4.92 ± 1.2 | 11.96 ± 3.7* |
| Energy to $F_F$ (mJ) | 8.2 ± 2.8 | 11.7 ± 3.0* | 16.6 ± 3.5 * |
| **Cranial Dimensions** | | | |
| Skull Thickness (µm) | 0.201 ± 0.08 | ---- | 0.295 ± 0.05 * |
| Foramen Ovale Area (µm) | 0.337 ± 0.18 | ---- | 0.273 ± 0.11 |

*$p<0.05$ for comparison to WT mice, using one-way ANOVA followed by Fisher's PLSD post hoc tests.

**Inactivation of sclerostin elicits a blunted osteogenic effect in Lrp4$^{KI}$ mice**

In the previous section I evaluated the ability of Lrp4$^{KI}$ mice to maintain high bone mass in the presence of excessive sclerostin. Next, I evaluated the opposite condition regarding the sclerostin–Lrp4 interaction, i.e., whether Lrp4$^{KI}$ mice can elicit a full anabolic response when sclerostin is inactivated pharmacologically. Four weeks of treatment with sclerostin monoclonal antibody (Scl-mAb) increased whole body BMD significantly compared to saline treatment in both WT and Lrp4$^{KI}$ female mice, but the antibody-induced BMD gain exhibited by Lrp4$^{KI}$ mice was only about half of that exhibited by WT mice (Figure 22E). Large gains in μCT-derived parameters (trabecular and cortical bone mass in the femur and spine) were measured among WT mice in response to Scl-mAb, but a blunted response (roughly a third to a half of WT gains) was observed in Lrp4$^{KI}$ mice (Figure 22A-D). Scl-mAb treatment increased bone formation parameters significantly in WT mice but not in Lrp4$^{KI}$ mice (Figure 22F-H). In summary, the strong anabolic effects of sclerostin neutralization were compromised or absent in Lrp4$^{KI}$ mice, likely due to the mutation having similar functional (i.e., redundant) effects as Sost inactivation.

**Lrp4$^{KI}$ mice are partially protected from disuse-induced bone wasting**

Bone is a highly mechanosensitive tissue, and previous studies highlight the importance of canonical Wnt signaling, particularly sclerostin, in this process. Mechanical disuse induces an increase in Sost expression, and Sost genetic deletion or sclerostin pharmacologic neutralization prevents disuse-induced bone loss [86]. Given the accumulating evidence that the Lrp4 R1170W mutation confers properties to bone tissue that are similar to sclerostin neutralization, I explored the role of Lrp4$^{KI}$ in response to

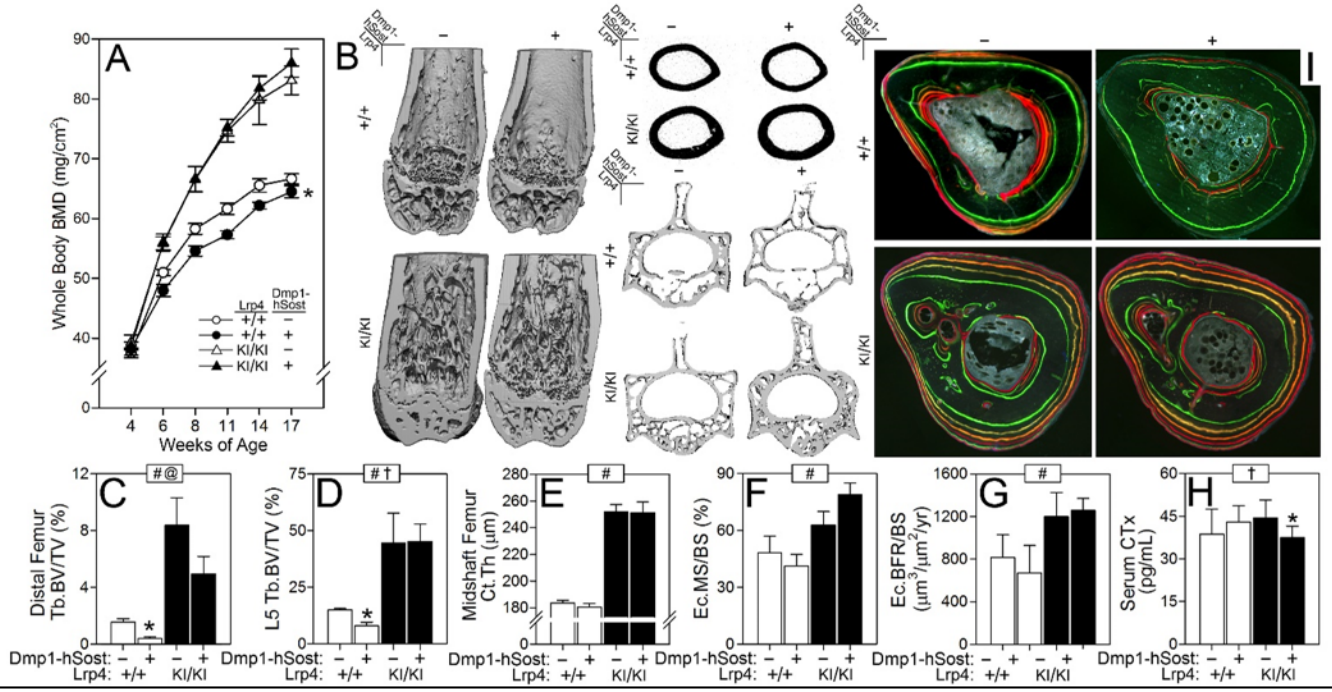


Figure 21. Lrp4$^{KI}$ mice are protected from the osteopenic effects of Sost overexpression. A) Whole body bone mineral density (BMD) in female Lrp4$^{+/+}$ mice was significantly reduced by the Dmp1-hSost transgene, which induces Sost overexpression in late stage osteoblasts and osteocytes, whereas Lrp4$^{KI}$ mice maintained high BMD regardless of Dmp1-hSost presence. (B-D) Trabecular bone volume fraction (Tb.BV/TV) in the distal femur and 5$^{th}$ lumbar vertebra (L5) were significantly reduced in 17-wk old female Lrp4 WT that carried the hSost transgene, but not in Lrp4$^{KI}$ mice that carried the hSost transgene. (E) Cortical thickness (Ct.Th) was not affected by the hSost transgene in either Lrp4 genotype. (F-G) Quantitative endocortical bone histomorphometry of the tibial cortex (I), calculated from 16-17 wks, revealed no effect of the transgene on the bone formation parameters mineralizing surface (MS/BS) bone formation rate (BFR/BS) in either Lrp4 genotype. (H) The serum resorption marker C-terminal telopeptide (CTx) was decreased by the hSost transgene in Lrp4$^{KI}$ mice overspressing Sost. Data from male mice are in Table S4. For panel A, *p<0.05 by repeated measures ANOVA for within Lrp4 genotype comparison of transgene presence, n=8-10/group. For panels C-H, data were tested using 2-way ANOVA with Lrp4 genotype and the Sost transgene as main effects. Inset at the top of each graph indicates significance of the main effects and interaction (#=Lrp4 genotype p<0.05; @=Dmp1-hSost p<0.05; †=interaction p<0.05). When at least one term was significant, Fisher's PLSD post-hoc tests were conducted and are indicated as *p<0.05. For panels C-E, n=8-10/group. For panels F-G, n=4-6/group. For panel H, n=6-7/group.

disuse mechanotransduction. $Lrp4^{KI}$ mice (12 wks of age) were subjected to 4 wks of unilateral mechanical disuse of the hindlimb using the Botulinum toxin-induced muscle paralysis model, and the degree of bone wasting was evaluated radiographically. The paralyzed limb of WT mice lost ~10% BMC, but $Lrp4^{KI}$ mice did not lose BMC in response to Botox (Figure 23A). However, while bone loss was spared in the paralyzed limb of $Lrp4^{KI}$ mice, I detected a significant failure to gain bone as was observed in the saline-treated limb of $Lrp4^{KI}$ mice (Figure 23A). Proximal tibial trabecular bone mass was significantly reduced by Botox in both WT and $Lrp4^{KI}$ mice, but the $Lrp4^{KI}$ mice lost roughly half as much bone as WT mice in response to paralysis (Figure 23B-D). Cortical bone loss was significant in Botox treated WT mice, but paralyzed limbs from $Lrp4^{KI}$ mice exhibited no difference from saline treated limbs. In summary, $Lrp4^{KI}$ mice exhibit less severe bone wasting in response to mechanical disuse than WT mice, suggesting that pharmacologically targeting the $3^{rd}$ β-propeller of Lrp4 during a disuse event might have therapeutic value in reducing bone loss.

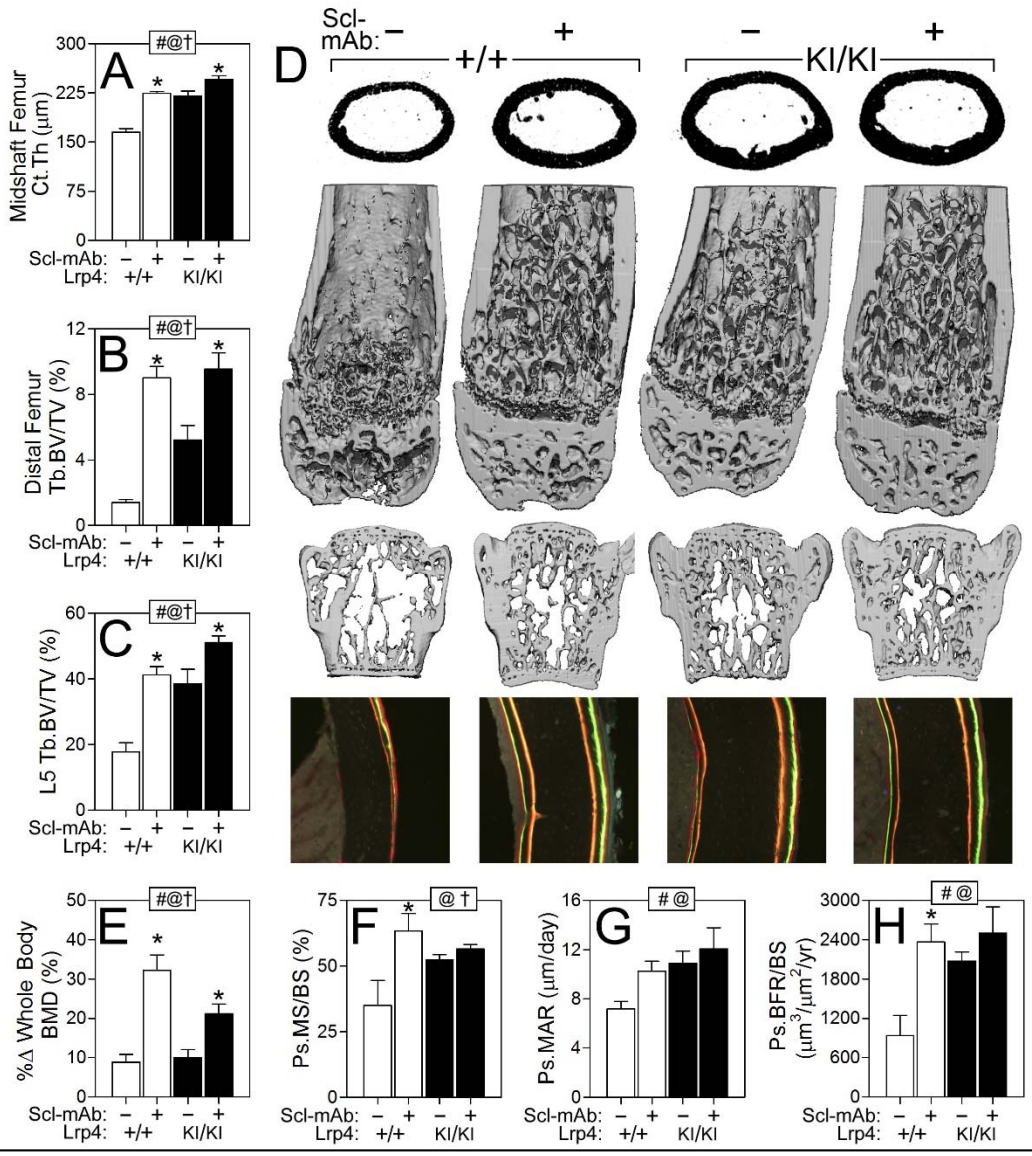


Figure 22. Response to pharmacologic inhibition of Sost is blunted in Lrp4$^{KI}$ mice. (A-C) Trabecular bone volume fraction (Tb.BV/TV) in the distal femur and 5$^{th}$ lumbar vertebra (L5), and cortical thickness (Ct.Th) in the mid-diaphyseal femur, were significantly increased in 16-wk old female Lrp4$^{KI}$ and WT (+/+) mice treated with sclerostin monoclonal antibody (Scl-mAb), but the gains were more pronounced in WT mice. (D) μCT reconstructions from the midshaft femur (upper) distal femur (middle) and vertebral body (lower) from representative +/+ and KI/KI mice treated with vehicle (-) or Scl-mAb (+). (E) Percent change in whole body bone mineral density (BMD) during the 4 week antibody treatment period was greater in WT mice compared to Lrp4$^{KI}$ mice. (F-H) The periosteal bone formation parameters mineralizing surface (MS/BS), mineral apposition rate (MAR), and bone formation rate (BFR/BS) were significantly increased in WT but not Lrp4KI mice in response to sclerostin antibody. For all data panels, data were tested using 2-way ANOVA with Lrp4 genotype and the Scl-mAb injection as main effects. Inset at the top of each graph indicates significance of the main effects and interaction (#=Lrp4 genotype $p<0.05$; @=Scl-mAb $p<0.05$; †=interaction $p<0.05$). When at least one term was significant, Fisher's PLSD post-hoc tests were conducted and are indicated as *$p<0.05$. For all panels, n=6-10/group.

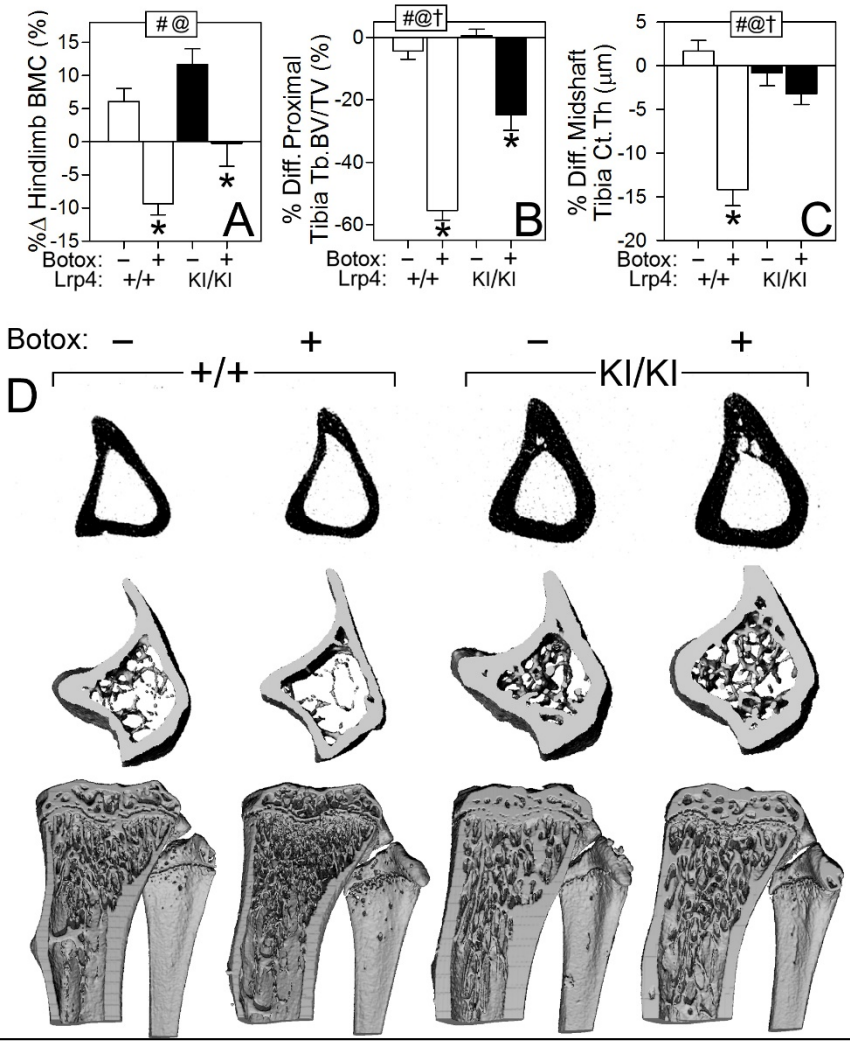


Figure 23. Lrp4$^{KI}$ mice are partially protected from disuse-induced bone loss. (A) Percent change in hindlimb bone mineral density (BMD) following 4 weeks of Botox-induced disuse. (B-C) Percent difference (side-to-side) in trabecular bone volume fraction (Tb.BV/TV) in the proximal tibia and cortical thickness (Ct.Th) in the mid-diaphyseal tibia, were significantly greater in Botox-treated WT mice compared to Botox-treated Lrp4$^{KI}$ mice. (D) μCT reconstructions at the proximal tibia from representative +/+ and KI/KI mice treated with Botox (+) or vehicle (-). Data were tested using 2-way ANOVA using Lrp4 genotype and Botox injection as main effects. Inset at the top of each graph indicates significance of the main effects and interaction (#=Lrp4 genotype $p<0.05$; @=Botox effect $p<0.05$; †=interaction $p<0.05$). When at least one term was significant, Fisher's PLSD post-hoc tests were conducted and are indicated as *$p<0.05$. For all panels, n=9-10/group.

Table 3. Radiographic analysis and serum measurements in WT and Lrp4-KI female mice with and without a Dmp1-hSost transgene

| | WT / NTG | WT / Dmp1-hSost | KI / NTG | KI / Dmp1-hSost |
|---|---|---|---|---|
| Whole Body BMC (17 wk; g) | 0.473 ± 0.02 | 0.446 ± 0.04* | 0.610 ± .0.07 | 0.639 ± 0.09 |
| **Femur µCT** | | | | |
| Tb.N (1/mm)[#@] | 2.11 ± 0.36 | 1.24 ± 0.46* | 2.42 ± 0.39 | 1.99 ± 0.48 |
| Tb.Th (mm)[#] | 0.038 ± 0.006 | 0.046 ± 0.013 | 0.067 ±0.010 | 0.063 ± 0.014 |
| Tb.Sp (mm)[#@†] | 0.49 ± 0.10 | 0.88 ± 0.26* | 0.41 ± 0.07 | 0.53 ± 0.15 |
| Tb.BMD (mg/cm$^3$)[#] | 923.7 ± 24.6 | 926.1 ± 31.7 | 948.9 ± 20.1 | 939.3 ± 18.2 |
| Tb.BMC (mg)[#@] | 0.05 ± 0.02 | 0.01 ± 0.01* | 0.28 ± 0.14 | 0.17 ± 0.11 |
| Ct.BMD (mg/cm$^3$)[#] | 1.07 ± 0.01 | 1.06 ± 0.02 | 1.09 ± 0.02 | 1.08 ± 0.02 |
| Ct.BMC (mg)[#] | 2.44 ± 0.14 | 2.35 ± 0.14 | 3.56 ± 0.34 | 3.54 ± 0.46 |
| **5$^{th}$ Lumbar µCT** | | | | |
| Tb.N (1/mm)[#] | 3.72 ± 0.2 | 2.41 ± 0.8 | 5.41 ± 2.5 | 5.13 ± 1.2 |
| Tb.Th (mm)[#] | 0.048 ± 0.003 | 0.056 ± 0.007 | 0.083 ± 0.011 | 0.085 ± 0.021 |
| Tb.Sp (mm)[#†] | 0.263 ± 0.16 | 0.440 ± 0.12* | 0.254 ± 0.23 | 0.204 ± 0.06 |
| Tb.BMD (mg/cm$^3$)[#] | 849.6 ± 14.1 | 863.1 ± 29.0 | 875.5 ± 3.83 | 877.9 ± 23.6 |
| Tb.BMC (mg)[#] | 0.237 ± 0.02 | 0.133 ± 0.06 | 0.617 ± 0.36 | 0.703 ± 0.27 |
| Serum sclerostin (pg/µL)[#] | 148.3 ± 19 | 131.2 ± 32 | 700.3 ± 291 | 778.8 ± 335 |

Symbols indicate significance of the main effects and interaction (#=Lrp4 genotype $p<0.05$; @=Dmp1-hSost $p<0.05$; †=interaction $p<0.05$). When at least one term was significant, Fisher's PLSD post-hoc tests were conducted and are indicated as *$p<0.05$.

.

Table 4. Radiographic analysis and serum measurements in WT and Lrp4-KI male mice with and without a Dmp1-hSost transgene

| | WT / NTG | WT / Dmp1-hSost | KI / NTG | KI / Dmp1-hSost |
|---|---|---|---|---|
| Whole Body BMC (17 wk; g) | 0.55 ± 0.10 | 0.55 ± 0.10 | 0.68 ± 0.08 | 0.72 ± 0.13 |
| Whole Body BMD (17 wk; g/cm$^2$) | 72.3 ± 8.6 | 73.2 ± 8.6 | 85.1 ± 7.3 | 89.9 ± 10.2 |
| **Femur µCT** | | | | |
| Tb.BV/TV (unitless) #† | 0.08 ±0.04 | 0.05 ± 0.02* | 0.12 ± 0.03 | 0.17 ± 0.04* |
| Tb.N (1/mm) #@† | 3.34 ± 0.68 | 1.98 ± 0.25* | 3.32 ± 0.27 | 3.56 ± 0.32 |
| Tb.Th (mm) #@ | 0.050 ± 0.01 | 0.058 ± 0.01* | 0.067 ± 0.00 | 0.072 ± 0.00 |
| Tb.Sp (mm) #@† | 0.307 ± 0.06 | 0.514 ± 0.06* | 0.287 ± 0.03 | 0.266 ± 0.03 |
| Tb.BMD (mg/cm$^3$) #† | 916.5 ± 19.6 | 925.0 ± 19.1* | 925.9 ± 9.8 | 936.1 ± 14.7* |
| Tb.BMC (mg) #† | 0.345 ± 0.19 | 0.184 ± 0.10 | 0.471 ± 0.13 | 0.793 ± 0.32* |
| Ct.BMD (mg/cm$^3$) # | 1.05 ± 0.03 | 1.04 ± 0.03 | 1.07 ± 0.01 | 1.08 ± 0.02 |
| Ct.BMC (mg) # | 2.58 ± 0.51 | 2.53 ± 0.19 | 3.47 ± 0.17 | 3.84 ± 0.47 |
| Ct.Th (mm) # | 0.198 ± 0.03 | 0.198 ± 0.01 | 0.243 ± 0.01 | 0.244 ± 0.03 |
| **5$^{th}$ Lumbar µCT** | | | | |
| Tb.BT/TV (unitless) #@ | 0.24 ± 0.09 | 0.08 ± 0.01* | 0.43 ± 0.05 | 0.40 ± 0.14 |
| Tb.N (1/mm) #@† | 4.99 ± 0.5 | 2.09 ± 0.3* | 6.37 ± 0.7 | 5.29 ± 1.4 |
| Tb.Th (mm) # | 0.051 ± 0.01 | 0.060 ± 0.01 | 0.072 ± 0.00 | 0.078 ± 0.01 |
| Tb.Sp (mm) #@† | 0.190 ± 0.02 | 0.479 ± 0.07* | 0.141 ± 0.03 | 0.198 ± 0.11 |
| Tb.BMD (mg/cm$^3$) | 874.5 ± 14.1 | 871.7 ± 11.3 | 856.4 ± 8.0 | 870.2 ± 17.3 |
| Tb.BMC (mg) #† | 0.40 ± 0.16 | 0.13 ± 0.03* | 0.58 ± 0.02 | 0.59 ± 0.22 |
| Serum sclerostin (pg/µL) # | 143.3 ± 37 | 121.6 ± 23* | 1007 ± 173 | 993.4 ± 109 |

Symbols indicate significance of the main effects and interaction (#=Lrp4 genotype $p<0.05$; @=Dmp1-hSost $p<0.05$; †=interaction $p<0.05$). When at least one term was significant, Fisher's PLSD post-hoc tests were conducted and are indicated as *$p<0.05$

## ***Chapter 5: Discussion***

While the importance of Wnt signaling in bone is clear, our current understanding of this pathway in bone cell mechanotransduction has been largely focused on the Wnt co-receptor Lrp5 and the soluble inhibitor Sost. However, numerous other Wnt pathway components are involved in the response to mechanical stimuli in bone, but our understanding of these other molecules is somewhat limited. Here, I explore the role of β-catenin in osteocytes in the context of a disuse environment. In addition, I define the role a less well-known Wnt signaling modulator—Lrp4.

**Regulation of β-catenin in osteocytes is necessary for mechanotransduction in disuse**

The downstream Wnt signaling modulator β-catenin has been explored in animal models of enhanced loading, where it was found to be necessary for load-induced bone formation [58, 59]. Activation of the Wnt signaling pathway results in the accumulation of β-catenin. Conversely, β-catenin is degraded in the absence of mechanical signal, such as in musculoskeletal disuse. β-catenin is involved in the regulation of adherins junctions at the cell-cell contact points , and it also functions as a binding partner for specific transcription factors in the nucleus. Whereas this study does not distinguish between the different actions of β-catenin in the cell (i.e., cell membrane versus nucleas), it does emphasize the necessity of β-catenin in regulating the response of osteocytes to mechanotransduction, particularly in reduced mechanical stimuli environments. Here, I employed a mouse model in which β-catenin was constitutively and inducibly activated in osteocytes, and subjected mice to two different methods of disuse. In both models, constitutive activation of β-catenin resulted in some degree of protection from disuse-induced bone loss, suggesting β-catenin regulation is critical for mechanotransduction in

bone. The Dmp1-Cre:ERt2 promoter, like all mouse models, is imperfect. While Dmp1-Cre:ERt2 was engineered to target osteocytes, other cell types expressing low levels of Dmp1 are also activated by tamoxifen. Additionally, the recombination efficiency of Dmp1-Cre:ERt2 is low (10-15% recombination in boht the βcatCa and flox loss-of-function alleles, see Chapter 3). While this leaves a large number of cells with intact β-catenin activity, the resulting recombination efficieny was enough to elicit a protective effect in bone. Finally, one of the largest drawbacks of using the Dmp1-Cre:ERt2 driver is the utilization of tamoxifen to activate the Cre recombinase. The Cre:ERt2 transgene codes for a Cre fusion protein that remains cytosolic until the tamoxifen ligand encountered, which induces translocation to the nucleus where the Cre recombinase activity can have its effect on LoxP sites. The direct effects of tamoxifen in bone are well known [87, 88]; therefore extensive control experiments were included in the design to account for the anabolic/anti-catabolic effects of tamoxifen in bone. In this study, I balanced tamoxifen administration to activate Cre recombinase activity while also minimizing the anabolic effects of tamoxifen in bone. To this end, additional controls were included to account for the tamoxifen effect in bone. Although treatment with tamoxifen increased bone mass in both Cre-positive and Cre-negative mice, the presence of tamoxifen alone (Cre-negative, disuse treated mice) offered no measureable protection against the bone wasting effects of either disuse model. Those control experiments suggest that the skeletal rescue seen in Cre-positive, tamoxifen treated mice subjected to disuse were the result of β-catenin activation rather than tamoxifen. Additionally, the increase in bone parameters following tamoxifen administration alone (i.e., in ground control mice) appears to be similar in both Cre-positive and Cre-negative mice, though

this result was inconsistent (e.g., tibial BMC exhibited additional increases beyond the tamoxifen effect in Cre-positive ground mice), suggesting little additional benefit of βcat CA activation beyond the increases induced by tamoxifen. Although that effect was inconsistent (e.g., tibial BMC exhibited additional increases beyond the tamoxifen effect in Cre-positive ground mice), at least for some endpoints, βcat CA activation can have negligible effects that are only manifest when challenged by a disuse stimulus.

As part of this study, I also performed high-throughput RNA sequencing on osteocyte-enriched hindlimb bone lysates from tail suspended mice. The aim for those studies was geared toward hypothesis generation, to determine whether there were candidate genes or pathways that were associated with the protective effects of β-catenin activation on disuse induced bone loss that might serve as better targets for skeletal therapies in disuse. Those mice were sacrificed after 4 days to capture more acute changes in gene expression. I found a number of genes that were significantly upregulated in activated tail suspended mice that were either not affected or downregulated in the uninduced suspended controls. I are currently pursuing some of these candidates to understand their potential role in protection from disuse osteopenia as part of the Wnt signaling pathway. GO pathway analysis of altered gene activity indicated in *Gli1*, *Nell1* and *Wnt11*, which are all associated with Wnt signaling and osteoblast regulation.

The bone-wasting effects of disuse have been well characterized, and are commonly associated with clinical conditions such as prolonged bedrest, spinal cord injury, muscle paralysis, and immobilization (casting), among others. Treatments for disuse-induced bone loss are limited. The importance of canonical Wnt signaling in the

response of osteocytes to altered mechanical environments prompted us to investigate whether manipulating β-catenin during disuse might have therapeutic potential for skeletal preservation. I focused on an adult onset mouse model of β-catenin constitutive activation (CA) in osteocytes, in conjunction with two disuse-associated mechanotransduction models, to address the efficacy of β-catenin activation in preventing bone loss. I consistently found that while uninduced mice subjected to disuse lost bone mass as expected, mice with induction of β-cat CA were protected from the bone wasting effects of disuse.

Both the fluid shift (tail suspension) and muscle paralysis (Botox) models of disuse support the conclusion that that induction of β-catenin mitigates the bone wasting effects during disuse. Both models of disuse used here have benefits and limitations; tail suspension prevents regular locomotion within the cage, but muscle forces from kicking may still exert small forces on the bones. Additionally, stress hormones are increased in mice during tail suspension, and may have negative impacts on bone mass. Another consideration of this model is the shift in fluid to the forelimbs and head of the body during suspension. Conversely, muscle paralysis does not completely prevent loading in the treated hindlimb. Muscle atrophy was reduced in these experiments, but muscle function was not completely abolished following botulinum toxin A (Botox) administration. In addition, many of these measurements do not account for the systemic effects Botox may have on the contralateral limb, or the bone gain that may occur in response to locomotive compensation in the contralateral limb. Due to either the sex-dependent differences in response to disuse or the differences within each model system, I did note some differences in the responses to each model. The rescue effect of inducing

β-cat CA during disuse was stronger in the tail suspension than in the Botox experiment when evaluated based on the DXA result (which is largely a cortical bone measurement). For example, Botox-induced bone loss (hindlimb BMD) was not statistically different between induced and uninduced mice (though the former was not different from controls whereas the latter was). However, when evaluated based on the μCT results (a trabecular compartment measurement), both models yielded roughly equal efficacy of the β-cat CA rescue effect. Thus, β-catenin activation might be a better strategy for preserving whole bone properties (cortical and trabecular) in disuse conditions involving fluid shift than for paralysis-based disuse, where cortical bone might be more susceptible to loss.

The results of the β-catenin study indicate that β-catenin is a key regulator of the bone-wasting response in a disuse mechanical environment, matching similar findings in studies of other key Wnt signaling molecules in disuse. Mice with gain of function missense mutations in Lrp5 are protected from disuse-induced bone wasting [71], as are as mice with deletion of the Wnt inhibitor Sost [86, 89]. Additionally, pharmacological neutralization of Sost prevents bone wasting during disuse [90]. Targeting of the Wnt signaling pathway as a therapy for osteoporosis and other bone diseases has been explored, with the use of Sost antibody as a potential therapeutic target. Lithium chloride (LiCl) is a clinically approved treatment for depression, schizophrenia, bipolar disorder, and other mood disorders. LiCl inhibits GSK3β, a major component of the β-catenin degradation complex [91], which is responsible for phosphorylating β-catenin at serine-threonine residues in exon 3. Thus, while LiCl is probably an inappropriate choice for patients subjected to disuse (due to side effects), epidemiological analysis of patients

taking LiCl for other reasons, who happen to also encounter a disuse event, might reveal the translational capacity of β-catenin activation for preserving bone mass.

β-catenin is responsible for multiple modes of regulation in osteocytes, and constitutive activation of β-catenin in this study does not distinguish between these pathways. β-catenin is involved in modulating the mechanotransduction response through its functions at the plasma membrane via cell-cell junctions, gap junctions and in the nucleus as a transcription factor and regulator of multiple gene expression pathways. Increased β-catenin accumulation by constitutive activation of β-catenin likely increases both membrane and nuclear accumulation of β-catenin, although changes in cellular distribution of β-catenin following constitutive activation have not been defined. Additional non-canonical effects of Wnt/B-catenin signaling in bone cannot be ruled out [92]. The RNAseq results provided here will provide further insight into the regulatory/gene transcription role of β-catenin in response to disuse.

The β-catenin study had several limitations that should be acknowledged. First, tamoxifen is not the ideal choice for a chemical inducer of Cre activity, as discussed earlier, due to its direct effects on bone metabolism. Our aim was to start the disuse experiments in adult mice that had a relatively normal skeleton (i.e., avoid a constitutive Cre that might generate an HBM phenotype before the disuse experiment was initiated). There are limited choices for adult-onset (inducible) Cre induction in osteocytes. I did a battery of additional experiments to account for the increases in bone mass following treatment with tamoxifen, but there might be other effects of tamoxifen that I could not resolve. Another limitation of the study was the use of a single sex for each disuse treatment (females for disuse, males for Botox). This study design was chosen due to the

high number of mice required for each experiment (including all the tamoxifen controls) as well as animal welfare concerns. Previous disuse studies have found no sex-dependent differences in response to disuse, suggesting that use of a single sex for each stimulus probably has little effect on the general conclusions. Third, these studies cannot distinguish between the nuclear role and the plasma membrane role of β-catenin. β-catenin plays a very important role in modulating cell mechanics via its function at cell–cell junctions, where it interacts with p120 catenin, vinculin, and the actin cytoskeleton, among other structural proteins. β-catenin regulates expression of Cx43 and gap junction formation between osteocytes [93], and is also critical for mediating transcription of Wnt target genes in the nucleus, via its interaction with Tcf and Lef1 transcription factors. Constitutive activation of β-catenin would presumably have effects on protein longevity and function at both sites, but the relative contribution of these loci cannot be addressed by the current experiments.

In conclusion, these findings indicate that targeting/blocking of β-catenin degradation in bone cells could have therapeutic implications in mechanically induced bone disease. The advancement of nanotechnology has made organ targeting of compounds more precise and effective, and the potential to target β-catenin selectively in bone might be a viable approach to preserving bone mass during disuse. More broadly, this data support the crucial role of Wnt signaling in bone metabolism, and highlight the therapeutic value of manipulating a downstream node in the canonical pathway to improve skeletal disease.

**Lrp4 mediates bone homeostasis and mechanotransduction through Sost**

While the role of the soluble inhibitor Sost in Wnt signaling has been explored extensively, the role of the novel Sost facilitator in bone, Lrp4, is less clear. Here, I generated a mouse model to mimic the high bone mass phenotype observed in SOST2 patients using Crispr/Cas9 to generate the R1170W point mutation. As seen in patients, mice with the Lrp4 R1170W mutation exhibited high bone mass and dramatic increases in circulating sclerostin levels. Additionally, I were able to utilize this mouse to evaluate the role of Lrp4 in ways that cannot be measured in human patients, including muscle function, bone formation and the effect of treatments in the presence of altered Lrp4. I found that that Lrp4 is necessary for Sost inhibition even when sclerostin is highly overexpressed. Additionally, altered Lrp4 has partial effects on both the response to sclerostin antibody as well as disuse in mice.

Understanding the role of individual molecules in Wnt signaling is critical for treatment of low bone mass and bone disease. While numerous therapeutics exist for treatment of low bone mass, most of them are driven towards preventing further bone loss, rather than building new bone. In addition, each of the established bone therapies is associated with side effects ranging from cardiovascular events to increased cancer risk. The recent FDA approval of romosozomab marks the first anabolic bone therapy on the market, but also has a black-box label due to associated side effects. The work shown here provides potential insight into novel therapeutic targets or concurrent therapies to enhance available drugs.

High bone mass (HBM)-causing mutations in genes coding for secreted or plasma membrane-bound Wnt signaling components represent rare glimpses into molecular

targeting opportunities to improve bone health and fracture resistance in osteoporotic patients. Targets that can be modulated to produce anabolic action in the skeleton are particularly attractive, given the paucity of approved and pipeline osteoanabolic agents. The identification of sclerosteosis-like patients harboring missense mutations in LRP4 [1] has furthered our understanding of accessory proteins involved in extracellular Wnt inhibition, and also provided additional avenues for therapeutic development. I engineered an orthologous mouse model to one of the HBM human families identified with an HBM-causing LRP4 missense mutation, which yielded an HBM phenotype and provided a tool to study more mechanistic questions beyond those suited to clinical studies (e.g., bone strength, tissue protein levels). I found that the Lrp4 R1170W knockin mice recapitulate the skeletal phenotype observed in SOST2 patients, and that the phenotype is driven largely by anabolic action.

Moreover, I were able to identify several additional traits associated with Lrp4 3βCD mutation that have not been reported in SOST2 patients, including changes to the dentition (also observed in other Lrp4 models [94], compromised muscle function, and increased levels of sclerostin in osteocyte-enriched protein lysates from bone tissue. Conversely, I failed to find some traits in the murine model that have been identified in patients (e.g., skull thickness, phenotype in the heterozygous state). The reduction in muscle function in Lrp4KI mice is surprising. Certain missense mutations in the 3rd β-propeller of LRP4 (e.g., E1233K and R1277H) can cause congenital myasthenic syndrome (CMS), a non-autoimmune disorder associated with progressive muscle weakness. CMS mutations located on the outer edge of the 3rd β-propeller impair Lrp4 interaction with both Agrin and MuSK—key interactions for neuromuscular junction

assembly and maintenance [85]. However, cell culture models show that overexpression of R1170W impairs Wnt signaling but has no effect on Agrin-induced MuSK signaling, suggesting that centrally located missense mutations (e.g. R1170W) affect Wnt but not Agrin/MuSK, whereas those located on the propeller edge have the inverse effect. These data do not identify a direct role for the R1170W mutation in regulating muscle function; other indirect explanations (e.g., R1170W-induced increase in circulating sclerostin might impair muscle function) cannot be ruled out.

Another interesting finding was the increased levels of sclerostin protein in bone extracts. Human LRP4 HBM patients [83], other mouse models of Lrp4 mutation [62, 95], and WT mice treated with Lrp4 neutralizing antibody [63] all have increased levels of circulating sclerostin, which I confirmed in my R1170W model. Additionally, I also found increased sclerostin protein in bone, which was surprising given (1) Lrp4's purported role in retaining sclerostin at high levels in the local bone environment (which is presumably inhibited by the Lrp4 HBM mutations), and (2) previous reports of decreased sclerostin in the osteocytes of Lrp4 knockin mice (R1170Q), as assessed by immunohistochemistry [95]. One explanation for the increase in tissue sclerostin despite a lack of its primary retention mechanism (functional Lrp4) that is consistent with previous data is the self-regulation of sclerostin expression observed when sclerostin signaling is inhibited genetically or pharmacologically [96].

Investigation of the interaction between Lrp4 and sclerostin has thus far been restricted to cell culture experiments involving overexpression of various signaling components, which have the potential to be problematic or misleading specifically in Wnt-related in vitro studies [97]. I designed in vivo experiments to better understand this

interaction in a more physiologic context, and did so using excessive (hSost transgene) and depleted (Scl-Ab) sclerostin levels in $Lrp4^{KI}$ mice. $Lrp4^{KI}$ mice were largely immune to changes in levels of sclerostin, where $Lrp4^{KI}$ mice overexpressing Sost failed to manifest the osteopenic effects of the transgene, and antibody-treated Lrp4KI failed to gain as much bone as treated WT mice (though they did exhibit significant gains for several parameters). Whereas those experiments do not prove a direct role in binding alterations, they do suggest that Lrp4 3βCD mutations disturb the normal function of sclerostin in regulating bone mass in an in vivo context, both positively and negatively.

To provide a translational context to Lrp4 clinical utility, I explored the role of Lrp4 in mediating disuse osteoporosis. Wnt is a major regulator of mechanical signaling in bone, and I have previously reported therapeutic effects of modulating Lrp5, Sost, and β-catenin in mechanical models [71, 86, 98]. Here, I evaluated the utility of Lrp4 modulation in a muscle paralysis model of bone loss. $Lrp4^{KI}$ mice exhibited significant protection from the bone wasting effects of lower limb paralysis, suggesting that pharmacologic targeting of Lrp4 during or soon after a disuse injury might have clinical benefit.

**Future directions**

Gaining an improved understanding of the role of Wnt signaling proteins in the regulation of bone in response to mechanical environment has the potential to develop novel therapeutics for low bone mass diseases, as well as increase our understanding of the function of these pathways in overall bone maintenance and health. The work shown here provides many different pathways to explore future targets, bone therapies and unanswered questions. In the model in which degradation-resistant β-catenin mice were

subjected to disuse, this work suggests disruption of normal β-catenin regulation protects bone during disuse. Future work will be done to characterize the novel targets discovered here critical for the β-catenin mediated response to mechanical deprivation in osteocytes.

One key area for future work is further characterization of Lrp4. Here, I have demonstrated the critical role for a key component of Lrp4 in Sost facilitator function, which has been hypothesized based on cell culture expriments, but not tested *in vivo* to date. Further characterization of Lrp4-Sost facilitator function are currently underway via fluorescent resonance energy transfer (FRET) studies. Here, I are exploring the direct interaction of Lrp4, Lrp5 and sclerostin in the presence of normal (wild-type) Lrp4 and R1170W Lrp4. The R1170W Lrp4 mice are also being utilized to explore the muscle phenotype identified in these studies, but not characterized further here. The generation and characterization of a bone-specific deletion of Lrp4 (Prx1-Cre;Lrp4$^{flox/flox}$) is ongoing. This mouse model will differ from the R1170W Lrp4 mutant mouse in two key ways. Firstly, this will be a bone-specific deletion of Lrp4 instead of a global knock-in mutation, limiting the effects of other tissues (such as muscle). This will improve our understanding of Lrp4 function in bone specifically, rather than global alteration of Lrp4 and the role of the specific 3$^{rd}$ beta-propeller central domain and its role in Sost function. Secondly, this bone-specific deletion model will effect not only Sost function, but also other Wnt inhibitors interacting with Lrp4 in bone and will disrupt Agrin-MuSK signaling in bone, which presents another possible avenue of exploration in the Lrp4 signaling mechanisms in bone. Because Lrp4 is also critical in CMS, understanding the effects of this disease in bone will broaden the scope of this work.

Finally, the overall aim of this work is to identify potential targets for therapeutic treatments in low bone mass disease. The β-catenin study presented here provides proof-of-concept for targeting intracellular Wnt signaling nodes for treating low bone mass disease, particularly in the context of bedrest or microgravity-induced bone wasting. While β-catenin has not previously been ideal as a therapeutic target due to the importance of β-catenin in other tissues as well as cancer, technological advances in tissue-specific drug targeting make the possibilities of utilizing β-catenin, or downstream targets of β-catenin a possibility in the future. Given the dramatic rescue effect of β-catenin (strong protective effects despite low recombination rates), B-catenin would be an ideal target for low bone mass disease treatment when targeted drug treatment becomes a reality.

Targeting of Lrp4 perhaps provides a more tenable focus for low bone mass therapies. While Lrp4 is globally expressed, and critical in NMJs formation, I have identified a critical role of the 3$^{rd}$ beta-propeller central domain in bone specifically. Future work is aimed at identification of pharmacological targeting of Lrp4 via either antibody treatment (currently being explored) or small molecule-targeting of the 3$^{rd}$ beta-propeller central domain.

Previous work, as well as the work shown here, identifies Wnt signaling as an ideal target for low bone mass therapies. This is demonstrated by the recent regulatory approval for clinical use of sclerostin-neutralizing antibody in several countries (US, Japan, Canada, South Korea, Australia), and has opened the door for widespread use of the first Wnt-based therapy for bone health. Whether other components (e.g., Lrp4) alone or in conjunction with sclerostin targeting can provide additional benefits to patients

remains to be determined, but Lrp4 targeting for low bone mass states appears attractive from a preclinical perspective. Advances in drug delivery technology may soon provide tissue-specific targeting strategies for therapies once considered unusable due to systemic effects, including β-catenin.

## ***APPENDIX 1: Permissions***

### Request for Rights Figure 5



**Title:** WNT signaling in bone homeostasis and disease: from human mutations to treatments

Logged in as: Whitney Bullock N/A

LOGOUT

**Author:** Roland Baron, Michaela Kneissel

**Publication:** Nature Medicine

**Publisher:** Springer Nature

**Date:** Feb 6, 2013



## Order Completed

Thank you for your order.

This Agreement between N/A -- Whitney Bullock ("You") and Springer Nature ("Springer Nature") consists of your license details and the terms and conditions provided by Springer Nature and Copyright Clearance Center.

Your confirmation email will contain your order number for future reference.

printable details

| | |
|---|---|
| License Number | 4653080232783 |
| License date | Aug 20, 2019 |
| Licensed Content Publisher | Springer Nature |
| Licensed Content Publication | Nature Medicine |
| Licensed Content Title | WNT signaling in bone homeostasis and disease: from human mutations to treatments |
| Licensed Content Author | Roland Baron, Michaela Kneissel |
| Licensed Content Date | Feb 6, 2013 |
| Licensed Content Volume | 19 |
| Licensed Content Issue | 2 |
| Type of Use | Thesis/Dissertation |
| Requestor type | academic/university or research institute |
| Format | electronic |
| Portion | figures/tables/illustrations |

| | |
|---|---|
| Number of figures/tables/illustrations | 1 |
| High-res required | no |
| Will you be translating? | no |
| Circulation/distribution | <501 |
| Author of this Springer Nature content | no |
| Title | The Role of Wnt Signaling in Bone Mechanotransduction |
| Institution name | Indiana University |
| Expected presentation date | Sep 2019 |
| Portions | Figure 1. Wnt Signaling: A simplified view |
| Requestor Location | N/A<br>635 BARNHILL DRIVE<br>INDIANAPOLIS, IN 46202<br>United States Attn:<br>N/A |

**PERMISSIONS FOR FIGURE 9**

## Copyright and license to publish

The text below explains the process for reusing content that was originally published in JBC. If you want to reuse previously published content in a new submission to JBC and need guidance regarding permissions, please click here.

**For authors:**

Effective with initial submissions from January 1, 2018, authors must agree that if their manuscript is accepted, they will grant ASBMB an exclusive, irrevocable License to Publish their work; the copyright remains with the authors.

Manuscripts initially submitted prior to January 1, 2018 are subject to JBC's former policy whereby, as a condition of publication, authors transfer copyright to ASBMB upon acceptance.

Authors of manuscripts, submitted at any time, need not contact the journal to request permission to reuse their own material. Authors who granted ASBMB exclusive license to publish and authors who transferred copyright to ASBMB, are allowed to do the following:

a. to use all or part of the work in compilations or other publications of the Authors' own commercial and
noncommercial works (includes theses/dissertations), to use figures, photos, and tables created by them and contained in the work, to present the work orally in its entirety, and to make copies of all or part of the work for the Authors' use for lectures, classroom instruction or similar uses. If the author is employed by an academic institution, that institution also may reproduce the article for teaching purposes.

b. to post the accepted manuscript version of the work, the "Paper in Press," on the author's personal web page, their personal or institutional repository, or their funding body's archive or designated noncommercial repository, provided that a link to the article in the *Journal of Biological Chemistry* is included.
c. to post a manuscript version of the work on not-for-profit preprint servers provided that the Authors retain distribution rights to the work, that ASBMB formatted final files are not posted, and that a link to the article in the *Journal of Biological Chemistry* is included.
d. to post the final edited PDFs, created by ASBMB, to their own departmental/university websites, provided that the posting does not happen until 12 months after publication of the work in the *Journal of Biological Chemistry*, and that a link to the article in the *Journal of Biological Chemistry* is included.

Reuse of JBC content must include the following: This research was originally published in the Journal of Biological Chemistry. Author(s). Title. J. Biol. Chem. Year; Vol:pp-pp. © the American Society for Biochemistry and Molecular Biology *or* © the Author(s).

Authors may choose to publish their article under the JBC's paid open access publishing option, Author's Choice, which means that for an additional publication fee: 1) the final, edited PDF and full text html of their article will be immediately available on jbc.org and in PubMed Central (PMC) without the usual 12-month embargo period, and 2) the article will be distributed under the CC-BY license which automatically grants all commercial and noncommercial use of the article to all, as long as appropriate attribution is given to the original work.

**Parties who are not authors on the article For noncommercial use:**

Parties other than the authors seeking to reuse JBC content for noncommercial purposes are welcome to copy, distribute, transmit and adapt the work at no cost and without permission as long as they attribute the work to the original source using the citation above. Examples of noncommercial use include:

- Reproducing a figure for educational purposes, such as schoolwork or lecture presentations.
- Appending a reprinted article to a Ph.D. dissertation.

**For commercial use:**

Parties other than the authors seeking to reuse JBC content for commercial purposes must obtain permission to do so. Navigate to the article of interest and click the "Request Permissions" button on the middle navigation bar (see diagram below), and obtain permission through copyright.com. Examples of commercial use include:

- Reproducing a figure in a book published by a commercial publisher.
- Reproducing a figure in a journal article published by a commercial publisher.


**For noncommercial and commercial use of content published under CC-BY license**

For JBC content that was published under JBC's paid open access publishing option, Author's Choice, the article was distributed under the CC-BY license which automatically grants all commercial and noncommercial use of the article to all, as long as appropriate attribution is given to the original work.

## ***References***


1. Leupin, O., et al., *Bone overgrowth-associated mutations in the LRP4 gene impair sclerostin facilitator function.* J Biol Chem, 2011. **286**(22): p. 19489-500.
2. Whitney A. Bullock, L.I.P., Alexander G. Robling, and Fredrick M. Pavalko, *Mechanotransduction in Bone Formation and Maintenance*, in *Primer on the Metabolic Bone Diseases and Disorders of Mineral Metabolism*, K. Lyons, Editor. 2018, Wiley-Blackwell.
3. Bullock, W.A., F.M. Pavalko, and A.G. Robling, *Osteocytes and mechanical loading: The Wnt connection.* Orthod Craniofac Res, 2019. **22 Suppl 1**: p. 175-179.
4. Riddle, R.C. and T.L. Clemens, *Bone Cell Bioenergetics and Skeletal Energy Homeostasis.* Physiol Rev, 2017. **97**(2): p. 667-698.
5. Baron, R. and M. Kneissel, *WNT signaling in bone homeostasis and disease: from human mutations to treatments.* Nat Med, 2013. **19**(2): p. 179-92.
6. Becker, D.J., M.L. Kilgore, and M.A. Morrisey, *The societal burden of osteoporosis.* Curr Rheumatol Rep, 2010. **12**(3): p. 186-91.
7. Burge, R., et al., *Incidence and economic burden of osteoporosis-related fractures in the United States, 2005-2025.* J Bone Miner Res, 2007. **22**(3): p. 465-75.
8. Robling, A.G., A.B. Castillo, and C.H. Turner, *Biomechanical and molecular regulation of bone remodeling.* Annu Rev Biomed Eng, 2006. **8**: p. 455-98.
9. Bonivtch, A.R., L.F. Bonewald, and D.P. Nicolella, *Tissue strain amplification at the osteocyte lacuna: a microstructural finite element analysis.* J Biomech, 2007. **40**(10): p. 2199-206.
10. Klein-Nulend, J., et al., *Pulsating fluid flow increases nitric oxide (NO) synthesis by osteocytes but not periosteal fibroblasts--correlation with prostaglandin upregulation.* Biochem Biophys Res Commun, 1995. **217**(2): p. 640-8.
11. Ponik, S.M., J.W. Triplett, and F.M. Pavalko, *Osteoblasts and osteocytes respond differently to oscillatory and unidirectional fluid flow profiles.* J Cell Biochem, 2007. **100**(3): p. 794-807.
12. Tatsumi, S., et al., *Targeted ablation of osteocytes induces osteoporosis with defective mechanotransduction.* Cell Metab, 2007. **5**(6): p. 464-75.
13. Komori, T., *Mouse models for the evaluation of osteocyte functions.* J Bone Metab, 2014. **21**(1): p. 55-60.
14. Wang, Y., et al., *Strain amplification and integrin based signaling in osteocytes.* J Musculoskelet Neuronal Interact, 2008. **8**(4): p. 332-4.
15. Stern, A.R. and D.P. Nicolella, *Measurement and estimation of osteocyte mechanical strain.* Bone, 2013. **54**(2): p. 191-5.
16. Donahue, T.L., et al., *Mechanosensitivity of bone cells to oscillating fluid flow induced shear stress may be modulated by chemotransport.* J Biomech, 2003. **36**(9): p. 1363-71.
17. Dubash, A.D., et al., *Chapter 1. Focal adhesions: new angles on an old structure.* Int Rev Cell Mol Biol, 2009. **277**: p. 1-65.
18. Pavalko, F.M., et al., *A model for mechanotransduction in bone cells: the load-bearing mechanosomes.* J Cell Biochem, 2003. **88**(1): p. 104-12.

19. Bidwell, J.P. and F.M. Pavalko, *The Load-Bearing Mechanosome Revisited.* Clin Rev Bone Miner Metab, 2010. **8**(4): p. 213-223.
20. Yavropoulou, M.P. and J.G. Yovos, *The molecular basis of bone mechanotransduction.* J Musculoskelet Neuronal Interact, 2016. **16**(3): p. 221-36.
21. Norvell, S.M., et al., *Fluid shear stress induces beta-catenin signaling in osteoblasts.* Calcif Tissue Int, 2004. **75**(5): p. 396-404.
22. McAllister, T.N. and J.A. Frangos, *Steady and transient fluid shear stress stimulate NO release in osteoblasts through distinct biochemical pathways.* J Bone Miner Res, 1999. **14**(6): p. 930-6.
23. Zhang, Y.L., J.A. Frangos, and M. Chachisvilis, *Mechanical stimulus alters conformation of type 1 parathyroid hormone receptor in bone cells.* Am J Physiol Cell Physiol, 2009. **296**(6): p. C1391-9.
24. Tahimic, C.G., et al., *Regulation of Ligand and Shear Stress-induced Insulin-like Growth Factor 1 (IGF1) Signaling by the Integrin Pathway.* J Biol Chem, 2016. **291**(15): p. 8140-9.
25. Rangaswami, H., et al., *Cyclic GMP and protein kinase G control a Src-containing mechanosome in osteoblasts.* Sci Signal, 2010. **3**(153): p. ra91.
26. Plotkin, L.I., T.L. Speacht, and H.J. Donahue, *Cx43 and mechanotransduction in bone.* Curr Osteoporos Rep, 2015. **13**(2): p. 67-72.
27. Goodenough, D.A. and D.L. Paul, *Beyond the gap: functions of unpaired connexon channels.* Nat Rev Mol Cell Biol, 2003. **4**(4): p. 285-94.
28. Penuela, S., R. Gehi, and D.W. Laird, *The biochemistry and function of pannexin channels.* Biochim Biophys Acta, 2013. **1828**(1): p. 15-22.
29. Plotkin, L.I. and T. Bellido, *Beyond gap junctions: Connexin43 and bone cell signaling.* Bone, 2013. **52**(1): p. 157-66.
30. Turner, C.H. and A.G. Robling, *Exercise as an anabolic stimulus for bone.* Curr Pharm Des, 2004. **10**(21): p. 2629-41.
31. Orriss, I.R., *The role of purinergic signalling in the musculoskeletal system.* Auton Neurosci, 2015. **191**: p. 124-34.
32. Li, Y.S., J.H. Haga, and S. Chien, *Molecular basis of the effects of shear stress on vascular endothelial cells.* J Biomech, 2005. **38**(10): p. 1949-71.
33. Seref-Ferlengez, Z., et al., *P2X7R-Panx1 Complex Impairs Bone Mechanosignaling under High Glucose Levels Associated with Type-1 Diabetes.* PLoS One, 2016. **11**(5): p. e0155107.
34. Thompson, W.R., C.T. Rubin, and J. Rubin, *Mechanical regulation of signaling pathways in bone.* Gene, 2012. **503**(2): p. 179-93.
35. Lieben, L. and G. Carmeliet, *The Involvement of TRP Channels in Bone Homeostasis.* Front Endocrinol (Lausanne), 2012. **3**: p. 99.
36. Lu, H.F., et al., *Mechanical loading induced expression of bone morphogenetic protein-2, alkaline phosphatase activity, and collagen synthesis in osteoblastic MC3T3-E1 cells.* Chin Med J (Engl), 2012. **125**(22): p. 4093-7.
37. Thorsen, K., et al., *In situ microdialysis in bone tissue. Stimulation of prostaglandin E2 release by weight-bearing mechanical loading.* J Clin Invest, 1996. **98**(11): p. 2446-9.

38. Tanaka, H., S. Kanako, and S. Abe, *Prostaglandin E2 receptor selective agonists E-prostanoid 2 and E-prostanoid 4 may have therapeutic effects on ovalbumin-induced bronchoconstriction.* Chest, 2005. **128**(5): p. 3717-23.
39. Li, J., D.B. Burr, and C.H. Turner, *Suppression of prostaglandin synthesis with NS-398 has different effects on endocortical and periosteal bone formation induced by mechanical loading.* Calcif Tissue Int, 2002. **70**(4): p. 320-9.
40. Burra, S. and J.X. Jiang, *Connexin 43 hemichannel opening associated with Prostaglandin E(2) release is adaptively regulated by mechanical stimulation.* Commun Integr Biol, 2009. **2**(3): p. 239-40.
41. Saura, M., C. Tarin, and C. Zaragoza, *Recent insights into the implication of nitric oxide in osteoblast differentiation and proliferation during bone development.* ScientificWorldJournal, 2010. **10**: p. 624-32.
42. Basso, N. and J.N. Heersche, *Effects of hind limb unloading and reloading on nitric oxide synthase expression and apoptosis of osteocytes and chondrocytes.* Bone, 2006. **39**(4): p. 807-14.
43. Gong, Y., et al., *LDL receptor-related protein 5 (LRP5) affects bone accrual and eye development.* Cell, 2001. **107**(4): p. 513-23.
44. Van Wesenbeeck, L., et al., *Six novel missense mutations in the LDL receptor-related protein 5 (LRP5) gene in different conditions with an increased bone density.* Am J Hum Genet, 2003. **72**(3): p. 763-71.
45. Little, R.D., et al., *A mutation in the LDL receptor-related protein 5 gene results in the autosomal dominant high-bone-mass trait.* Am J Hum Genet, 2002. **70**(1): p. 11-9.
46. Sawakami, K., et al., *The Wnt co-receptor LRP5 is essential for skeletal mechanotransduction but not for the anabolic bone response to parathyroid hormone treatment.* J Biol Chem, 2006. **281**(33): p. 23698-711.
47. Saxon, L.K., et al., *Analysis of multiple bone responses to graded strains above functional levels, and to disuse, in mice in vivo show that the human Lrp5 G171V High Bone Mass mutation increases the osteogenic response to loading but that lack of Lrp5 activity reduces it.* Bone, 2011. **49**(2): p. 184-93.
48. Cui, Y., et al., *Lrp5 functions in bone to regulate bone mass.* Nat Med, 2011. **17**(6): p. 684-91.
49. Niziolek, P.J., M.L. Warman, and A.G. Robling, *Mechanotransduction in bone tissue: The A214V and G171V mutations in Lrp5 enhance load-induced osteogenesis in a surface-selective manner.* Bone, 2012. **51**(3): p. 459-65.
50. Zhao, L., et al., *Inactivation of Lrp5 in osteocytes reduces young's modulus and responsiveness to the mechanical loading.* Bone, 2013. **54**(1): p. 35-43.
51. Poole, K.E., et al., *Sclerostin is a delayed secreted product of osteocytes that inhibits bone formation.* FASEB J, 2005. **19**(13): p. 1842-4.
52. Balemans, W., et al., *Increased bone density in sclerosteosis is due to the deficiency of a novel secreted protein (SOST).* Hum Mol Genet, 2001. **10**(5): p. 537-43.
53. Loots, G.G., et al., *Genomic deletion of a long-range bone enhancer misregulates sclerostin in Van Buchem disease.* Genome Res, 2005. **15**(7): p. 928-35.
54. Semenov, M., K. Tamai, and X. He, *SOST is a ligand for LRP5/LRP6 and a Wnt signaling inhibitor.* J Biol Chem, 2005. **280**(29): p. 26770-5.

55. Robling, A.G., et al., *Mechanical stimulation of bone in vivo reduces osteocyte expression of Sost/sclerostin.* J Biol Chem, 2008. **283**(9): p. 5866-75.
56. Tu, X., et al., *Sost downregulation and local Wnt signaling are required for the osteogenic response to mechanical loading.* Bone, 2012. **50**(1): p. 209-17.
57. Harris, S.E., et al., *DMP1 and MEPE expression are elevated in osteocytes after mechanical loading in vivo: theoretical role in controlling mineral quality in the perilacunar matrix.* J Musculoskelet Neuronal Interact, 2007. **7**(4): p. 313-5.
58. Javaheri, B., et al., *Deletion of a single beta-catenin allele in osteocytes abolishes the bone anabolic response to loading.* J Bone Miner Res, 2014. **29**(3): p. 705-15.
59. Kang, K.S., J.M. Hong, and A.G. Robling, *Postnatal beta-catenin deletion from Dmp1-expressing osteocytes/osteoblasts reduces structural adaptation to loading, but not periosteal load-induced bone formation.* Bone, 2016. **88**: p. 138-145.
60. Maurel, D.B., et al., *Beta-Catenin Haplo Insufficient Male Mice Do Not Lose Bone in Response to Hindlimb Unloading.* PLoS One, 2016. **11**(7): p. e0158381.
61. Zong, Y. and R. Jin, *Structural mechanisms of the agrin-LRP4-MuSK signaling pathway in neuromuscular junction differentiation.* Cell Mol Life Sci, 2013. **70**(17): p. 3077-88.
62. Xiong, L., et al., *Lrp4 in osteoblasts suppresses bone formation and promotes osteoclastogenesis and bone resorption.* Proc Natl Acad Sci U S A, 2015. **112**(11): p. 3487-92.
63. Chang, M.K., et al., *Disruption of Lrp4 function by genetic deletion or pharmacological blockade increases bone mass and serum sclerostin levels.* Proc Natl Acad Sci U S A, 2014. **111**(48): p. E5187-95.
64. Boudin, E., et al., *The Lrp4R1170Q Homozygous Knock-In Mouse Recapitulates the Bone Phenotype of Sclerosteosis in Humans.* J Bone Miner Res, 2017. **32**(8): p. 1739-1749.
65. Ayturk, U.M., et al., *Modeling Degenerative Disk Disease in the Lumbar Spine: A Combined Experimental, Constitutive, and Computational Approach.* Journal of Biomechanical Engineering-Transactions of the Asme, 2012. **134**(10).
66. Harada, N., et al., *Intestinal polyposis in mice with a dominant stable mutation of the beta-catenin gene.* Embo j, 1999. **18**(21): p. 5931-42.
67. Brault, V., et al., *Inactivation of the beta-catenin gene by Wnt1-Cre-mediated deletion results in dramatic brain malformation and failure of craniofacial development.* Development, 2001. **128**(8): p. 1253-64.
68. Powell, W.F., Jr., et al., *Targeted ablation of the PTH/PTHrP receptor in osteocytes impairs bone structure and homeostatic calcemic responses.* J Endocrinol, 2011. **209**(1): p. 21-32.
69. Indra, A.K., et al., *Temporally-controlled site-specific mutagenesis in the basal layer of the epidermis: comparison of the recombinase activity of the tamoxifen-inducible Cre-ER(T) and Cre-ER(T2) recombinases.* Nucleic Acids Res, 1999. **27**(22): p. 4324-7.
70. Kalajzic, I., et al., *In vitro and in vivo approaches to study osteocyte biology.* Bone, 2013. **54**(2): p. 296-306.
71. Niziolek, P.J., et al., *Missense Mutations in LRP5 Associated with High Bone Mass Protect the Mouse Skeleton from Disuse- and Ovariectomy-Induced Osteopenia.* PLoS One, 2015. **10**(11): p. e0140775.

72. Bouxsein, M.L., et al., *Guidelines for assessment of bone microstructure in rodents using micro-computed tomography.* J Bone Miner Res, 2010. **25**(7): p. 1468-86.
73. Dempster, D.W., et al., *Standardized nomenclature, symbols, and units for bone histomorphometry: a 2012 update of the report of the ASBMR Histomorphometry Nomenclature Committee.* J Bone Miner Res, 2013. **28**(1): p. 2-17.
74. Luks, V.L., et al., *Lymphatic and other vascular malformative/overgrowth disorders are caused by somatic mutations in PIK3CA.* J Pediatr, 2015. **166**(4): p. 1048-54.e1-5.
75. Ayturk, U.M., et al., *An RNA-seq protocol to identify mRNA expression changes in mouse diaphyseal bone: applications in mice with bone property altering Lrp5 mutations.* J Bone Miner Res, 2013. **28**(10): p. 2081-93.
76. Dobin, A., et al., *STAR: ultrafast universal RNA-seq aligner.* Bioinformatics, 2013. **29**(1): p. 15-21.
77. Liao, Y., G.K. Smyth, and W. Shi, *featureCounts: an efficient general purpose program for assigning sequence reads to genomic features.* Bioinformatics, 2014. **30**(7): p. 923-30.
78. Robinson, M.D. and A. Oshlack, *A scaling normalization method for differential expression analysis of RNA-seq data.* Genome Biol, 2010. **11**(3): p. R25.
79. Robinson, M.D., D.J. McCarthy, and G.K. Smyth, *edgeR: a Bioconductor package for differential expression analysis of digital gene expression data.* Bioinformatics, 2010. **26**(1): p. 139-40.
80. Turner, C.H. and D.B. Burr, *Basic biomechanical measurements of bone: a tutorial.* Bone, 1993. **14**(4): p. 595-608.
81. Organ, J.M., et al., *Reduced skeletal muscle function is associated with decreased fiber cross-sectional area in the Cy/+ rat model of progressive kidney disease.* Nephrol Dial Transplant, 2016. **31**(2): p. 223-30.
82. Grüneboom, A., et al., *A network of trans-cortical capillaries as mainstay for blood circulation in long bones.* Nature Metabolism, 2019. **1**(2): p. 236-250.
83. Fijalkowski, I., et al., *A Novel Domain-Specific Mutation in a Sclerosteosis Patient Suggests a Role of LRP4 as an Anchor for Sclerostin in Human Bone.* J Bone Miner Res, 2016. **31**(4): p. 874-81.
84. Shen, C., W.C. Xiong, and L. Mei, *LRP4 in neuromuscular junction and bone development and diseases.* Bone, 2015. **80**: p. 101-108.
85. Ohkawara, B., et al., *LRP4 third beta-propeller domain mutations cause novel congenital myasthenia by compromising agrin-mediated MuSK signaling in a position-specific manner.* Hum Mol Genet, 2014. **23**(7): p. 1856-68.
86. Robling, A.G., et al., *Sost, independent of the non-coding enhancer ECR5, is required for bone mechanoadaptation.* Bone, 2016. **92**: p. 180-188.
87. Jardi, F., et al., *A shortened tamoxifen induction scheme to induce CreER recombinase without side effects on the male mouse skeleton.* Mol Cell Endocrinol, 2017. **452**: p. 57-63.
88. Zhong, Z.A., et al., *Optimizing tamoxifen-inducible Cre/loxp system to reduce tamoxifen effect on bone turnover in long bones of young mice.* Bone, 2015. **81**: p. 614-619.

89. Lin, C., et al., *Sclerostin mediates bone response to mechanical unloading through antagonizing Wnt/beta-catenin signaling.* J Bone Miner Res, 2009. **24**(10): p. 1651-61.
90. Spatz, J.M., et al., *Sclerostin antibody inhibits skeletal deterioration due to reduced mechanical loading.* J Bone Miner Res, 2013. **28**(4): p. 865-74.
91. Grimes, C.A. and R.S. Jope, *The multifaceted roles of glycogen synthase kinase 3beta in cellular signaling.* Prog Neurobiol, 2001. **65**(4): p. 391-426.
92. Kondoh, S., et al., *Estrogen receptor alpha in osteocytes regulates trabecular bone formation in female mice.* Bone, 2014. **60**: p. 68-77.
93. Xia, X., et al., *Prostaglandin promotion of osteocyte gap junction function through transcriptional regulation of connexin 43 by glycogen synthase kinase 3/beta-catenin signaling.* Mol Cell Biol, 2010. **30**(1): p. 206-19.
94. Ahn, Y., et al., *Multiple modes of Lrp4 function in modulation of Wnt/beta-catenin signaling during tooth development.* Development, 2017. **144**(15): p. 2824-2836.
95. Boudin, E., et al., *The Lrp4 R1170Q homozygous knock-in mouse recapitulates the bone phenotype of sclerosteosis in humans.* J Bone Miner Res, 2017.
96. Witcher, P.C., et al., *Sclerostin neutralization unleashes the osteoanabolic effects of Dkk1 inhibition.* JCI Insight, 2018. **3**(11).
97. Goel, S., et al., *Both LRP5 and LRP6 receptors are required to respond to physiological Wnt ligands in mammary epithelial cells and fibroblasts.* J Biol Chem, 2012. **287**(20): p. 16454-66.
98. Bullock, W.A., Hoggatt, A., Horan, D. J., Yokota, H., Sebastian, A., Loots, G. G., Pavalko, F. M., Robling, A. G., *Expression of a degradation-resistant beta-catenin mutant in osteocytes protects the skeleton from mechanodepravation-induced bone wasting.* J Bone Miner Res, 2019. **in press**.

# ***Curriculum Vitae***

**Whitney Ann Bullock**

## Education

**2014-2019** Doctor of Philosophy
Major: Anatomy and Cell Biology; Minor: Life Sciences
Indiana University, Indianapolis, IN

**2007-2010** Bachelor of Science
Major: Animal Sciences; Minor: Biotechnology
Purdue University, West Lafayette, IN

## Accomplishments

NIH 1 F31 AR068901-01A1
"Accessory membrane and intracellular mediators in bone cell mechanotransduction."
Role: PI
Award start date: July 1, 2017

NIH 5T32AR065971-02
"Comprehensive Training Program in Musculoskeletal Research"
Role: Graduate Trainee
July 2016- July 2017

## Publications

**Bullock, W.** Hoggatt, A., Horan D., Elmendorf A., Sato A., Bellido T., Loots G., Pavalko F., and Robling A., *Lrp4 mediates bone homeostasis and mechanotransduction through interaction with sclerostin in vivo.* iScience 2019 20:205-215. doi:10.1016/j.isci.2019.09.023 PMID:31585407

Lewis, K., Chio, R., Pemberton, E., **Bullock, W.,** Firulli, A., Robling, A. *Twist1 Inactivation in Dmp1-Expressing Cells Increases Bone Mass but Does Not Affect the Anabolic Response to Sclerostin Neutralization.* Int J Mol Sci. 2019 20(18). piiE4427. doi: 10.3390/ijms20184427 PMID:31505764

**Bullock, W.,** Hoggatt, A, Horan D, Lewis Z, Yokota H, Hann S, Warman M, Sebastian A, Loots G, Pavalko F, Robling A. *Expression of Degradation-Resistant B-catenin Mutant in Osteocytes Protects the Skeleton From Mechanodeprovation-Induced Bone Wasting.* JBMR 2019. In press. doi:10.1002/jbmr.3812 PMID: 31173667

Yang H, Xu X, **Bullock W,** Main RP. *Adaptive changes in micromechanical environments of cancellous and cortical bone in response to in vivo moadig and disuse.* J Biomech 2019 89:85-94. doi: 10.1016/j.jbiomech.2019.04.021 PMID: 31047696

**Bullock, W.,** Plotkin, L., Robling, A., Pavalko, F. "Mechanotransduction in bone formation/maintenance" *Primer on the Metabolic Bone Diseases and Disorders of Mineral Metabolism, 9th Edition*

**Bullock W**, Pavalko FM, Robling AG. *Osteocytes and mechanical loading: The Wnt Connection*. Orthod Craniofac Res. 2019 May;22 Suppl 1:175-179. doi: 10.1111/ocr.12282. PMID: 31074153

Witcher P., Rachles S., Horan D., **Bullock W.**, Lim KE., Kang KS., Adaniya A., Ross R., Loots G, Robling A. *Genetic disruption of compensatory WNT inhibitor expression reveals a context-dependent, highly osteoanabolic role for DKK1 inhibition in the skeleton.* JCI Insight 2018 3(11): pii 98673. doi: 10.1016/j.bone.2018.10.007 PMID:30409757

**Bullock W**, Robling A. *WNT-mediated Modulation of Bone Metabolism: Implications for WNT Targeting to Treat Extraskeletal Disorders*. Toxicol Pathol. 2017 Oct;45(7):864-868. doi: 10.1177/0192623317738170. Epub 2017 Nov 5. PubMed PMID: 29105581; PubMed Central PMCID: PMC5688020.

Robling A, Kang K, **Bullock W**, Foster W, Murugesh D, Loots G, Genetos D. Sost, independent of the non-coding enhancer ECR5, is required for bone mechanoadaptation. Bone. 2016 Nov;92:180-188. doi: 10.1016/j.bone.2016.09.001. Epub 2016 Sep 4. PubMed PMID: 27601226.

Niziolek P, **Bullock W**, Warman M, Robling A. Missense Mutations in LRP5 Associated with High Bone Mass Protect the Mouse Skeleton from Disuse- and Ovariectomy-Induced Osteopenia. PLoS One. 2015 Nov 10;10(11):e0140775. doi: 10.1371/journal.pone.0140775. eCollection 2015. PubMed PMID: 26554834; PubMed Central PMCID: PMC4640505.

Gaharwar A, Kishore V, Rivera C, **Bullock W**, Wu CJ, Akkus O, Schmidt G. Physically crosslinked nanocomposites from silicate-crosslinked PEO: mechanical properties and osteogenic differentiation of human mesenchymal stem cells. Macromol Biosci. 2012 Jun;12(6):779-93. doi: 0.1002/mabi.201100508. Epub 2012 Apr 19. PubMed PMID: 22517665.

Kishore V, **Bullock W**, Sun X, Van Dyke WS, Akkus O. Tenogenic differentiation of human MSCs induced by the topography of electrochemically aligned collagen threads. Biomaterials. 2012 Mar;33(7):2137-44. doi: 10.1016/j.biomaterials.2011.11.066. Epub 2011 Dec 15. PubMed PMID: 22177622; PubMed Central PMCID: PMC3279298.

**Awards**

Young Investigator Award, ASBMR Annual Conference 2019, Orlando Florida.

1st Place Poster. Indiana Center for Musculoskeletal Research International meeting 2019. *Bone and Muscle Interactions: the Mechanical and Beyond,* Indianapolis Indiana.

Poster selected for Plenary Session, 2015 ASBMR meeting

**Presentations**

**Whitney A. Bullock**, April Hoggatt, Daniel J. Horan, Andrew Elmendorf, Amy Y. Sato, Teresita Bellido, Gabriela G. Loots, Fredrick M. Pavalko, and Alexander G. Robling. *Lrp4 mediates bone mass and mechanotransduction through interaction with sclerostin in vivo.* ASBMR Annual Meeting, Orlando Florida, September 2019.

**Whitney A. Bullock**, April Hoggatt, Daniel J. Horan, Andrew Elmendorf, Amy Y. Sato, Teresita Bellido, Gabriela G. Loots, Fredrick M. Pavalko, and Alexander G. Robling. *Lrp4 mediates bone mass and mechanotransduction through interaction with sclerostin in vivo.* Indiana Center for Musculoskeletal Research International meeting 2019-*Bone and Muscle Interactions: the Mechanical and Beyond,* Indianapolis Indiana

**Whitney Bullock**, Alexander Robling. *Point Mutation in Lrp4 Sost Binding Pocket Increases Bone Mass in Mice*. ORS Sun Valley Workshop August 2017.

"Targeted Deletion of Src from Osteocytes Increases Trabecular Bone Mass in Mice." Poster presentation, 2016 ASBMR, Atlanta, GA

"β-catenin gain-of-function mutation in osteocytes confers protective effects from disuse-induced bone loss." Poster presentation, 2015 ASBMR, Seattle, WA